Siegfried Arneitz, BSc.

Recovery and recrystallization study of an Al(Mg) alloy using difference dilatometry and electron backscatter diffraction

MASTER'S THESIS

to achieve the university degree of

Diplom-Ingenieur

Master's degree programme: Advanced Materials Science

submitted to

Graz University of Technology

Supervisor

Assoc. Prof. Wolfgang Sprengel

Institute of Materials Physics

Graz, June 2019

AFFIDAVIT

I declare that I have authored this thesis independently, that I have not used other than the declared sources/resources, and that I have explicitly indicated all material which has been quoted either literally or by content from the sources used. The text document uploaded to TUGRAZonline is identical to the present master‘s thesis.

31.05.2018

Date

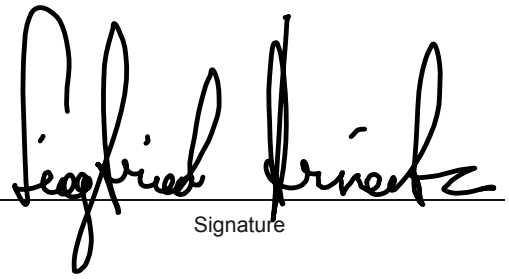

Signature

Abstract

Recovery and recrystallization in metals after deformation are in general accompanied by irreversible releases of excess volume due to changes in the number of grain boundaries, dislocation density or vacancy concentration. This results in macroscopic length changes. Applying the technique of difference-dilatometry, i.e., simultaneous measurement of length changes as function of time and temperature with respect to a fully recrystallized reference sample allows to distinguish between reversible and irreversible effects for quantitative studies. Such kind of measurements were performed in combination with electron backscatter diffraction (EBSD) on a commercial Al-3wt%Mg (AW5754) alloy. The dilatometric measurements were carried out with different linear heating rates (0.1 to 6.0 $\mathrm{K\,min^{-1}}$) on samples with various degrees of plastic deformation (-0.01 $< \varepsilon <$ -0.67; $\varepsilon > -2$) and heated up to different temperatures ranging from 100 to 500 °C. The measurement distinguished also between different measurement directions with respect to the direction of deformation. The influence of Al_6(Mn,Si,Fe) particles, which were aligned alongside the initial hot- rolling direction of the production process was also examined. Furthermore, the microstructure of the samples in different stages of recovery and recrystallization were quenched-in and analyzed by EBSD.

The dilatometric measurements found an anisotropy in the annealing behaviour of the material depending on the direction of observation. Perdendicular to the direction of deformation, a steady decrease in relative length in comparison to a fully recrystallized reference sample was observed during annealing. Parallel to the direction of deformation, an initial increase in length in the low temperature regime (up to 200 °C) was followed by a decrease in length change in the high temperature regime. At about 60 °C the onset of static recovery was observed for all conditions investigated. The onset temperature for recrystallization varied according to the strain that had been applied. For larger deformation the onset of recrystallization occurred at lower temperatures. However, the onset temperature for nucleation during recrystallisation was found to be independent on the grade of deformation. Measurements with extremely low and extremely high deformed samples showed, that the boundary value of ε for recrystallisation to occur is located around $\varepsilon = -0.04$. For temperatures above 400 °C a fully recrystallized microstructure was observed.

The unique combination of in-situ dilatometry with EBSD also allows for an analysis of the kinetics of recovery and recrystallization which cannot be obtained from post-mortem analysis alone. An attempt to calculate the activation energies of recovery and recrystallisation was made and a dependence of these apparent activation energies on the grade of deformation previously introduced to the sample was found.

The observed quantitative correlations between the volume changes, e.g., due to the change in the dislocation density, and the observed changes in the microstructure gives access to valuable parameters for modelling of recovery and recrystallization processes in those alloys.

Contents

1 Introduction

Aluminum alloys have many beneficial properties. Their low density, high strength and hardness and convenience in processing make them suitable for many applications like lightweight construction, astronautics and in the production of structural elements, just to name a few.

The main subject of this thesis is the examination of the commercial aluminum alloy AW5754. Contrary to precipitation hardened aluminum alloys, this type of alloy does not form a second phase during cooling. Therefore, it is not prone to ageing effects. To get the ideal properties for this type of alloy, a special rolling and heating procedure is applied. This procedure, as well as the formation, migration and annihilation of dislocations is the cause for a well defined microstructure, which is of high importance for the properties of the material.

Microstructure examination is often only possible with intricate and expensive methods. Nevertheless, fundamental knowledge of the microstructure of a material for the simulation of large-scale industrial processes, especially in aluminum industry, is of utmost importance. An easier way of microstructure examination would possibly be enabled by dilatometry, which is the measurement of length changes with changing temperature. During heating, irreversible length changes in a dilatometry sample are often caused by a change in the microstructure of the sample. Length changes can be detected by dilatometry and the aim of this master thesis is to find a correlation between these irreversible length changes and already well- known restructuring processes considering microstructural changes. The microstructural changes can, e.g., be analysed and visualised by electron backscatter diffraction (EBSD). The results gained from dilatometry and EBSD can be very useful for finding parameters necessary for the development of above-mentioned models.

This master thesis was supervised by Prof. Sprengel from the Institute for Materials Physics at TU Graz and took place in close cooperation with the *Christian Doppler Laboratory for Design of high-performance alloys by thermomechanical processing* lead by Prof. Cecilia Poletti from the Institute of Materials Science, Joining and Forming of the TU Graz. The resulting parameters from the measurements of this thesis can be important starting points for the development of certain models which are aimed to be used for the computer simulation of entire production processes. With the assistance of finely adjusted models, the number of practical tests necessary for the implementation of new industrial processes may be reduced significantly, which will also result in cost reduction.

2 Basics

2.1 Basics of 5xxx aluminum alloys

The 5xxx alloys consist of aluminum with a variable portion of magnesium as an alloying element. Compared to most other alloying elements for aluminum, magnesium is, to some extent, soluble in aluminum even at room temperature. If the magnesium content is kept below a certain value, no precipitates are formed when cooled down after hot rolling. Aluminum alloys of the 5xxx series are therefore not age hardenable, the final materials properties are achieved only by a controlled deformation and a subsequent heat treatment.

Aluminum 5xxx alloys are therefore classified as work- hardenable alloys, with a moderate to high strength. Some of their beneficial properties are a good weldability, good corrosion resistance even in harsh environments and high strength in comparison to other non age hardenable alloys.

To refine the alloy properties, manganese is added in small portions. Nevertheless, the positive effect on the properties of the material by the addition of magnesium is more significant than by the addition of manganese.

Aluminum 5xxx alloys are used for shipbuilding, pressure vessels, in transportation and construction just to mention a few examples.

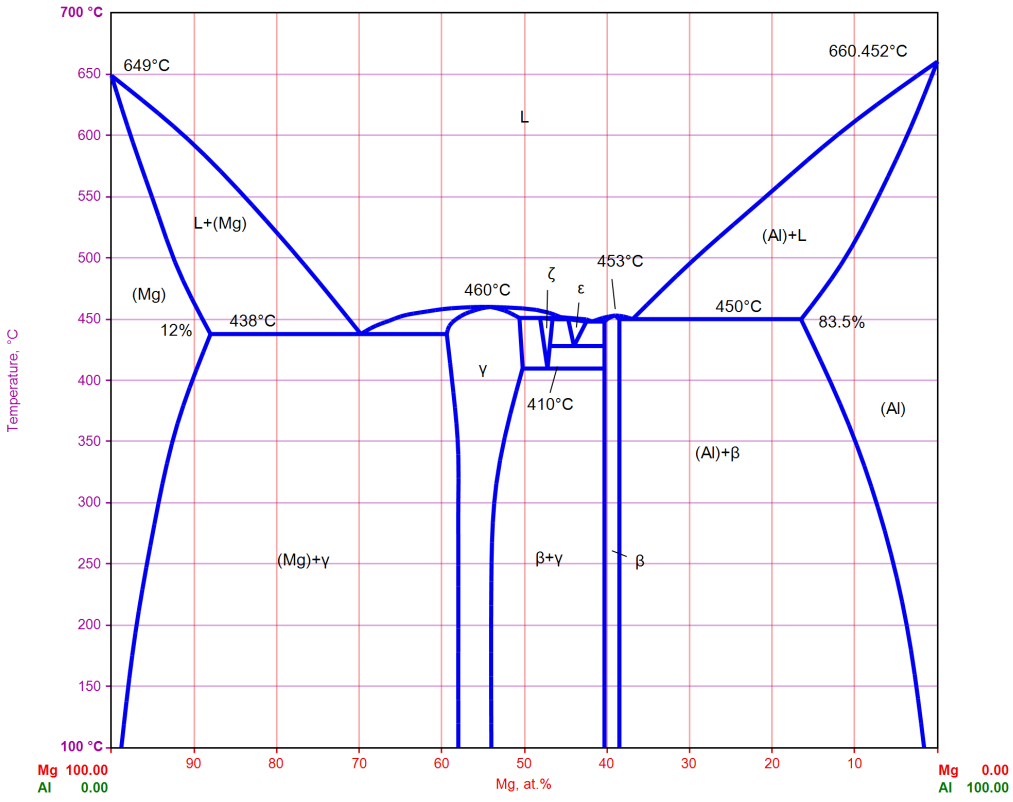

Figure 2.1.1: *Equilibrium phase diagram of the aluminum magnesium system [1]*

The material of concern for this master's thesis was a commercial aluminum 5754 alloy, with about 3 wt% magnesium.

2.2 Recrystallisation and Recovery

One important step during processing of metals is the forming step. Metals can be deformed hot or cold, nevertheless for both processes it is important to understand the underlying principles of motion and annealing of lattice defects built up during deformation.

In a single crystal, deformation cannot proceed along all directions, but only along certain planes, so-called slip planes, which are characteristic for each crystal structure. Each crystal lattice has a certain number of slip planes. In polycrystalline material deformation can occur in any direction due to the random orientation of its grains. Materials that crystallize in a lattice with a high number of slip planes, i.e., with fcc- structure, are usually better deformable than materials, that crystallize in a lattice with a lower number of slip planes.

During the deformation of a material, lattice defects like vacancies and dislocations are formed. The energy introduced during deformation is stored in these defects, which act like a barrier against further deformation. Nevertheless, a certain amount of these defects, depending on their ability to move in the matrix, will anneal out during the course of deformation as dynamic recovery. Moreover, vacancies usually move easier and faster than dislocations already at lower temperature. The number of defects remaining in the matrix will also be dependent on the material itself as well as on its purity. These remaining lattice defects can lead to recovery and/or recrystallisation during a second annealing step at elevated temperatures. Recovery and recrystallisation are two correlated and competing processes when it comes to consuming the energy stored in the material. A higher occurrence of the first can, e.g., lead to a hindrance for the latter. The basic principles and the similarities and differences of both processes will be discussed in the following paragraphs.

Recovery processes comprise rearrangement and/ or annealing of vacancies and dislocations. Recovery concerning dislocation motion occurs in five stages according to Fig. 2.2.2 [2]. During each stage, the amount of dislocations is subsequently reduced to release stored energy. In stage II, the accumulation of dislocations in certain regions lead to the formation of cells and the stored energy is released via the formation of low- angle grain boundaries (LAGB). In stage III, dislocations of opposite signs within these cells annihilate or migrate to the previously formed LAGB. For the annihilation of dislocations, their migration is necessary. Dislocations residing on the same glide plane (A and B) may annihilate by gliding towards each other, while the annihilation of dislocations residing on different glide planes (C and D) requires preceding climbing steps (Fig.2.2.1). The latter have a higher activation energy and can therefore only proceed at higher temperatures in comparison to the first, which occurs even at room temperature for many materials.
Further annihilation and rearrangement of dislocations in the cell walls lead to the formation of sub grains with pronounced LAGB. To reduce the amount of stored energy, the rearrangement of triple point junctions, which are the locations where three LAGB meet, to form junctions with angles of 120° is also highly favored.
Since the energy stored in LAGB is proportional to the radius of the sub grain, they include, sub grain growth can lead to a further release of energy in stage V. [2].

The onset of recovery is dependent on the ability of dislocations to move, which is, as mentioned above, dependent on different factors. First, the material itself plays an important role. In materials, with a high stacking fault energy, it is easy for dislocations to glide and climb, therefore recovery can start at lower temperatures. In materials with a low stacking fault energy, the movement of dislocations is less favorable, recovery starts at higher temperatures and other processes like twinning or recrystallisation at higher temperatures may occur. Moreover, solute atoms or fine dispersoids of another phase may hinder the movement of dislocations and therefore increase the temperature, at which recovery starts.

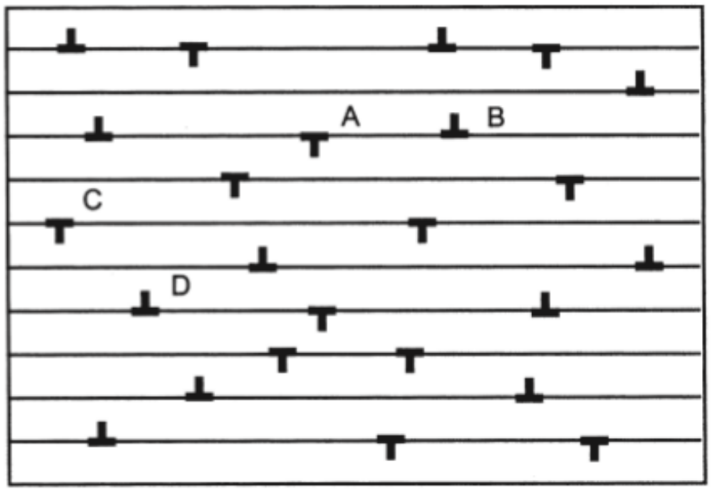

Figure 2.2.1: *Dislocation residing on different slip planes. A and B need one preceding gliding step to annihilate, while C and D, C and B or D and A need two preceding processes to annihilate: glide and climb [2]*

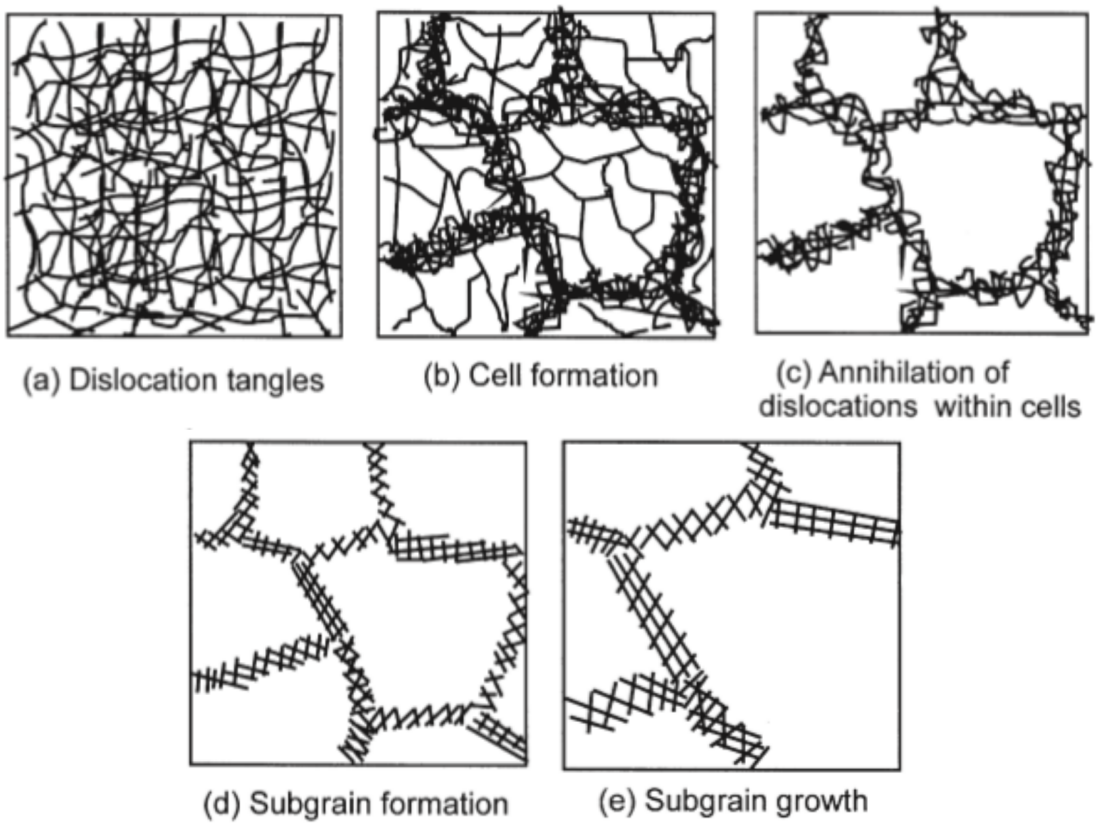

Figure 2.2.2: *Five stages of recovery: Tangles of dislocation arrange and annihilate to form cells with regions of lower and higher dislocation density (a and b) with subsequent further annihilation of dislocations within these cells (c). Rearrangement and annihilation of dislocations within low angle boundaries lead to subgrains with distinct boundaries (d) which can increase in size under the right conditions (e) [2]*

Recrystallisation is a microstructural transformation subsequent to recovery and occurs in two regimes: Nuceleation and Growth. A nucleus can be defined as a newly formed crystallite of low energy, separated from other deformed or previously recovered regions via high angle grain boundaries (HAGB). Nucleation is a complex process as the nucleation rate is dependent on different factors like temperature, introduced strain and previously occured recovery and may not even remain constant during the course of recrystallisation. [2].
Following nucleation is the growth of the newly formed crystallites. The growth rate of the crystallites $\dot{\mathrm{R}}$, i.e., the change of the radius R of the curvature over time, which equals the velocity v_b of HAGBs is given by the boundary mobility M times the driving pressure P_d (2.1).

$$v_b = \dot{R} = MP_d \tag{2.1}$$

$$P_d = E_D = \alpha\rho G b^2 \tag{2.2}$$

The driving pressure P_d in a deformed material is the stored energy E_D, which is given by equation 2.2 (with the shear modulus G, dislocation density ρ, a factor $\alpha \sim 0.5$ and the Burger's vector b).

Opposing the driving pressure there are retarding forces P_c, resulting from a gain in surface energy (2.3, γ_b = specific energy of the HAGB, R = radius of the curvature of the grain) that may even prevent growth in small grains ($< 1\,\mu m$) or from the pinning of the moving HAGB by solutes or second phase particles.

$$P_c = \frac{2\gamma_b}{R} \tag{2.3}$$

The driving pressure P_d itself may also be lowered by preceding recovery and therefore recovery can retard or even prevent recrystallisation. Recrystallisation behavior overall is dependent on following parameters:

- amount of deformation
- temperature during deformation
- annealing temperature
- annealing time
- initial grain size
- heating rate
- concentration of solutes and second phases

For recrystallisation to occur, there is a minimum amount of strain, usually around a true strain of $\varepsilon = 0.01$ to 0.03, that has to be introduced to the material. The higher the amount of deformation, the higher the energy stored in the material, which results in a lower onset temperature for recrystallisation. Moreover, a higher deformation will lead to more nucleation sites at which new crystallites form and therefore, the final grain size of the material after recrystallisation will be smaller.
The temperature during deformation is also important, since a higher temperature will increase the rate of recovery during the deformation process which will result in a reduced amount of stored energy after deformation and as mentioned above, this stored energy is necessary for recrystallisation. If the temperature during deformation is high enough, even recrystallisation may occur (dynamic recrystallisation).

Annealing temperature and annealing time are no independent parameters. A higher annealing temperature leads to an earlier onset of recrystallisation, since nucleation proceeds faster. Therefore, the annealing time to get a fully recrystallised material is overall longer at lower annealing temperatures. A higher annealing temperature will also lead to more nucleation sites and subsequently to a smaller grain size of the recrystallized material.
Since HAGB are possible nucleation sites, the initial grain size of the starting material also effects recrystallisation. A material with larger initial grains has a lower area fraction of HAGB and therefore provides less possible nucleation sites. When annealing two samples with different initial grain sizes at the same temperature, both deformed with the same strain, the onset of recrystallisation will be later in the sample with a larger initial grain size.

Heating rates up to the annealing temperature may also affect the recrystallisation behavior, since a lower heating rate leaves more time for recovery to consume stored energy at lower temperatures which will affect later recrystallisation.

Solutes and a second phase also have an influence on recrystallisation. The movement of grain boundaries, which is crucial for recrystallisation to occur is hindered by solute hetero atoms and finely dispersed particles due to Zener pinning. However, larger particles can act as possible nucelation sites during recrystallisation due to particle stimulated nucleation (PSN). Nuclei for recrystallisation are believed to form preferentially at the interface between the matrix and the particle or in zones of heterogeneous deformation closely around the particles [2].

Figure 2.2.3 shortly sums up a few relations considering recrystallisation.

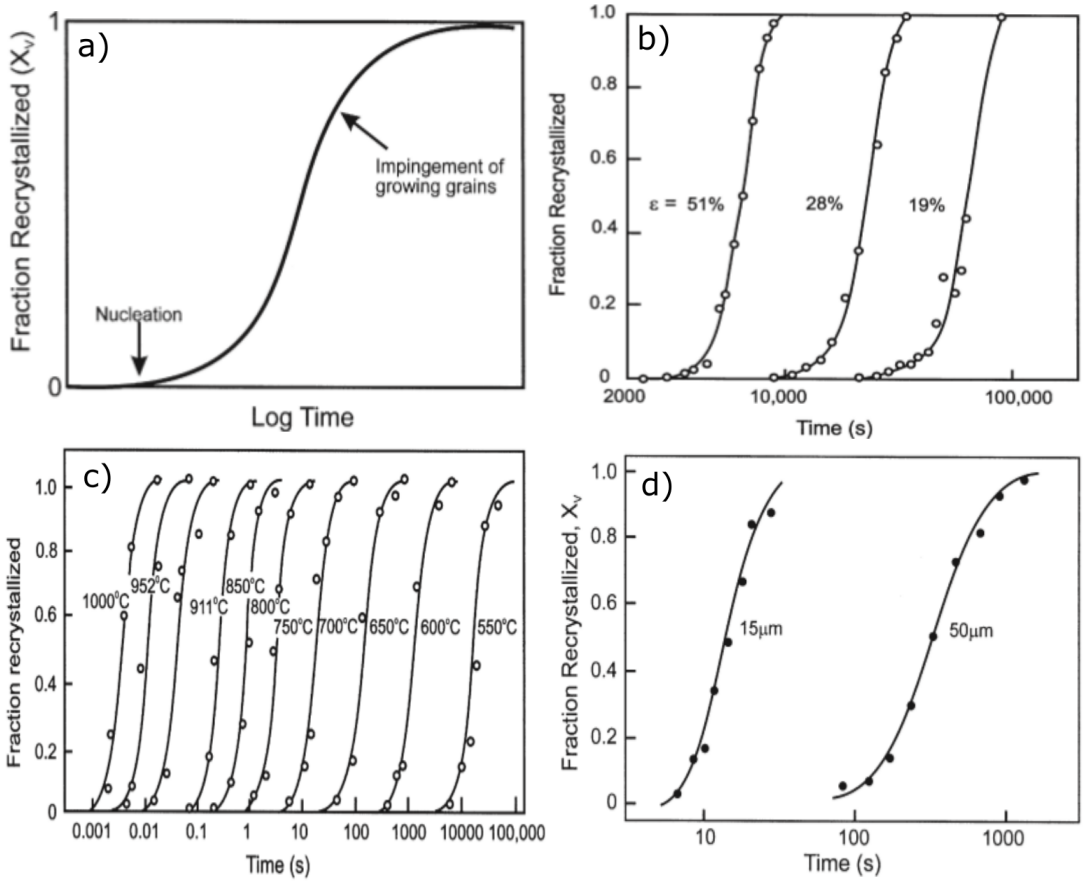

Figure 2.2.3: *a) Overview over the process of recrystallisation: After some time t_N, nucleation of new crystallites starts and recrystallisation can proceed. When comparing the recrystallisation behaviour of different materials or at different conditions, usually, the value t_{50} is taken, which is the time, after that 50% of recrystallisation has occured.*
b) When annealing samples of the same material, deformed with a different strain at the same temperature, a higher grade of deformation will result in an earlier onset of recrystallisation. However, the overall time for recrystallisation to proceed will remain the same.
c) When annealing samples of the same material and deformed with the same amount of strain at different temperatures, a higher anneling temperature will result in an earlier onset of recrystallisation.
d) When annealing two samples with the same amount of deformation at the same temperature, the one with the lower initial grain size will start to recrystallise first. This is due to the fact, that in a material with a lower initial grain size, there is a higher density of grain boundaries at which nucleation can start. This will result in a smaller grain size in the recrystallized material too, due to a higher number of nuclei that form during nucleation. [2]

3 Experimental Methods

3.1 Difference Dilatometry

Dilatometry is the measurement of the length change of a material when heated or cooled. The dilatometer used for this master's thesis was a commercial *LINSEIS DIL L75/264VX* differential push- rod dilatometer. Differential measurement means, that two samples can be measured simultaneously, which makes it possible to measure any sample against a reference sample under the exact same conditions. In the present case the deformed sample was measured together with a well- recrystallized sample of the same material as reference.

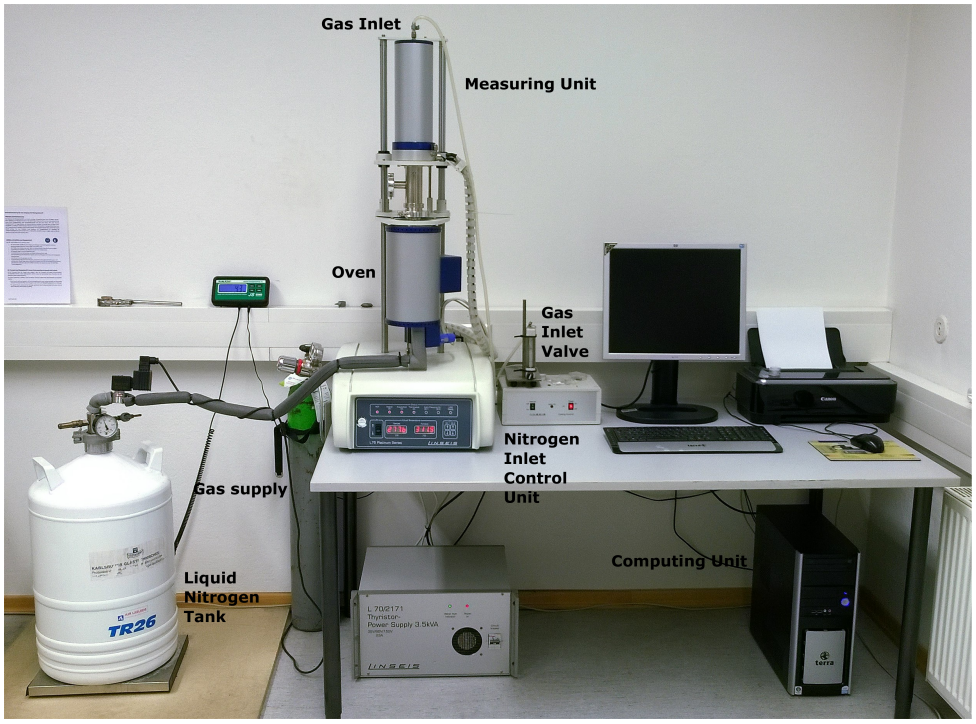

Figure 3.1.1: *LINSEIS DIL L75/264VX Differential Push Rod Dilatometer - setup*

Figure 3.1.1 shows a full view of the *LINSEIS DIL L75/264VX* dilatometer with a liquid nitrogen Dewar vessel for cooling and an argon gas supply for measurements in an inert gas atmosphere, as well as the nitrogen inlet control unit, the gas valve and the actual dilatometer with oven and measuring unit. Cold nitrogen gas is used for the cooling steps and a maximum cooling rate of $30\,\mathrm{K\,min^{-1}}$ can be achieved. All measurements can be performed under inert gas and in the case of this master's thesis, argon gas of 5N purity was used for all measurements.

A more detailed view of the dilatometer is shown in Fig. 3.1.2 with the armature (left image), the sample holder (central image) and push rods with the thermocouple (right image).

The *LINSEIS DIL L75/264VX* dilatometer uses a LVDT detector for the length change measurement, a schematic view of the measuring unit with two samples is shown in figure 3.1.3. The push rods apply a certain defined force (mN range) at the samples that remains constant during the measurement. Each change in length is detected by the LVDT detector of which a schematic view is given in figure 3.1.4.

A LVDT detector consists of one primary field coil and one secondary field coil parallel to it at each side. At the center of the three coils, a loose soft- iron core is placed which is

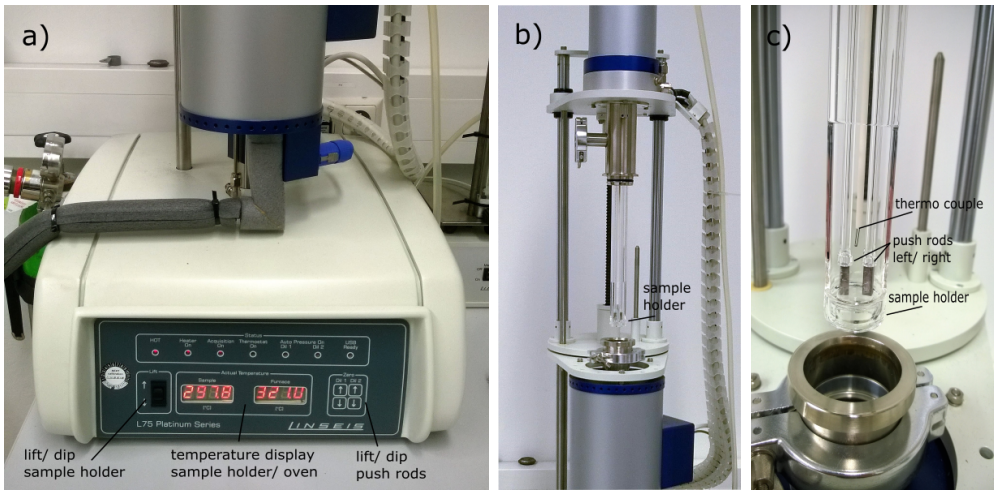

Figure 3.1.2: *LINSEIS DIL L75/264VX. a) service console. b) sample holder. c) sample holder with mounted samples*

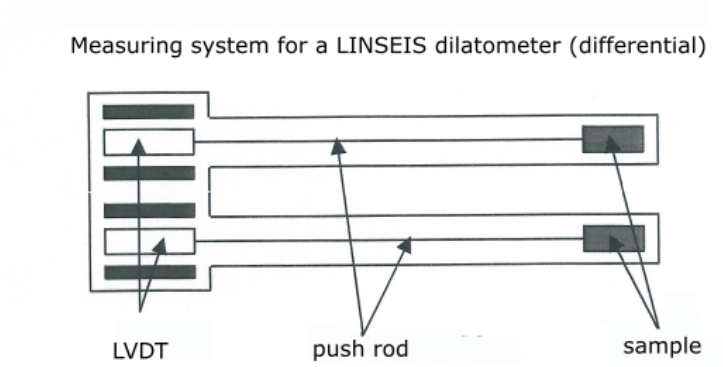

Figure 3.1.3: *Schematic view of the measuring unit inside the apparatus in vertical position [3]*

connected to one push rod each. At the primary field coil (A) an AC voltage with constant amplitude and frequency is applied which induces a current in the two secondary coils (B) via the soft- iron core. If the soft- iron core is in the middle position, the induced currents in the secondary coils compensate each other. If the push rod is moved due to an expansion of the sample, a voltage between the two secondary coils is formed which is proportional to the movement of the soft- iron core.

Figure 3.1.5 shows a more detailed description of the measuring system of the *LINSEIS DIL L75/264VX* dilatometer. The main part of the construction are two motors and two LVDT sensor units. The zero-point motor is responsible for the zero-point adjustment when placing a sample into the sample holder. During zero point adjustment, the push rods are pressed against the top surface of the sample with a certain pressure. This pressure remains constant during the whole measurement, which is assured by the load control motor and the load control LVDT sensor. The load control detector detects deviations from the set contact pressure that occur due to thermal expansions or contraction of the sample which is then corrected by the load control motor. The absolute movement of the rod is then detected by the measurement LVDT detector.

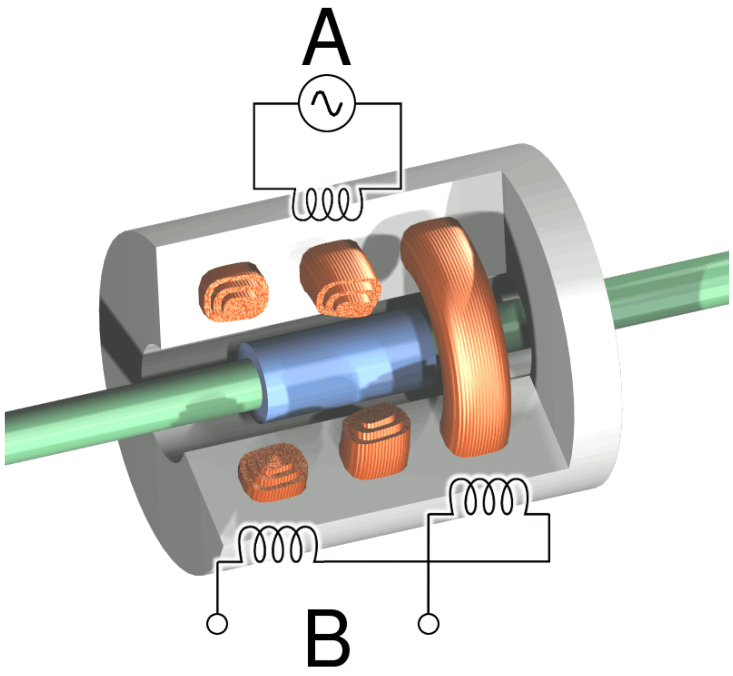

Figure 3.1.4: *Detailed view of an LVDT detector [4]*

The most important specifications of the dilatometer as given by the manufacturer are summed up in table 3.1.1.

Table 3.1.1: *Specifications of the dilatometer as given by the manufacturer*

Temperature range	$-150\,°C$ to $500\,°C$
Range of heating rates	0.1 to $50\,K\,min^{-1}$
measurement range	$\pm$ 25 to 2500 µm
max. vacuum	10^{-5} mbar
resolution	$\pm$ 0.125 nm/digit
accuracy	$\pm$ 1 % full scale
reproducibility	$\pm$ 150 nm

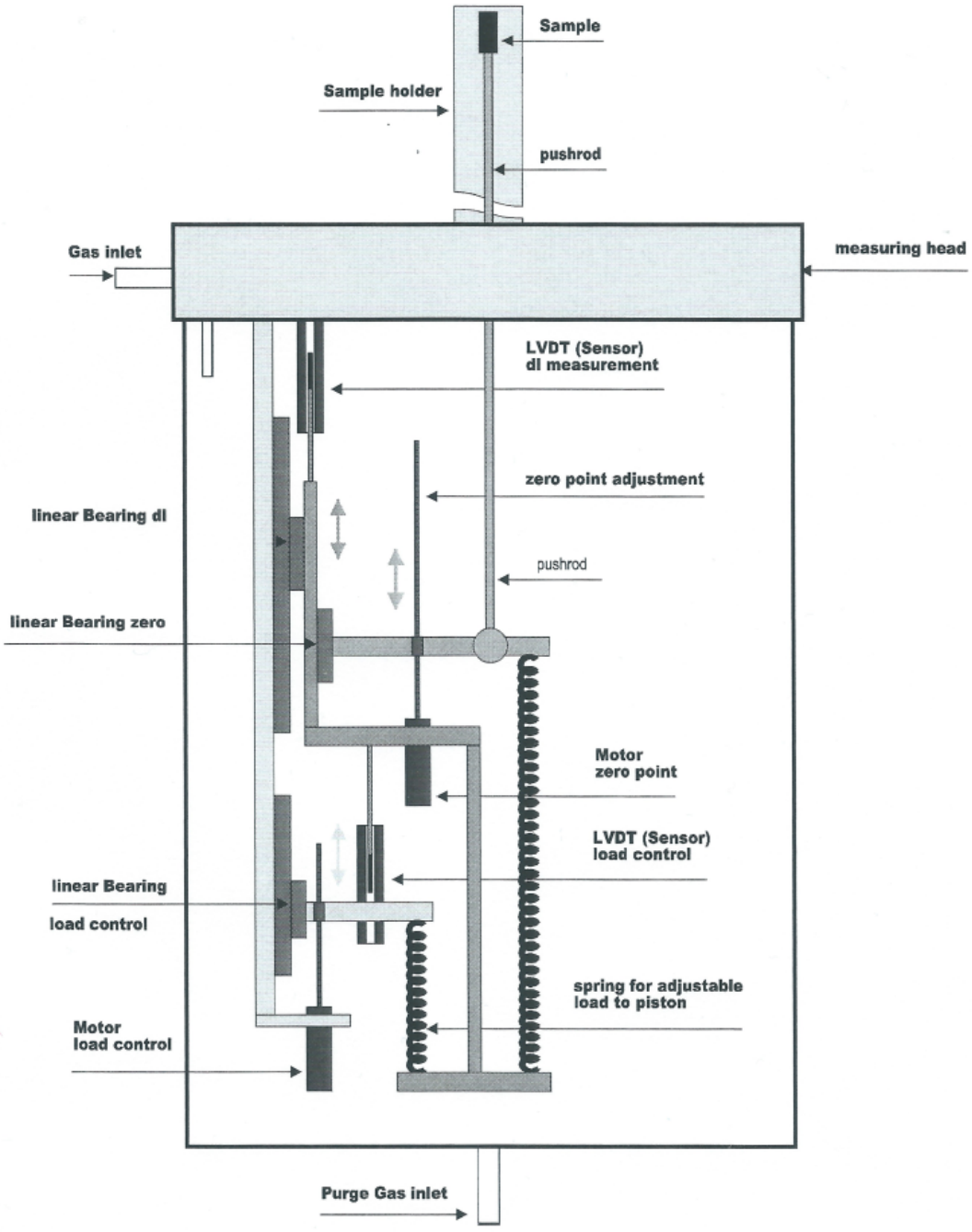

Figure 3.1.5: *Detailed description of the measuring system for one pushrod. Please note that this schematic is turned upside- down compared to the dilatometer used in this thesis. [3]*

3.1.1 Data Evaluation

This subsection will give an insight in how the measurement data was treated, before being evaluated. The evaluation of the data was performed by *QtiPlot*, a software designed for plotting and data evaluation. From the dilatometric measurements, two curves were obtained for the absolute length change, one for the reference, one for the sample. From the absolute length change curves, the relative length change curves are obtained by normalizing to the length of each sample ($^{\Delta L}/_{L_0}$) and then, the relative difference length change curves were calculated by substracting the reference curves from the sample curves. The resulting difference relative length change curves were then all set to zero at 30 °C for all measurements, i.e., $^{\Delta L}/_{L_{0(30\,°C)}} \equiv 0$.
The data was further treated by linear interpolation of the curves to 100 data points and by smoothing of the resulting curves with a *Moving Window Average* command. The *Moving Window Average* performs a smoothing according to function 3.1. The value n was set to 5 for the treatment of measurements with a heating rate of 1.5 K min^{-1} or faster and was set to 10 for the treatment of measurements with a lower heating rate.

$$z_i = \frac{1}{n} \sum_{j=i-\frac{n}{2}}^{j+\frac{n}{2}} y_i \tag{3.1}$$

The smoothed curves were then differentiated, where the calculation of the derivative was done by centered finite differences. All the dilatometric and derivative curves shown in this thesis were treated in a manner as described above. The evaluation of peak position and peak width was done by a Gaussain fit (Fig. 3.1.6). A good description on how *QtiPlot* works can be found in [5].

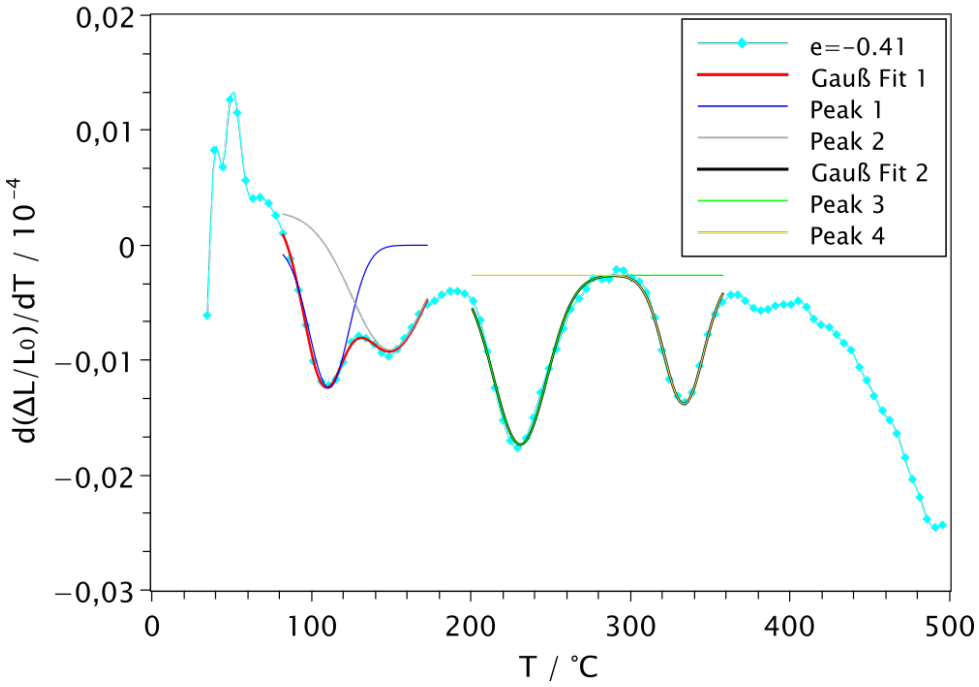

Figure 3.1.6: *Examplary derivative curve as received by data treatment in a manner mentioned above with a Gaussian fits to evaluate peak positions and peak widths.*

Table 3.1.2: *Correction factors as determined in the Bachelor thesis of K. Unger. [6] HR = heating rate, T_{corr} = correction value that has to be substracted from the measured temperature to obtain the actual temperature of the samples*

HR / $\mathrm{K\,min^{-1}}$	T_{corr} / K
0.75	0.7
1.5	1.4
4	3.8
6	5.7

Temperature correction Since samples are not heated directly, but instead by an oven, the measured temperature does not represent the real temperature of the sample. Therefore, the evaluated temperatures of interest had to be corrected by a certain value as the real temperature of the sample is always lower than the measured temperature. The necessary correction factors for the dilatometer as a function of the heating rate had been evaluated by K. Unger in the course of a Bachelor thesis and are shown in table 3.1.2.

3.1.2 Kissinger Analysis

A Kissinger plot as used in the course of this thesis is a logarithmic plot of the heating rate divided by the square of the peak temperature of the reaction/ process ($\frac{HR}{T_p^2}$) against the reciprocal peak temperature (Fig. 6.1.1), which represents the temperature at which the reaction rate ($\frac{dx}{dt}$) of the process is at maximum.

The activation energy E_A is calculated from the slope k of the linear fit considering relation 3.2.

$$k = \frac{E_a}{R} \tag{3.2}$$

This correlation can be derived as follows:
The rate of a reaction of n^{th} order is given by following equation, where x is the fraction of substance reacted, E_A is the activation energy of the process, R is the gas constant, T the reaction temperature and A a reaction dependent factor. This equation is also true, if the temperature is a function of time ($T(t)$).

$$\frac{dx}{dt} = A(1-x)^n e^{\frac{E_A}{RT}} \tag{3.3}$$

Differentiation of 3.3 leads to Eq. 3.4, where Φ is the heating rate.

$$\frac{d}{dt}\left(\frac{dx}{dt}\right) = \frac{dx}{dt}\left(\frac{E_A\Phi}{RT^2} - An(1-x)^{n-1}e^{\frac{E_A}{RT}}\right) \tag{3.4}$$

The reaction rate $\frac{dx}{dt}$ is at maximum, when the derivative (Eq. 3.4) equals zero, which leads to Eq. 3.5, with T_P as the temperature of maximum deflection and with the heating rate, HR, as $\Phi = \frac{dT}{dt}$.

$$\frac{E_A\Phi}{RT_P^2} = An(1-x)^{n-1}e^{\frac{E_A}{RT_P}} \tag{3.5}$$

Eq. 3.5 can be rewritten into Eq. 3.6 or Eq. 3.7

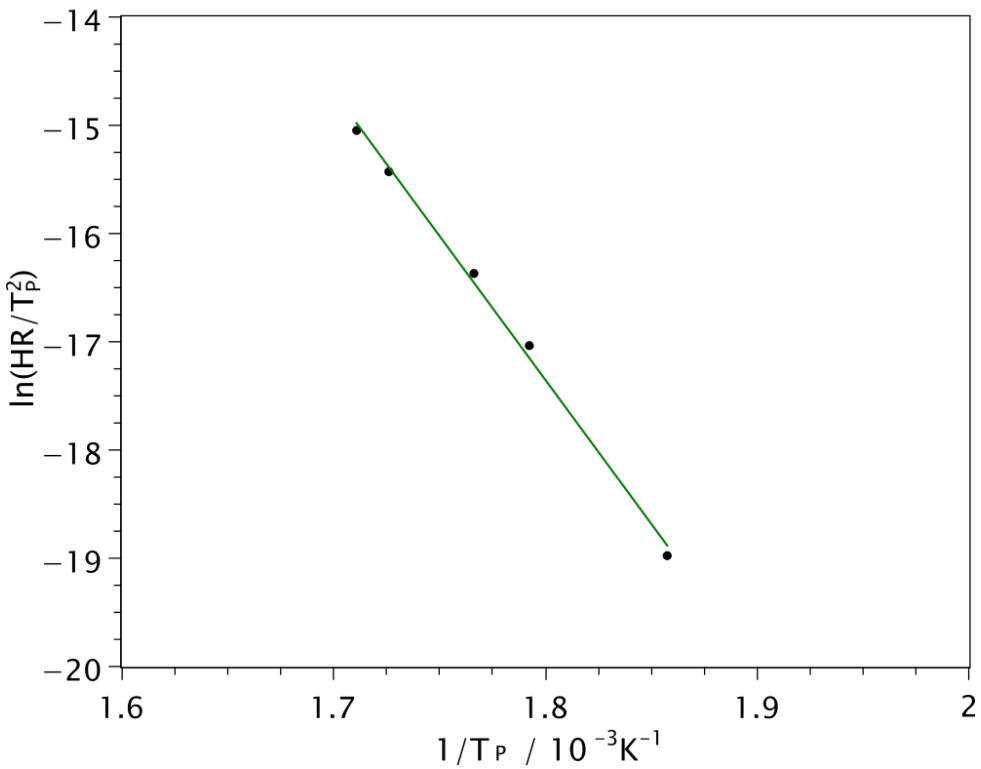

Figure 3.1.7: *Kissinger plot: Heating rates divided by the square of the peak temperatures are logarithmically plotted against different reciprocal peak temperatures obtained from measurements with different heating rates for samples with a deformation of* $\varepsilon = -0.61$ *to calculate the activation energy of the recrystallisation process.*

$$ln\left(\frac{\Phi}{T_P^2}\right) = -\frac{E_A}{R} * \frac{1}{T_P} + \left(ln(An(1-x)^{n-1}) - ln\left(\frac{E_A}{R}\right)\right) \tag{3.6}$$

$$ln\left(\frac{\Phi}{T_P^2}\right) = -\frac{E_A}{R} * \frac{1}{T_P} + C \tag{3.7}$$

When plotting $ln\left(\frac{\Phi}{T_P^2}\right)$ against $\frac{1}{T_P}$, the activation energy E_A of a thermally activated process is therefore given by the negative slope of the plot times the gas constant, as can be seen from Eq. 3.7 and was used as in Eq. 3.2 to calculate the activation energies of two different processes observed in this thesis.

3.2 Optical Microscopy

Most of the images taken for this thesis were done using polarized light microscopy and therefore, this section will focus on the details of this type of microscopy. The microscope used during the course of this thesis was a *Zeiss Axio Observer z1m.*

As one may expect, polarised light is used to make features visible, which cannot be detected with usual microscopy techniques. Polarised light is generated by a polarisation

filter, that only let pass light of a certain orientation. When passing an anisotropic material, birefringence occurs, the polarised light is refracted into two waves orthogonal in orientation. The projection of these two waves results in a wave orthogonal to the incident polarised light wave with a lower amplitude, which can pass a second filter orthogonal in orientation to the first one. Therefore, only anisotropic material can be seen bright in a polarised light microscope [7].

Aluminium is an isotropic material with cubic symmetry. However, when treating the surface of a polished aluminium sample with Weck's reagent [8], an orientated MnO_2 layer forms upon the surface by replacement according to the reaction given below in Eq. 3.8 [9]. MnO_2 is an anisotropic material and can therefore be seen in polarized light.

$$\mathrm{Al(s) + MnO_4{-}(aq) + 2\,H_2O \longrightarrow Al(OH)_4{-}(aq) + MnO_2(s)} \tag{3.8}$$

The intensity of the refracted light is dependent on the angle between the optical axis of the examined material and the polarisation of the light wave passing through. There is maximum intensity at 45°, and extinction at 0°.

Birefringence also results in a phase shift between the two refracted waves, since one wave can pass the material faster. Due to this shift, dependent on the wavelength of the incoming light wave, constructive of destructive interference occurs. Since a poly chromatic light source is used, certain colors are suppressed and certain colors are enhanced. The magnitude of the phase shift is dependent on the thickness of the sample layer and therefore sample layers of different thickness may appear in different colors. Reference [10] suggests, that the thickness of the deposited MnO_2 layer is dependent on the composition of the material it replaces. Therefore, different phases within a material can be visualized with this technique too.

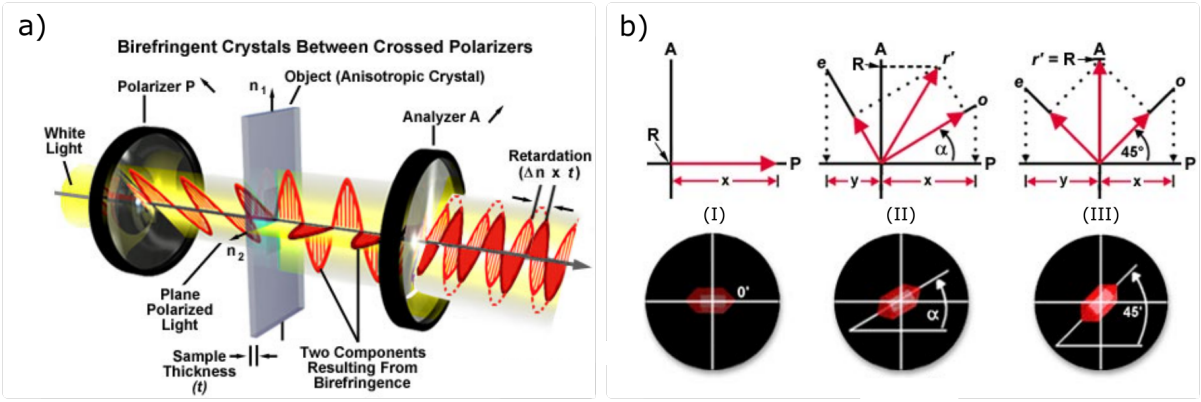

Figure 3.2.1: *Schematic view of a polarized light microscope (transmission microscope) (a). Behaviour of polarised light when crossing a birefringent sample (b): Extinction is reached when the optical axis of the material is parallel or* 90° *to the orientation of the incoming polarised light (I). Maximum intensity is reached, when the optical axis is oriented* ±45° *or* ±135° *to the orientation of the incoming polarised light (III). In between, the intensity of the light is lower (II) [11]. Similar principles are valid for reflection.*

3.3 Electron Backscatter Diffraction (EBSD)

EBSD is a technique to determine the crystal orientation at a certain point in a sample. EBSD measurements are performed by a scanning electron microscope, but unlike in SEM mode, the sample is tilted by 70°. When the incident electron hits the surface of a crystalline sample, it gets diffracted by the lattice plane of the crystal which results in Kikuchi- patterns (Fig.3.3.1). Different patterns are characteristic for different crystal orientations relative to the incident beam which makes it possible to identify the orientaion of different grains in a polycrystalline material. However, the composition of the material has to be known and the resolution limit is about 30 nm. The measured Kikuchi patterns are then compared with databases and deviations from the original patterns can be distinguished. Therefore, it is also possible to measure misorientation, which is caused by strain, to some extent [12].

The electron microscope used for the EBSD measurements during the course of this thesis was a *Tescan MIRA3*.

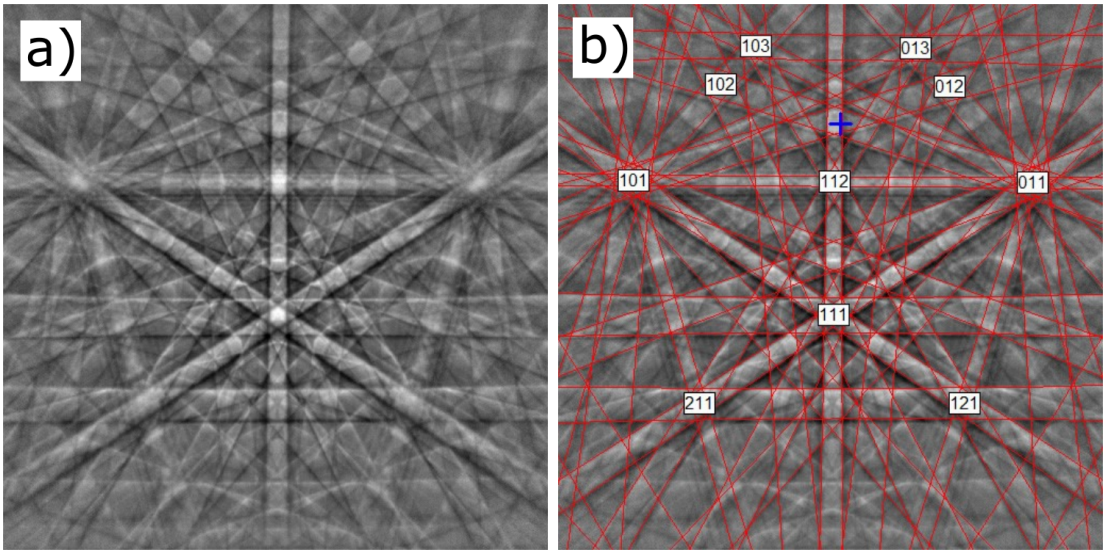

Figure 3.3.1: *Example for Kikuchi patterns (a) with assigned lattice planes (b) [13]*

Data Cleanup Before the evaluation of the data, a cleanup of the data has to be performed. This cleanup has to be performed with care, since it changes the data set, nevertheless, it is necessary for the better interpretation of the data. Two subsequent cleanup steps were done. First, a grain confidence index (CI) standardisation with a grain tolerance angle of 12 and a minimum grain size of 5 was applied and then, a neighbor CI correlation with a minimum confidence index of 0.1, which was stopped after one iteration, was performed using the *TSL OIM Analysis 8* software package.
The first cleanup step changes the CI of all points within a grain to the maximum CI within this grain. The grain boundary (GB) is defined as an area with a misorientaion larger than the grain tolerance angle. In the second cleanup step, CIs with a value below the set minimum are changed to the CI of the neighbor point with the highest CI.

Inverse Pole Figure (IPF) Images To show different grains within the sample, IPF images can be made, which show the crystal orientation of each grain. Grain boundaries and sub grain boundaries can be shown as well, if required. When changing the grain tolerance angle of the data set to 2°, sub grains within the sample can be shown. A minimum CI can be set in the data set, which was 0.6 for all evaluations of this thesis, to exclude regions with a low CI and to prevent making conclusion from too little information. To show either recrystallized or not recrystallized grains in an IPF map, a limit for the grain orientation spread (GOS) was set above (not recrystallized) or below (recrystallized) a value of 2°.

Grain Orientation Spread (GOS) and Grain Reference Orientation Deviation (GROD) Maps are two methods to show misorientaion in the sample, which are very similar. A GROD map shows the deviation in angle of each point in a grain from the mean orientation of the grain. In a GOS map, the average of these misorientations within a grain is shown.

Kernel Average Misorientation (KAM) The KAM is the average of the misorientation between the center of a kernel and the perimeter. An option to average the misorientation between the center and all points within this kernel is possible but was not performed for the evaluation in this thesis. The kernel is user- specified, for this thesis, the first nearest neighbor was considered. The KAM can be displayed either in maps or charts.

Grain Size (GS) and Sub Grain Size (SGS) To show the GS in a chart, the grain tolerance angle of the data set was set to 12°, when showing the SGS, it was set to 2°.

3.4 Differential Scanning Calorimetry (DSC)

DSC is the measurement of the change in heat flow of a sample during linear heating in comparison to an inert reference sample. Each thermally activated process that consumes or releases energy can be detected by DSC. There are two main types of DSC: heat- flux and power compensation DSC.

In heat- flux DSC , a sample and an inert reference are heated in a common furnace with a linear heating rate up to a certain temperature. Sample and reference are physically connected via a thermal conductible bridge, so if a thermally activated process occurs in the sample, heat is allowed to flow from the sample to the reference or vice versa and a corresponding temperature change can be detected.

In power compensation DSC , sample and reference are heated with a well- defined heating rate in seperate furnaces. If a thermally activated process occurs in the sample, the heat flow to the sample is either increased or decreased to maintain the same temperature as the reference, compensating the comsumption or release of energy caused by an endothermic or exothermic process. This change in heat flow is then recorded [14].

With both methods, the total heat generated or consumed during a thermally activated process, the heat capacity of the material as well as the temperature, at which the process

occurs, can be determined. To determine the latter, the same material has to be measured with at least three different heating rates, which will result in three different peak temperatures. With these different peak temperatures an extrapolation to a peak resulting from a theoretical heating rate of $0\,\mathrm{K\,min^{-1}}$ can be done to receive the temperature, at which this process occurs.

The DSC used for this thesis was a Netzsch STA 449F1 Jupiter, which is a heat- flux DSC.

4 Sample Preparation and Characterization

This chapter describes the preparation methods which were applied during the course of this thesis, as well as a few tests performed on the sample material to determine the necessary information about its properties.

The material was delivered by *Heck & Sevdic GbR* as a cold rolled, commercially pure AW 5754 aluminum sheet. To determine the exact composition of the material, samples were characterized using optical emission spectrometry. Table 4.0.1 shows the results of the analysis.

Table 4.0.1: *Results of the element analysis (in wt%) of the AW 5754 alloy used in this work. Bal.: Al; $\bar{c}$: concentration; s standard deviation.*

element	Mg	Fe	Si	Mn	Zn	Cu	Cr	Ti	Ni
$\bar{c}$	3,28	0,333	0,318	0,291	0,074	0,068	0,045	0,032	0,0083
s	0,036	0,0033	0,0041	0,0034	0,0068	0,0040	0,0001	0,0012	0,0002

For the deformation process, the sheet was cut into smaller cuboids of following dimensions: (10 x 10 x a) mm^3. [1] After deformation, the deformed cuboids were further cut into small bars with a base area of (3,5 x 3,5) mm^2 and a length of 8 to 12 mm. Figure 4.0.1 shows the orientation of the sample, where the original rolling direction as done in the production process is represented by x, the direction of deformation as applied in this work by y and the measurement direction using dilatometry by y or z, depending on the type of measurement.

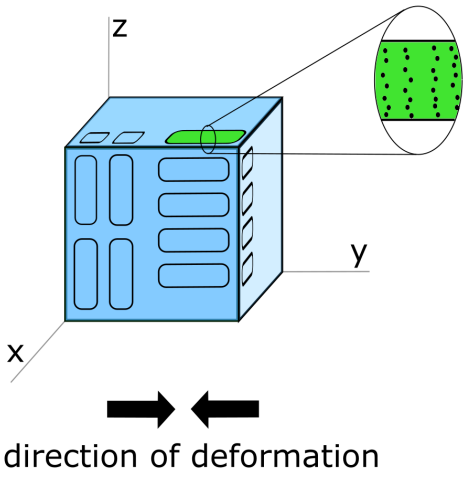

Figure 4.0.1: *Schematic view of the mentioned above cuboid to indicate the original rolling direction of the production process (x) and the direction of deformation as applied in this work (y). Please note, that due to the original rolling procedure in the production process, particles present in the material are aligned in x direction.*

[1] with 8 mm < a < 12 mm, depending on the subsequent grade of deformation

4.1 Preparation Methods

4.1.1 Deformation of the samples

Two methods were considered for the deformation of the aluminum samples.
The first method (G) was deformation using a *DSI Gleeble 3800 Hydrawedge*. The *DSI Gleeble 3800* is a machine capable of introducing deformation to samples by tension, compression or torsion at defined temperature and atmosphere (Fig. 4.1.1). The samples were cut into pieces of (10x10x15) mm^3 or (10x10x17) mm^3, depending on the grade of deformation and were put into the Gleeble. They were then deformed at a strain rate of $\dot{\varepsilon} = 0,1/s$.

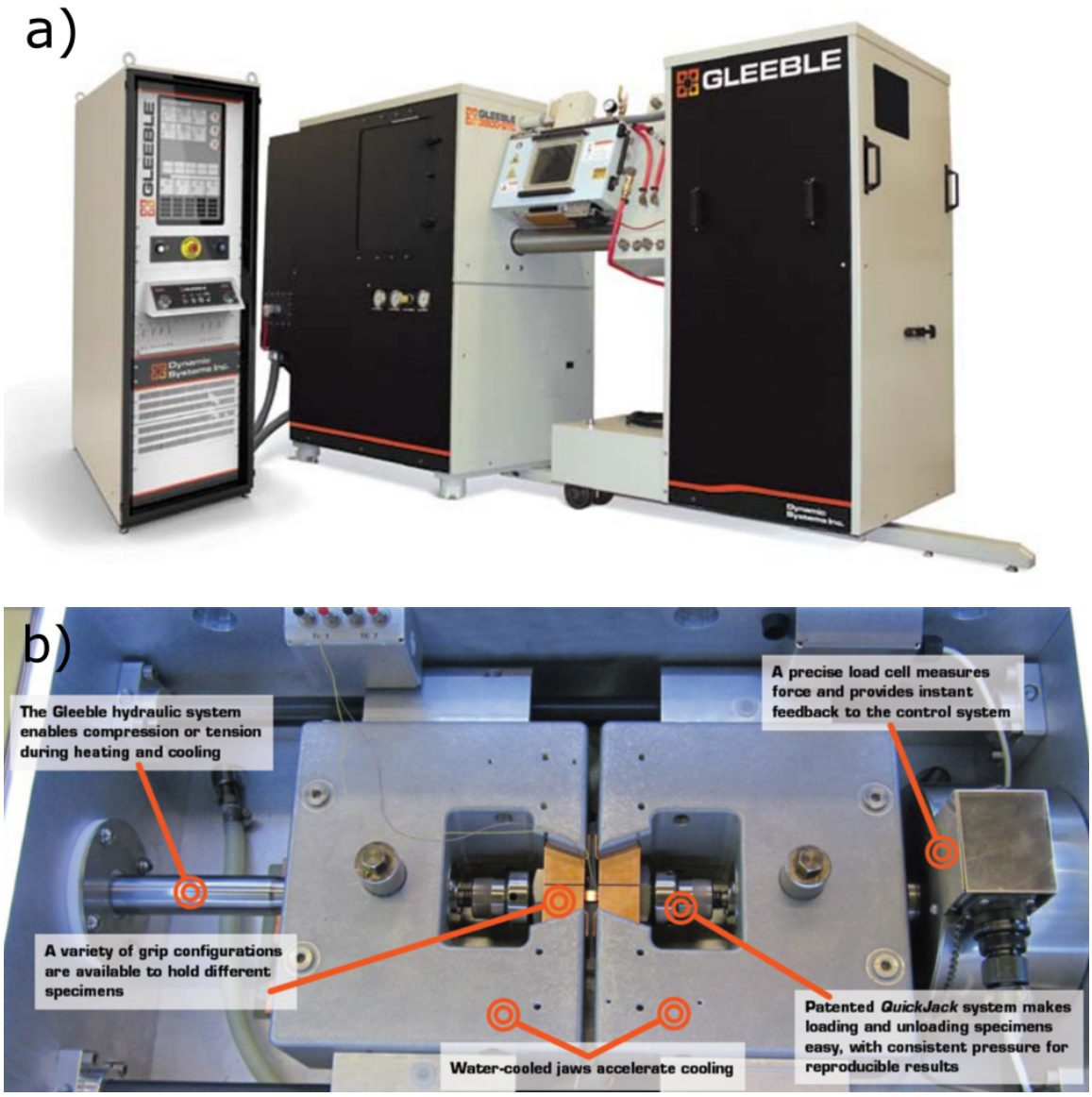

Figure 4.1.1: *a: Image of the DSI Gleeble 3800 Hydrowedge, b: more detailed view of the deformation chamber.[15]*

The second method (R) was deformation by a man powered cylindric roll as shown in

Fig. 4.1.2. With this method, the deformation had to be performed step wise, due to the fact that only little deformation per turn was possible. Moreover, after each rolling step, the sample was turned by 90° in the rolling plane to avoid bending of the sample and to obtain a similar mode of deformation as obtained by Gleeble.

In the following sections, these methods will be referred to as method G and R.

Figure 4.1.2: *Cylindric roll used for the deformation of the samples.*

4.1.2 Preparation for dilatometric measurements

As mentioned above, after deformation, samples were cut into small bars of (3.5 x 3.5 x a) mm^3. [2] as shown in Fig. 4.1.3. It should be mentioned, that the rods were cut from the center, since it has been verified, that the recrystallisation behaviour of the bulk center can be very different to that of the surface layers [16].

After cutting, the samples were ground at the edges to obtain a smooth, plane parallel surface, using the following method and apparatus (Fig. 4.1.3). The samples were glued in position using Uhu® superglue and ground until the surface of the bar was in plane with the brass inset of the apparatus. To grind the opposite surface of the bar, it was glued in at opposite position with the same plane as before to ensure a real plane parallelism of the two ground surfaces. After these steps, the bars were removed and ready for measurement in the dilatometer.

4.1.3 Preparation for Optical Microscopy

For the microscopy analysis, depending on the assignment of tasks, samples were taken before and after measurement in the dilatometer. The samples were embedded in a poly

[2] with 8 mm < a < 12 mm, depending on the grade of deformation

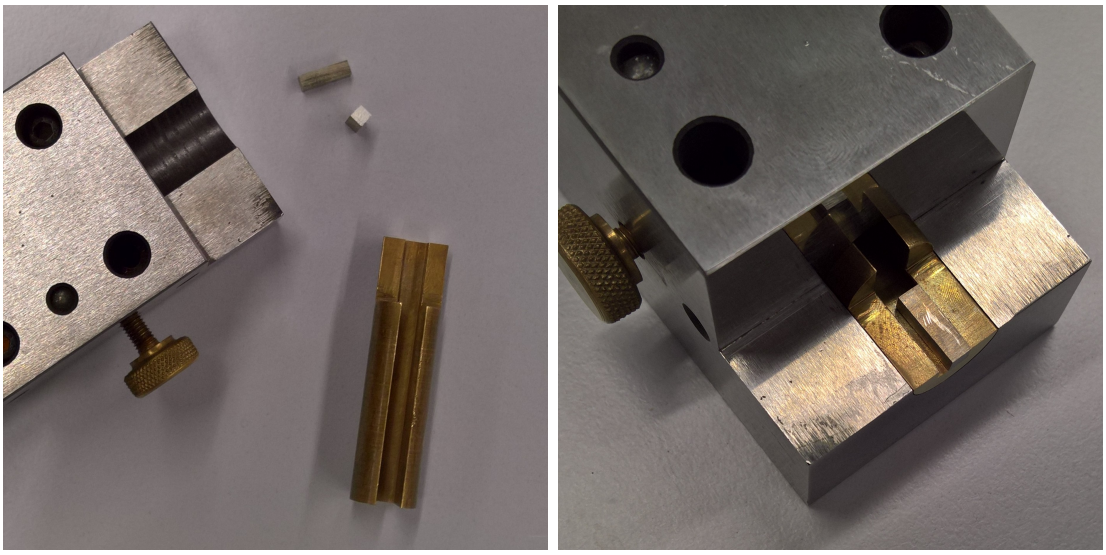

Figure 4.1.3: *Device used to prepare dilatometric samples with two parallel face sides as described in the text.*

acrylic resin and ground and polished with a Bühler grinding and polishing machine. Table 4.1.1 shows the subsequent grinding and polishing steps.

Table 4.1.1: *Grinding and Polishing steps*

Step	**1**	**2**	**3**	**4**	**5**	**6**	**7**	**8**	**9**	**10**
Grinding: Size / particles per cm^2	320	500	800	1200	2400	4000				
Polishing: Particle size / μm							9	3	1	0,01 (Chem)
Time / min	1	1	1,5	2	2	3	3	5	5	5

After polishing, the samples where washed with detergent and afterwards etched by Weck's etching solution [8]. Table 4.1.2 summarizes the etching procedure according to Ref. [17].

Table 4.1.2: *Etching Procedure*

	1^{st} etching step	**2^{nd} etching step**
etching solution	100 ml deionized water 2.8 g KOH	100 ml deionized water 4 g Potassium Permanganate after dissolution of $KMnO_4$: 1.4 g KOH
temperature	RT	RT
time	1 min	15 sec
procedure	dipping	dipping

The first etching step is used to remove dirt and part of the oxide layer as well as to refine the grain boundaries. During the second etching step, a layer of manganese oxide (pyrolusite) is deposited on to the polished and cleaned surface at the expense of aluminum, which can then be examined using polarized light.

After etching, the samples can be examined with an optical microscope with polarized light to distinguish different grains. As mentioned in section 3.2, not only different grains can be identified with polarized light microscopy, but also different phases and regions with a different concentration of alloying elements. However, if a second phase like a particle has a significantly more positive electrochemical potential than the matrix, only the latter will react with the etching reagent. Therefore, the manganese oxide layer covering a particle forms by replacing the surrounding matrix instead of the particle, which leads to a uniform layer over the course of a whole grain. Therefore, these kind of particles would be more difficult to detect, which can be both advantage and disadvantage at the same time. However, the case of particles that are possibly present in the material and how to make them visible will be discussed in a later section (see section 4.2.2).

It is also not possible to visualize sub grains and finer substructures with this method. When covering an highly disordered area with the manganese oxide layer, the resulting image under polarized light will not be as clear as the image of highly ordered areas. However, since a blurred image of the grain structure can be caused by many different factors (age of the etching solution, age of the components used to mix the etching solution, slight deviations in the polishing and grinding procedure for two different sample), this cannot be accounted as a reliable method to determine a possible disorder in a sample.
To get a more detailed view on a sample (e.g. disorder, dislocation density), EBSD measurements were performed for some selected samples . The sample preparation for an EBSD measurement will be discussed in the following section.

The technique mentioned above for sample preparation is the most commonly used in this thesis, so the term "prepared and etched" will be used in the following sections to describe a sample preparation according to this method. Any deviations from this practice will be mentioned.

4.1.4 Preparation for EBSD

For the EBSD measurements, the samples must have a very clean, flawless surface. To achieve this requirement the sample preparation procedure had to be modified. After the 1 µm polishing step, the samples were polished for half an hour with the chemical polishing agent (0.01 µm). The samples were then cleaned carefully with detergent and put into the vibropolishing machine for at least one hour with an acidic polishing solution. After cleaning with ethanol once again, the sample preparation for the EBSD measurements was finished.

4.1.5 Preparation for DSC

For the DSC measurements, samples of size (5 x 5 x 2.5) mm^3 were cut with one surface as smooth as possible.

4.2 Preliminary tests to determine the properties of the material

4.2.1 Preparation of the initial, recrystallized state

The as- received material was an industrially cold- rolled AlMg3 (alloy AW5754) plate. Since the degree of deformation was unknown, the sample was deformed and recrystallized to get a well- defined initial state of the microstructure. The samples should have a defined maximum possible grain size and should be fully recrystallized with a minimum dislocation density. To find the optimal starting parameters to obtain that condition, samples were deformed with two different grades of deformation and annealed for different time periods. The aim was to identify which grade of deformation results in the largest possible grains, the time after that recrystallisation is complete, and if and to which extent grain growth occurs after recrystallisation.

The test series were performed on samples denoted by series **0** and **A**. Table 4.2.1 shows the initial lengths, strain, recrystallisation time and direction of deformation for each sample.

Table 4.2.1: *Parameters for series 0 and A with initial length (l_0), true strain (ε) and annealing time (t_a)*

Series	Sample	l_0 / mm	ε	t_a / h
0	0	12,2	-0,33	4
0	1	19,4	-0,14	4
0	2	20,1	-0,25	4
0	4	20,1	-0,39	4
A	I+1	17	-0,36	1
A	I+2	17,2	-0,32	1
A	I+3	17	-0,34	1

direction of deformation = x (parallel to the rolling direction of the production process)

Series	Sample	l_0 / mm	ε	t_a / h
A	III-3	15	-0,16	1
A	III-4	15	-0,17	1
A	III-5	14,9	-0,16	2
A	III-6	15	-0,17	4
A	IV-1	17,3	-0,70	4
A	IV-2	16,3	-0,34	1
A	IV-3	17,4	-0,35	2
A	IV-5	16,95	-0,35	2
A	IV-6	17,1	-0,35	4

direction of deformation = y (perpendicular to the rolling direction of the production process)

Deformation in x direction, that is parallel to the rolling direction of the production process, most often lead to a kink in the sample which would have resulted in an inhomogeneous distribution of strain in the sample. That would cause a broad grain size distribution in the recrystallized sample, which is relatively unwanted for reproducible measurements. Therefore, only the samples deformed in y- direction were examined further.

Samples were either deformed with $\varepsilon = -0,17$ or $\varepsilon = -0,35$ and then annealed at 500 °C for 1, 2 or 4 hours for each ε. The high deformation ($\varepsilon = -0,7$) of sample A IV-1 happened as an accident with the Gleeble Machine. Nevertheless, it was also examined with a maximum heating time of 4 hours to examine the recrystallization structure at a high and inhomogeneous deformation. After heating, the samples were cooled in air, cut in half in the xy - plane (Fig. 4.2.1) and prepared and etched for grain size analysis with an optical microscope.

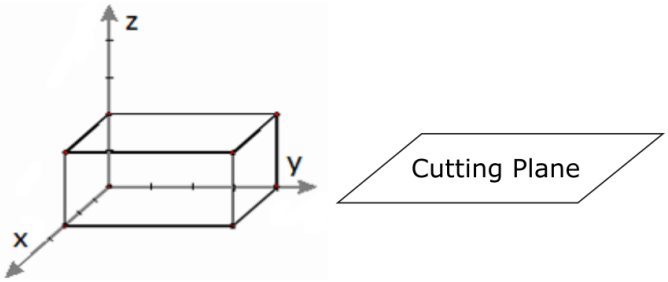

Figure 4.2.1: *Cutting plane for the sample series A III+IV for microstructure analysis by polarized light optical microscopy.*

Results: After preparation, the samples were examined in the microscope, pictures were taken and from the resulting images, the average grain size for each sample was determined using a counting procedure based on the number of grains per area according to [18]. Table 4.2.2 shows the grain sizes for each grade of deformation and annealing time.

Table 4.2.2: *Results of the grains size determination with annealing time (t_a), annealing temperature (T_a), true strain (ε) and grain size. Direction of deformation: y (except the as- received sample)*

sample	t_a / h	T_a / °C	ε	**grain size** / µm	micrograph
as received	0	no deform.	0	49,2± 1,8	Fig. 4.2.2 a)
A III- 3	1	500	-0.17	82,2 ± 3,5	Fig. 4.2.2 b)
A III- 4	1	500	-0.17	70,6± 8,2	Fig. 4.2.2 c)
A III- 5	2	500	-0.17	65,4±4,9	Fig. 4.2.2 d)
A III- 6	4	500	-0.17	72,2± 5,0	Fig. 4.2.2 e)
A IV-1	4	500	-0.7	not determinable	Fig. 4.2.3 a)
A IV-2	1	500	-0.35	41,2 ± 2,0	Fig. 4.2.3 b)
A IV-3	2	500	-0.35	35,8 ± 2,9	Fig. 4.2.3 c)
A IV-5	2	500	-0.35	35,6 ± 0,2	Fig. 4.2.3 d)
A IV-6	4	500	-0.35	34,6 ± 3,9	Fig. 4.2.3 e)

The results show, that the grain size of the as received sample is around 50 µm. A high deformation of $\varepsilon = -0,35$ and subsequent annealing at $T_a = 500\,°C$ for 1,2 and 4 hours leads to a mean average grain size of about 35 to 40 µm. A low deformation of $\varepsilon = -0,17$ and subsequent annealing leads to an average grain size of 65 to 70 µm . After one hour of annealing, for $\varepsilon = -0.17$, recrystallisation has started, but has not yet finished as figure 4.2.2 b) shows. After two hours, recrystallisation has finished and even after four hours no further grain growth seems to take place. For $\varepsilon = -0.35$, recrystallisation has finished after even one hour, when increasing the annealing time, no further grain growth occurs. Due to the results mentioned above, a treatment as done for sample A III-5 ($\varepsilon = -0.17$, $t_a = 2h$) was applied to all following samples before further preparation since it provides a well- recrystallized structure with grains as large as possible.

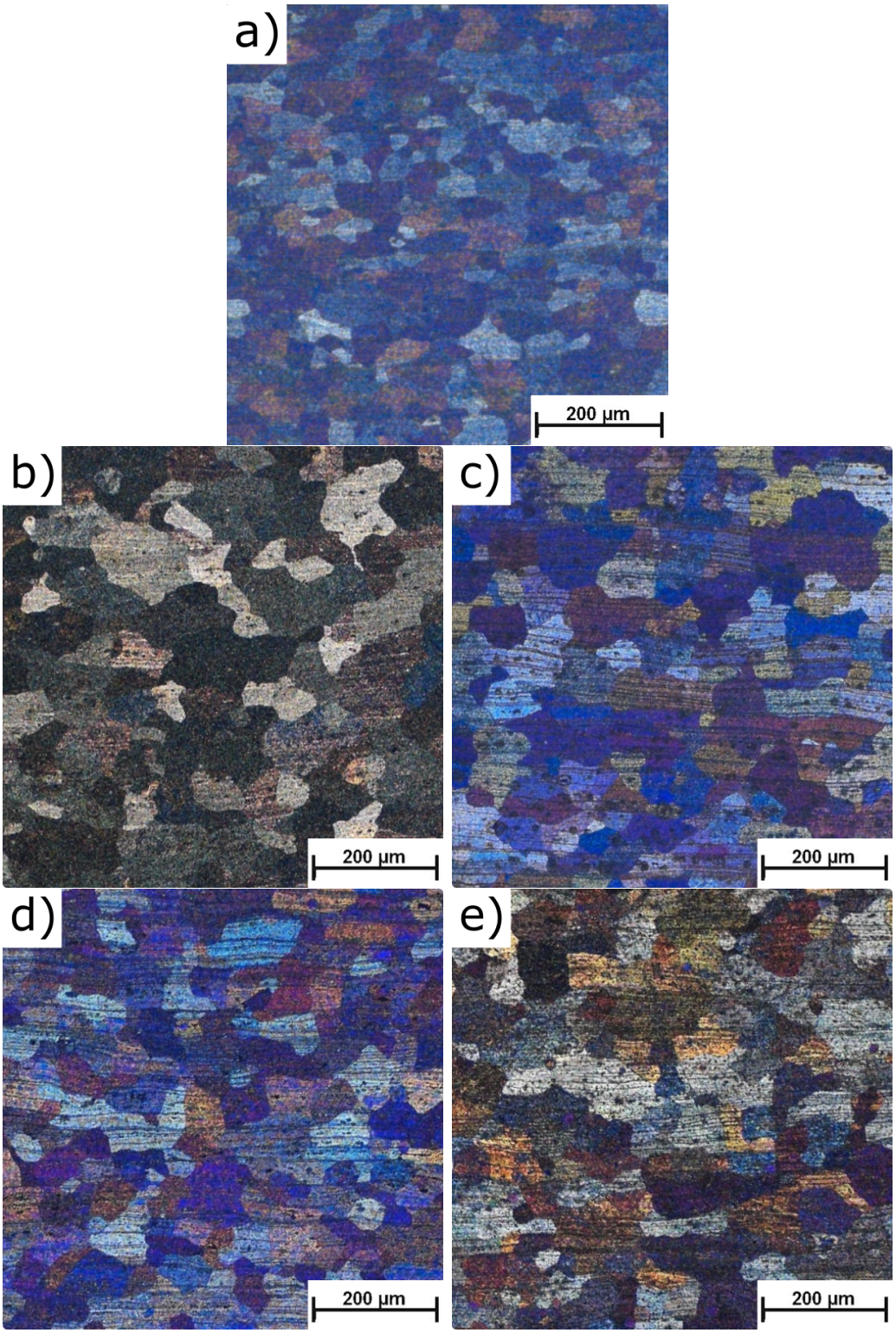

Figure 4.2.2: *Series A III (b-e) and original as- received sample from the manufacturer (a): The grain structure of the as- received sample is slightly more inhomogeneous than the grain structures of the recrystallized samples, which emphasizes the need for the preparation of an initial recrystallized grain structure before performing further experiments. The recrystallisation process in the deformed and annealed (b-e) sample seems to be complete after two hours of annealing (sample A III-4 (c)). Further annealing seems to result in no further grain growth (d-e). After only one hour of annealing, no defined grains with clear grain boundaries can be spot, so it seems, recrystallisation is not complete yet.*

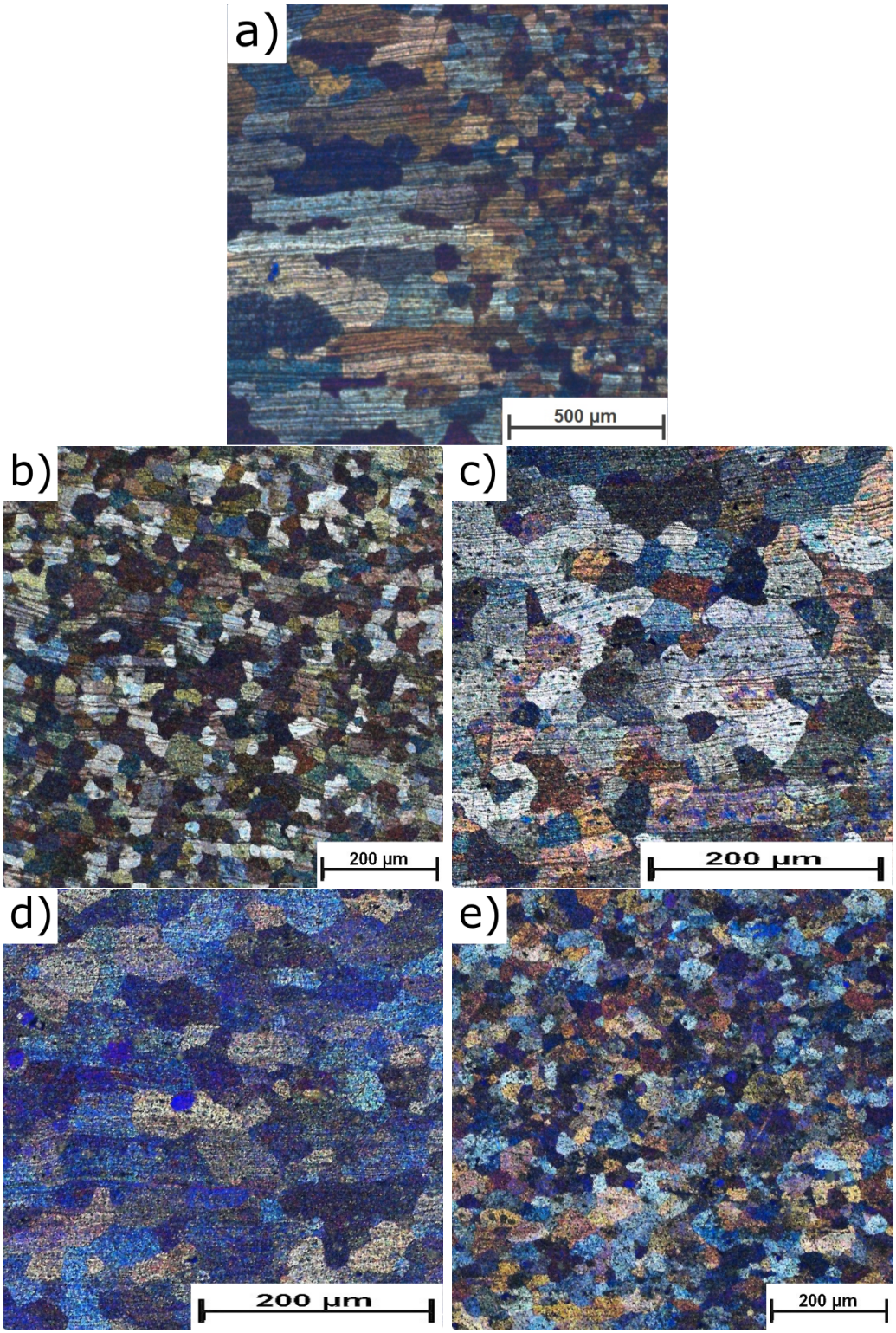

Figure 4.2.3: *Series A IV: Samples deformed with a deformation of* $\varepsilon = -0.35$ *(b-e) and* $\varepsilon = -0.7$ *(a) and annealed for 1 (b), 2 (c,d) and 4 (a,e) hours. The recrystallisation process seems to be finished after one hour and no further grain growth seems to occur, when increasing the annealing time. As mentioned in the text, sample AIV-1 (a) was deformed heavily and inhomogenously by accident which lead to an inhomogenous grain structure with verly small grains in the core of the sample and very large grains at the surface. These large grains are probably a result of abnormal grain growth, due to an highly imhomogenous deformation in the presence of second- phase particles [19, 20]*

4.2.2 Study of the particle behaviour during isothermal heating

As can be seen in Fig. 4.2.4, there are small particles in the material, aligned in the rolling direction of the production process (x) as done by the manufacturer, which are formed by impurities and alloying elements present in a commercially pure material. Considering the composition of the material (Tab. 4.0.1), these particles are most likely $Al_6(Mn, Fe)$ formed by iron and manganese during solidification [21]. $Al_6(Mn, Fe)$ particles occur in two modifications, one which is prefereably formed in the course of a preheating treatment at higher temperatures (550 °C) with subsequent slow cooling and one which is prefereably formed in the course of a preheating treatment at lower temperatures (510 °C) with subsequent faster cooling [22].

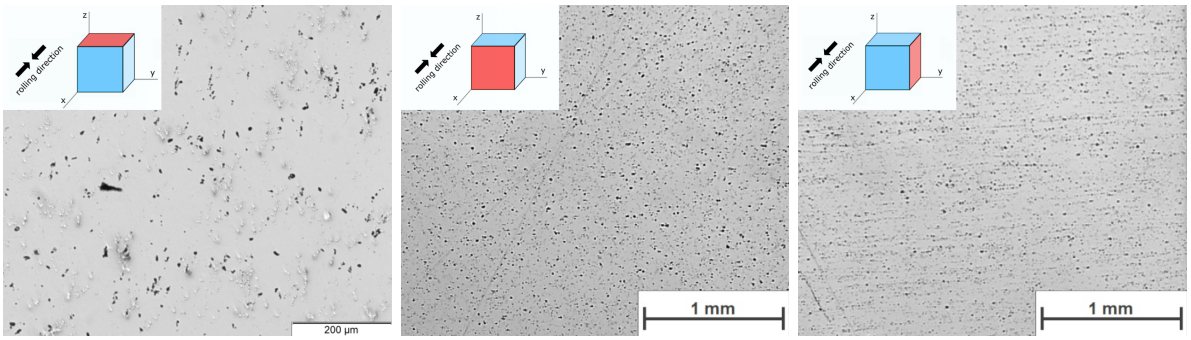

Figure 4.2.4: *Microscopy image of the as received material from different perspectives. As can be seen, the particles of interest are aligned alongside the rolling direction as done by the manufacturer (x- direction)*

Both types should not dissolve below 510 °C, but since they can affect the materials behaviour during recovery and recrystallisation, they have to be examined more closely. Very small particles can counteract recrystallisation due to their Zener pinning effect. Larger particles can facilitate the onset of recrystallisation due to particle stimulated nucleation (PSN) [23]. If these particles dissolve or change their size during heating in the range, where dilatometer measurements were conducted, which is between RT and 500 °C, the results of the measurements would not only be dependent on the chosen parameters, but also on the size and overall behavior of these particles, which would further complicate the situation.

Therefore, four samples the size of (10 x 10 x 5)mm^3 were taken from the as- received material. One sample (R) was ground and polished and directly examined under the microscope. The other three samples were put in an oven at 500 °C for 20 hours, one sample (W) was then water- quenched, one was air cooled (A) and one was cooled in an oven over the course of 40 hours (S). The samples were then ground, polished and examined under the microscope as shown in Fig. 4.2.5.

As can be seen, the particles actually do not change notably when heat treated at 500 °C. Since the particles have a size of roughly one micrometre and a somewhat plate-like shape, particles present in the material mostly seem to occur in the higher temperature modification mentioned in [22]. With this information, a Zener pinning effect in this material would be negligible as it is rather weak for particles of this size however, particle stimulated nucleation (PSN) can be taken into consideration [24].

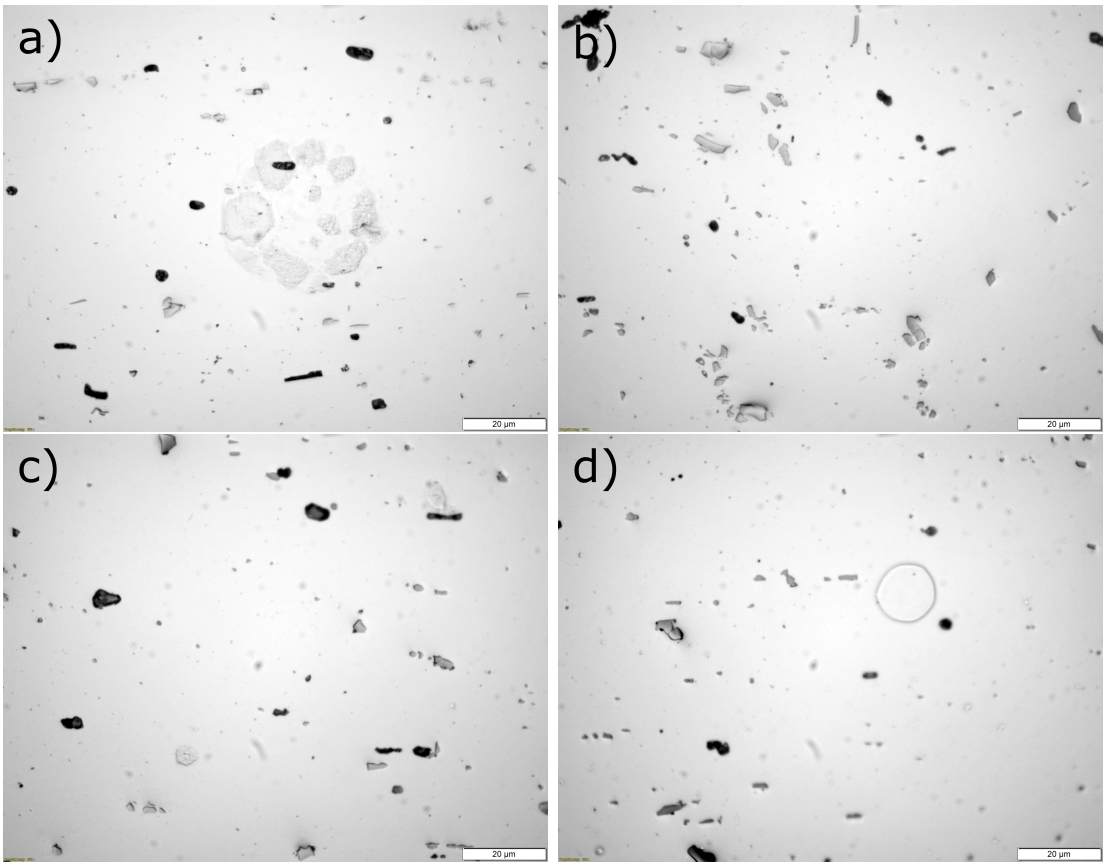

Figure 4.2.5: *Images of an as received (a), a water- quenched (b), an air- cooled (c) and a* $20\,\mathrm{K\,h^{-1}}$ *cooled sample (d). Particles do not seem to change in size or shape during the course of annealing. Different cooling rates also seem to have no effect on these to parameters. Medium grey areas are preparation artifacts.*

DSC- measurements were performed for a water- quenched and a slowly cooled ($40\,\mathrm{K\,h^{-1}}$) sample with 20 and $6\,\mathrm{K\,min^{-1}}$ (Fig. 4.2.6). All four measurements show only one peak around 500 °C during cooling. This peak can be explained as the device probably overheated above 500 °C during the heating run, so some of the smaller particle of low temperature modification dissolved and during cooling they again precipitated.
However, if particles could dissolve below 500 °C, at least one peak should be seen in the heating regime. When cooled back to room temperature (RT), particles would precipitate again and a second peak could be seen in the same region as the peak recorded during heating.

With the results of these tests, interference of these particles during the annealing process were not taken into consideration in the analysis of the results due to the fact, that they do not change in the heating regime of the measurements.

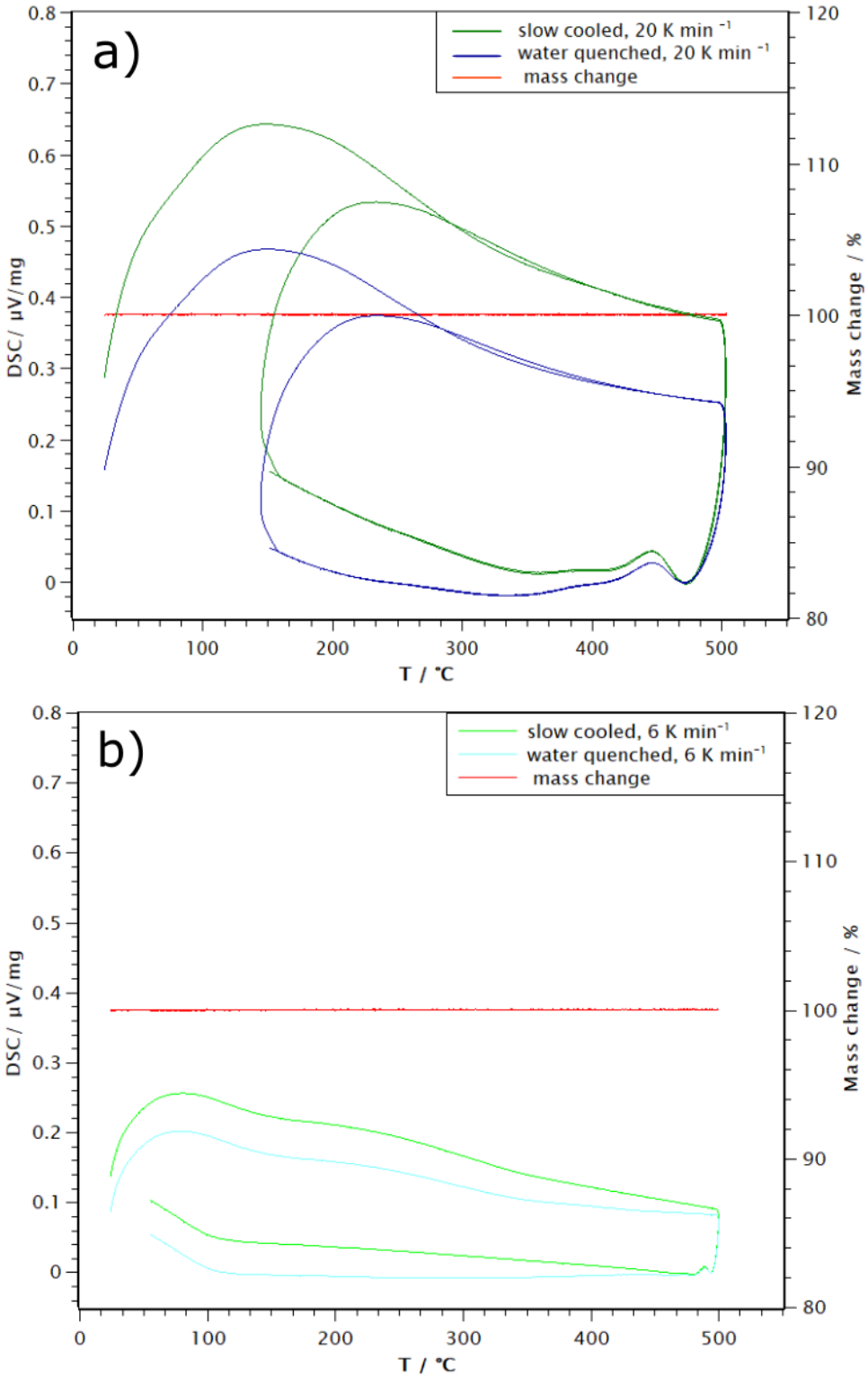

Figure 4.2.6: *DSC measurements of a water- quenched and a* $40\,\mathrm{K\,h^{-1}}$ *cooled sample with different heating and cooling rates (* $20\,\mathrm{K\,min^{-1}}$ *(a) and* $6\,\mathrm{K\,min^{-1}}$ *(b)). One peak can be seen in both measurements. When roughly interpolating these peaks to a peak obtained from a hypothetical heating rate of* $0\,\mathrm{K\,min^{-1}}$*, one gets* $507\,^{\circ}\mathrm{C}$ *for the peak temperature, which is near the dissolution temperature* $510\,^{\circ}\mathrm{C}$ *of the dispersoids of low-temperature modification mentioned in [21]. Please note, that the large peaks in the low temperature regimes cannot be taken into consideration, since the DSC used for the measurements usually is used for the examination of ceramics. Therefore, the accuracy of the device is not assured for measurements at temperatures below* $200\,^{\circ}\mathrm{C}$ *to* $300\,^{\circ}\mathrm{C}$*.*

5 Results

Three different types of measurements have been performed. The first section will deal with the results of dilatometer measurements with linear heating rates up to 500 °C. The main focus of this section is on the information, one can get only from dilatometer curves such as the onset temperatures of certain processes or the amount of volume release during these processes. In the second section, measurements that were performed on the basis of the results of the first two measurement types will be discussed, where samples were measured in the dilatometer with a linear heating rate and were quenched after reaching certain temperatures between 0 and 500 °C. The quenched samples were then further examined with EBSD to get a more detailed view on the microstructure and on the possible processes apparent during linear heating. In the third section, results of isothermal length change measurements are shown, which were made to confirm and verify the insights gained from the previous two experiment approaches.

Starting conditions for each measurement The temperature program of each measurement has the same starting conditions to ensure the comparability and reproducibility of the results. The oven with the samples first was cooled from room temperature to −20 °C, held at this temperature for 15 minutes and then heating started with a heating rate characteristic for each measurement (see Fig. 5.0.1). This procedure was done due to the issue, that linearity of sample heating could already be established after heating to 10 or 20 °C. For the same reason, 30 °C could then be taken as reference point for the start of each measurement.

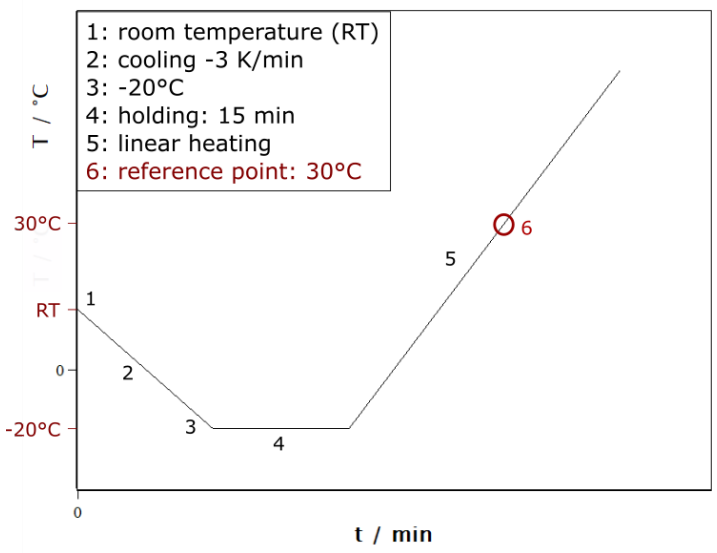

Figure 5.0.1: *Starting conditions for each measurement. The first step is cooling from room temperature (RT) to* −20 °C *(2), the temperature was held for* 15 min *(4) and then, programmed linear heating (5) started.*

5.1 Difference Dilatometry with linear heating rates

The objective of these two measurement series was to study the behavior of the deformed samples upon heating in a temperature range between 30° and 500° C. Figure 5.1.1 shows a schematic temperature program used for the following two measurement series.

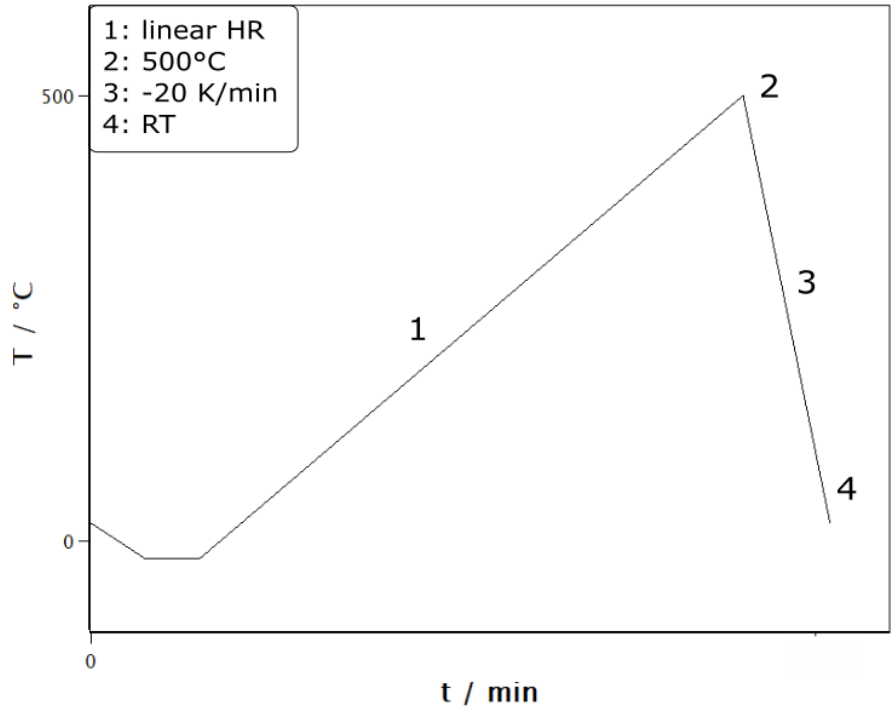

Figure 5.1.1: *Schematic temperature program used for the measurements parallel and perpendicular to the direction of deformation heated with a linear heating rate (1).*

There were several measurements performed with different heating rates on samples with different grades of deformation. Table 5.1.1 summarizes the different conditions under which these two measurement series were performed.

As can be seen from tab. 5.1.1, the most important difference between the two series is the measurement direction, one series of samples were measured parallel to the direction of deformation and one series measured perpendicular to the direction of deformation (Fig. 5.1.2).

One further important difference was the mode of deformation. Samples of the series measured parallel to the direction of deformation were deformed only by method G (Gleeble), samples of the series measured perpendicular were mostly deformed by method R (Rolling). Measurements in the perpendicular direction of samples, which were deformed by method G were performed to show, that the mode of deformation has no recognizeable effect on the results of the measurements.

Table 5.1.1: *Different parameters under which measurements perpendicular and parallel to the direction of deformation were performed. MD: measurement direction, G: deformation using the Gleeble machine, R: deformation using rolling*

parameters		MD: parallel	MD: perpendicular
induced strain ε	-0.17	•	–
	-0.25	•	•
	-0.35	•	•
	-0.41	•	•
	-0.55	•	•
	-0.61	•	•
	-0.67	•	–
heating rate HR ($\mathrm{K\,min^{-1}}$)	0.1	–	•
	0.75	•	•
	1.5	•	•
	4	•	•
	6	•	•
method of deformation	G	•	–
	R	•	•
measurement direction	y	•	–
	z	–	•

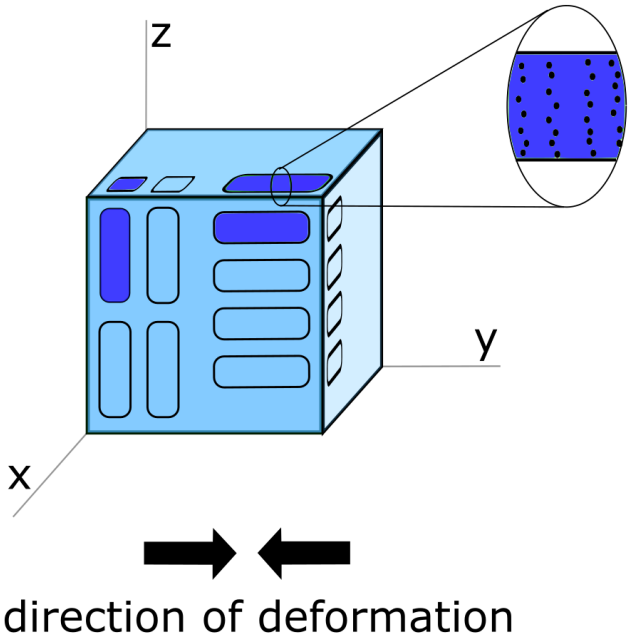

Figure 5.1.2: *Orientation of the samples (marked dark blue) cut from the deformed material as used in the two series. Samples were cut either parallel to z (perpendicular to the direction of deformation) or parallel to y direction (parallel to the direction of deformation) as shown in the image. Inclusions resulting from the solidification are present in the material and are aligned alongside x direction due to the rolling process as performed by the manufacturer.*

5.1.1 Measurements perpendicular to the direction of deformation

Measurements with five different heating rates combined with five grades of deformation were performed to get an idea of the influence that these two parameters can have on the annealing processes in the aluminum sample. Measurements with a heating rate of $0.1\,\mathrm{K\,min^{-1}}$ were performed to simulate conditions in a quasi- equilibrium to gain a more detailed insight into the ongoing processes. Also, extremely low and high deformed samples were measured with two different heating rates. These measurements which complement the results of the previous measurements will be discussed in a subsequent paragraph.

To possibly identify different processes occurring during annealing, the derivatives of the dilatometer curves were formed (Fig. 5.1.4b). In general, in a difference dilatometer curve with its corresponding derivative (see Fig. 5.1.3), which are both representative for all measurements in this series, four distinct peaks can be distinguished, one around 100 °C and one around 150 °C, which will be assigned to a stage I as well as one peak around 200 °C and one around 300 °C, which will be assigned to a stage II. The assignment of two peaks to one stage is due to their overlapping in many measurements, which is probably caused by two competing processes in each of these two temperature regimes. Overall, the dilatometer curves of the perpendicular series can be grouped into three stages I, II and II, where stage I will be sub classified into Ia and Ib and stage II will be sub classified into IIa and IIb due to the forecited occurrence of two peaks in each of these two stages. Also as mentioned before, due to their proximity, the two peaks in stage I are merging into one broad peak in most measurement curves. The two peaks in stage II are overlapping in some curves. These four peaks can be found more or less distinctive in each curve of this series (with some exceptions for the measurements of the extremely high and low deformed samples, which will be discussed more thoroughly in the corresponding paragraph). Considering the absolute length changes, the dilatometer curves in this series show a slight decrease in length change in stage I from the beginning, followed by a more steep decrease in stage II terminating with a slight decrease in stage III. (Fig. 5.1.3).

Furthermore, a fifth peak can be assigned around 450 °C, which was found in a few other measurements. Nevertheless, in most of the measurements of this series, this peak does not show up, therefore, no further attention will be paid to a process probably happening in this temperature range (III).

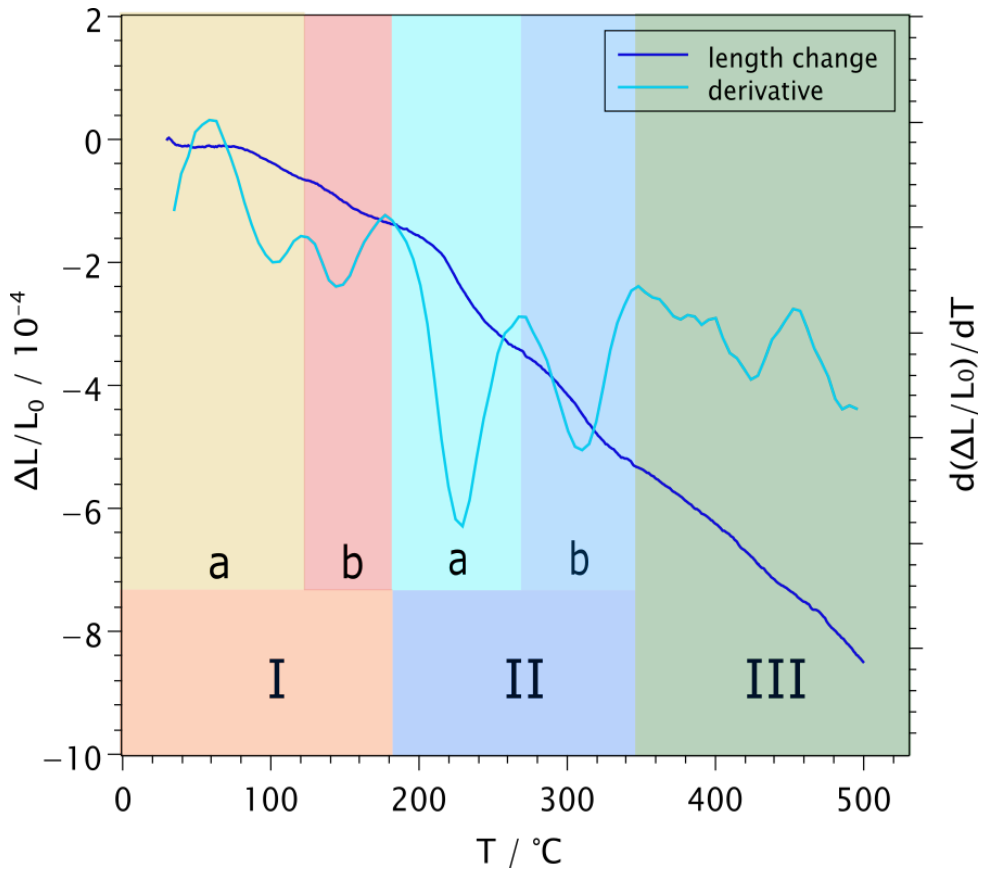

Figure 5.1.3: *General appearance of dilatometric results measured perpendicular (⊥) to the deformation direction: Dilatometric difference curve with its corresponding derivative for $\varepsilon = -0.35; HR = 1.5K/min$. The irreversible length change is plotted against the temperature. The different processes occurring in the material during linear heating are identified by the positions of the peaks found in the derivative which leads to the assignment of three separate stages I, II and III, of which I and II can be further sub classified into a and b.*

So two separate processes can be distinguished to occur in stage I and II due to the peaks assigned according to the derivative curve. The overlap of processes may be by coincidence, but there also might be a correlation between them.

Figure 5.1.4 shows the difference length change curves and the corresponding derivative curves for a heating rate of $1.5\,\mathrm{K\,min^{-1}}$. When comparing the peak positions of different grades of deformation (see Fig. 5.1.4b), one can see, that the peaks in stage II are overlapping too at higher grades of deformation. So it seems as if the peaks found around 200 °C do not change their positions upon changing the grade of deformation. The position of the peaks found around 300 °C on the other hand is dependent on the grade of deformation. The higher the grade of deformation, the more the position of the peaks is shifted to lower temperatures. So to examine the dependence of the peak positions on the heating rate and the grade of deformation, the position of each peak in this measurement series is summarized in Fig. 5.1.5 and given in table 5.1.2.

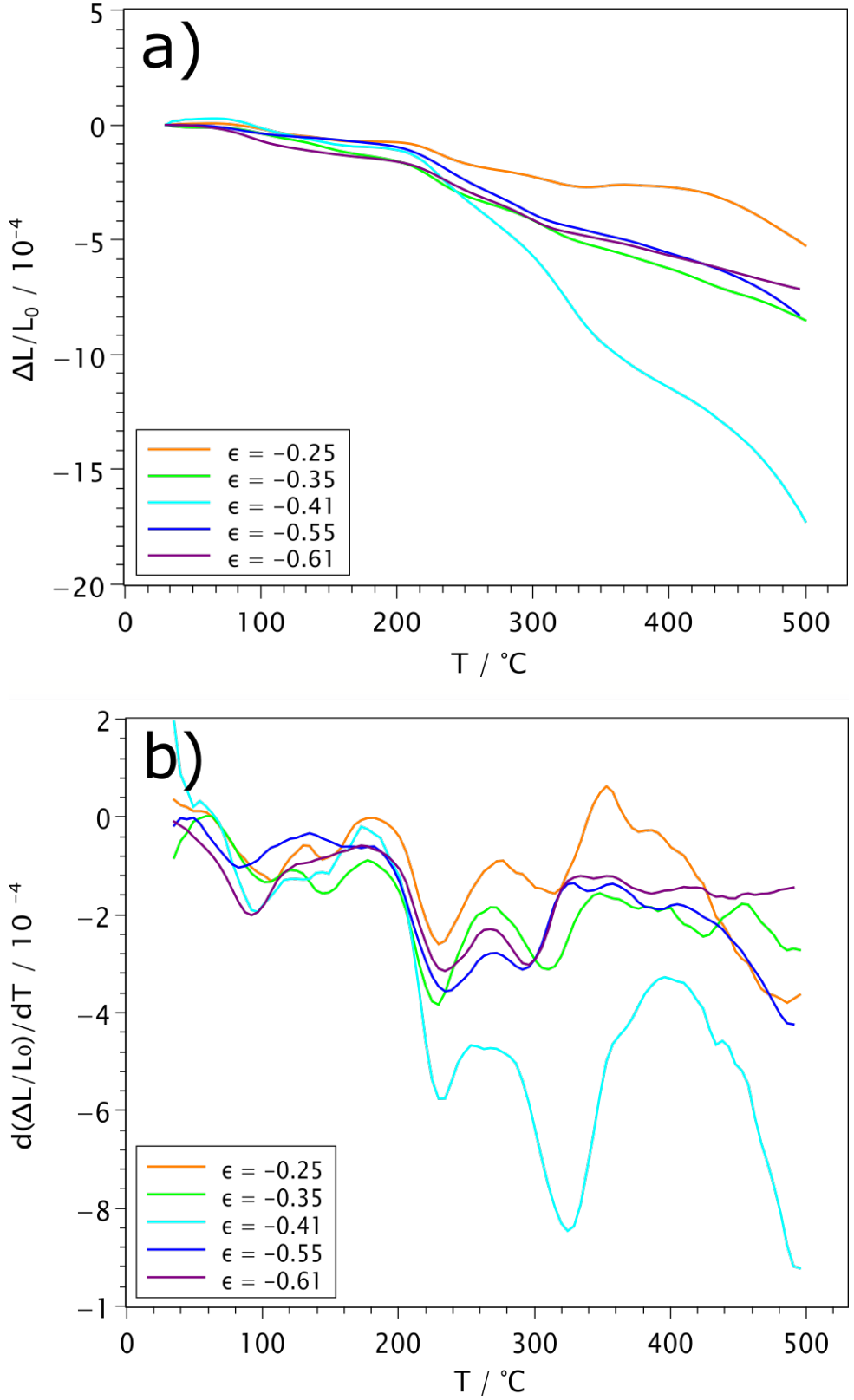

Figure 5.1.4: *Dilatometric results measured perpendicular to the deformation direction: Irreversible length change* $\frac{\Delta L}{L_0}$ *(a) and corresponding derivatives (b) for HR* $1.5\,\mathrm{K\,min^{-1}}$. *The two overlapping peaks around* $100\,^{\circ}\mathrm{C}$ *can be separately spot best for* $\varepsilon = -0.25$ *and* $\varepsilon = -0.35$

Comparing the positions of the peaks of the whole measurement series, the peaks found around 150 °C and 200 °C do not change their position when changing the heating rate or the grade of deformation; whereas the peaks found around 100 °C and 300 °C do change their position.
The position of the peak in stage Ia shifts to higher temperatures with increasing heating rate and shifts to lower temperatures with increasing grade of deformation of the sample, which is also true for the peak found at 300 °C. A possible explanation for this phenomenon will be given in the discussion section (chapter 6.1 and 6.2).

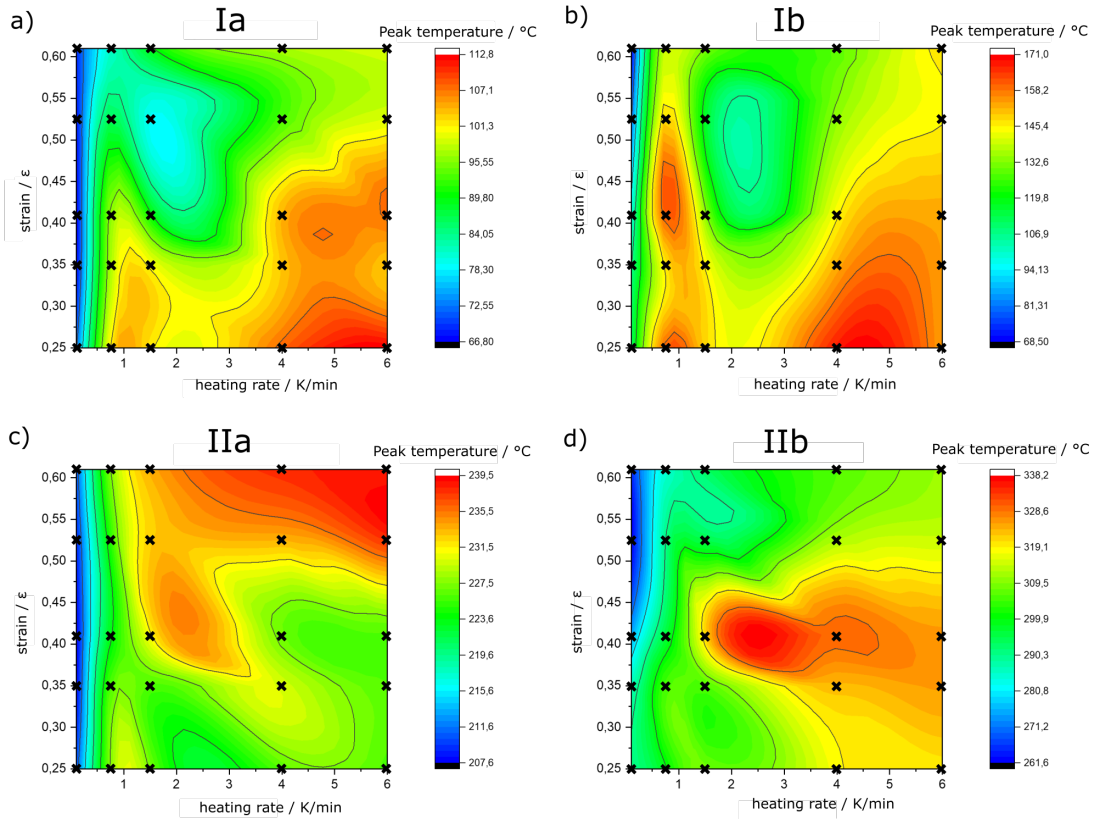

Figure 5.1.5: *Peak temperature variation for the peaks found in stage Ia (a), Ib (b), IIa (c) and IIb (d) in a two dimensional, interpolated representation with the measured data points marked by ×. Comparison of the variation of peak temperatures with the grade of deformation or the heating rate leads to the conclusion, that peaks found in stage Ib and IIa do not change their position when changing one of the mentioned above parameters, but the peaks found in stage Ia and IIb do so. Upon increasing the heating rate, the temperatures at which these peaks are found increase, upon increasing the grade of deformation, the temperatures at which the peaks are found decrease.*

Table 5.1.2: *Temperatures (°C) of maximum reaction rate of the processes in stage I and II for measurements performed perpendicular to the direction of deformation, HR = heating rate (*$\mathrm{K\,min^{-1}}$*)*

Peak	HR \ ε	**-0.25**	**-0.35**	**-0.41**	**-0.55**	**-0.61**
Ia	**0.1**	72.0	67.3	66.9	68.3	-
	0.75	101.7	97.5	96.3	84.6	81.0
	1.5	101.7	100.8	90.4	80.4	89.3
	4	107.7	103.4	104.2	92.7	97.3
	6	112.6	103.2	107.5	98.0	99.1
Ib	**0.1**	111.4	106.5	98	-	-
	0.75	160.7	146.8	160.6	145.1	139.5
	1.5	148.4	144.9	134.3	118.4	132.1
	4	167.7	-	144.8	132.3	-
	6	-	153.7	152.9	144.6	147.4
IIa	**0.1**	210.5	207.9	207.7	209.5	-
	0.75	227.9	226.2	223.3	225.8	227.6
	1.5	227.3	226.0	231.2	232.6	233.7
	4	226.3	230.0	227.0	235.4	237.9
	6	225.9	226.3	226.0	239.2	238.1
IIb	**0.1**	290.2	286.4	275.3	261.7	265.2
	0.75	299.3	305.6	296.3	289.3	284.8
	1.5	308.7	306.1	321.1	290.2	293.1
	4	318.4	323.4	329.5	309.1	306.2
	6	319.6	325.7	326.0	312.8	311.4

Table 5.1.3: *Temperatures (°C) of maximum reaction rate of the processes in stage I and II of additional measurements performed perpendicular to the direction of deformation to show the reproducibility of the measurements, HR = heating rate (*$\mathrm{K\,min^{-1}}$*)*

Peak	HR \ ε	**-0.25**	**-0.35**	**-0.41**	**-0.55**	**-0.61**
Ia	**1.5**	89.4	78.8	75.5	92.8	86.3
	4	86.3	85.8	86.9	93.5	93.2
Ib	**1.5**	139.7	151.1	140.1	139.6	145.3
	4	122.3	130.2	143.4	128.9	142.8
IIa	**1.5**	235.1	233.9	231.5	233.9	234.4
	4	237.3	228.7	235.3	236.2	237.3
IIb	**1.5**	327.9	312.1	308.6	288.3	287.6
	4	330.4	326.5	312.6	314.5	305.8

Measurements of samples with extremely low and extremely high deformation
Five measurements were performed, three with very low deformed samples with a heating rate of $0.1\,\mathrm{K\,min^{-1}}$, one with a very high deformed sample with a heating rate of $0.1\,\mathrm{K\,min^{-1}}$, and one with a very high deformed sample with a heating rate of $4\,\mathrm{K\,min^{-1}}$.

Of the four peaks mentioned previously in this section, peaks around 200 and 300 °C can be easily identified in the derivative curves (Fig.5.1.6b). The peak around 200 °C (IIa) is apparent in all five measurements, although the intensity of this peak decreases at the expense of the peak found around 300 °C when moving from a very low deformation to a very high deformation.
The peak around 300 °C (IIb) is apparent in both measurements of very high deformed samples and can be identified to some extent for $\varepsilon = -0.04$. So the process happening around 300 °C seems to need a minimum amount of deformation to take place, some kind of threshold value which may be located around $e = -0.04$. Furthermore, the process happening around 200 °C does not need this kind of threshold value. However, if there is enough deformation introduced to the sample for process IIb (at 300 °C) to occur, process IIa (at 200 °C) is not the dominant process any more. So these two processes seem to be correlated, that means if the subsequent process can take place, it takes place at the expense of the previous process. This correlation can also be seen in the measurement heated with $4\,\mathrm{K\,min^{-1}}$ where both peaks are shifted to higher temperatures due to the faster heating rate.

The peaks around 100 °C and 150 °C seem to occur in all five measurements, but they are more pronounced in derivative curves of samples with a higher deformation. So the processes that cause these two peaks seem to need no threshold value of deformation, but are nevertheless somehow dependent on the grade of deformation, if only to a small extent.

One important remark, that can be made from the results obtained from the dilatometer curves in Fig. 5.1.6 a is the fact, that there seems to be no correlation between the total length change and the grade of deformation. This missing correlation appears also in the other measurements of the "perpendicular" series, but when having a look at the total length changes of extremely high and extremely low deformed samples in Fig. 5.1.6, it can be seen that there is almost no difference in length change between these two extremes. Intuitively, this seems to be not reasonable, as one would expect a greater length change when measuring a sample with a higher amount of disorder previously introduced to the sample. Nevertheless, an attempt to explain this findings will be made in the discussion section with the consideration of results gained from other measurements too (see chapter 6.3).

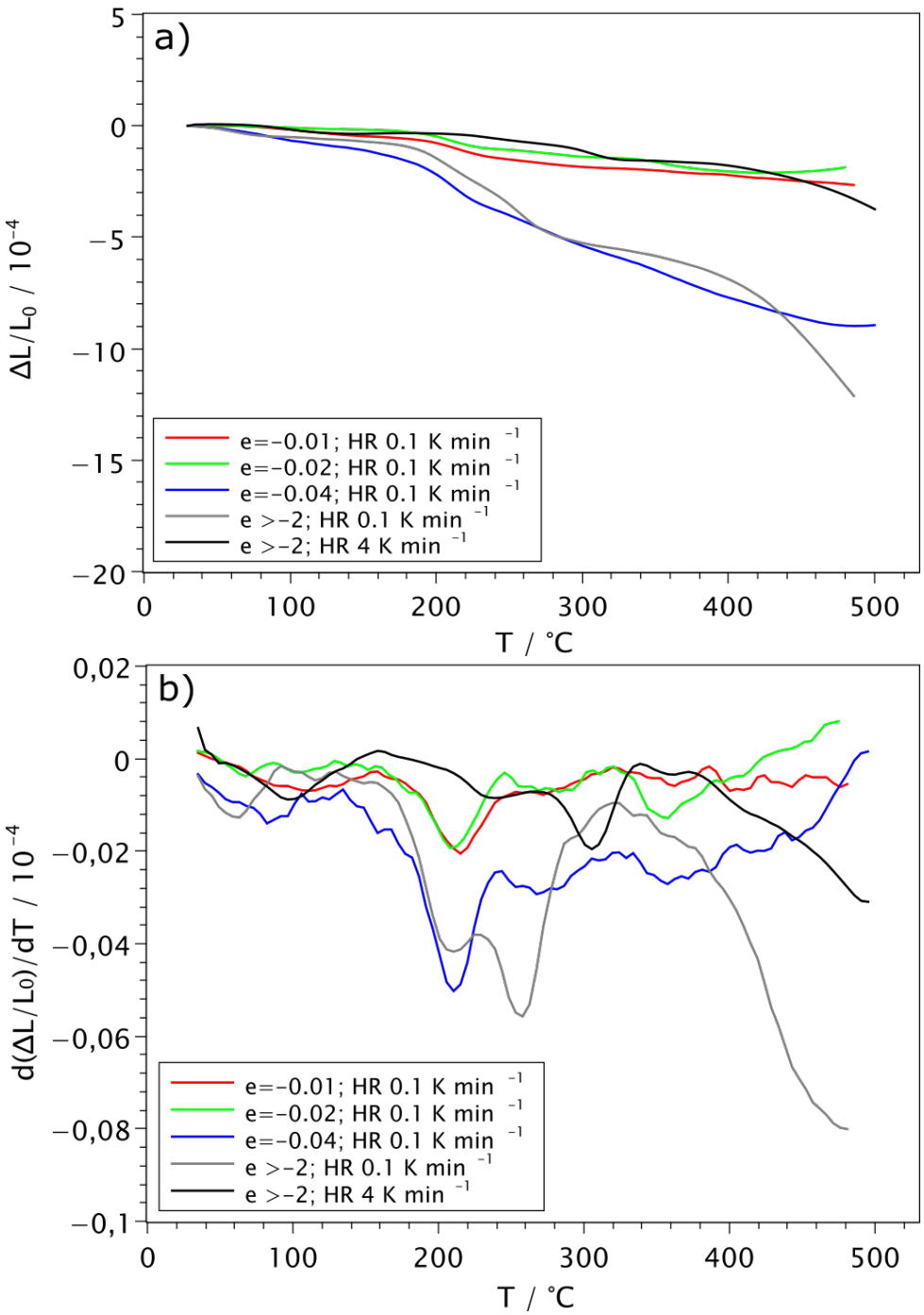

Figure 5.1.6: *Results of the dilatometric measurements done perpendicular to the direction of deformation with extremely low and extremely high grades of deformation (a) with the the corresponding derivatives (b). The two processes occurring in stage II can clearly be distinguished. However, process IIb seems not to take place if the grade of deformation is lower than a certain threshold value. However, if this threshold value is exceeded, process IIb takes place at the expense of the correlated process in IIa. Moreover, the total irreversible change in length in these measurements does not seem to be dependent on the grade of deformation.*

Table 5.1.4: *Temperatures (°C) of maximum reaction rate of the processes in stage I and II for measurements performed perpendicular to the direction of deformation with extremely low and extremely high deformed samples, HR = heating rate (*$\mathrm{K\,min^{-1}}$*)*

Peak	ε / HR	**-0.01**	**-0.02**	**-0.04**	**>-2**
Ia	**0.1**	81.4	66.1	84.7	59.4
	4	-	-	-	98.2
Ib	**0.1**	109.6	107.2	113.1	116.3
	4	-	1-	-	-
IIa	**0.1**	214.9	209.8	209.6	208.1
	4	-	-	-	246.8
IIb	**0.1**	-	-	271.3	255.5
	4	-	-	-	306.0

5.1.2 Measurements parallel to the direction of deformation

For this measurement series, additional measurements for deformations $\varepsilon = -0.17$ and $\varepsilon = -0.67$ but no measurements with a heating rate of $0.1\,\mathrm{K\,min^{-1}}$ were performed, contrary to the measurement series done perpendicular to the direction of deformation as reported in section 5.1.1.

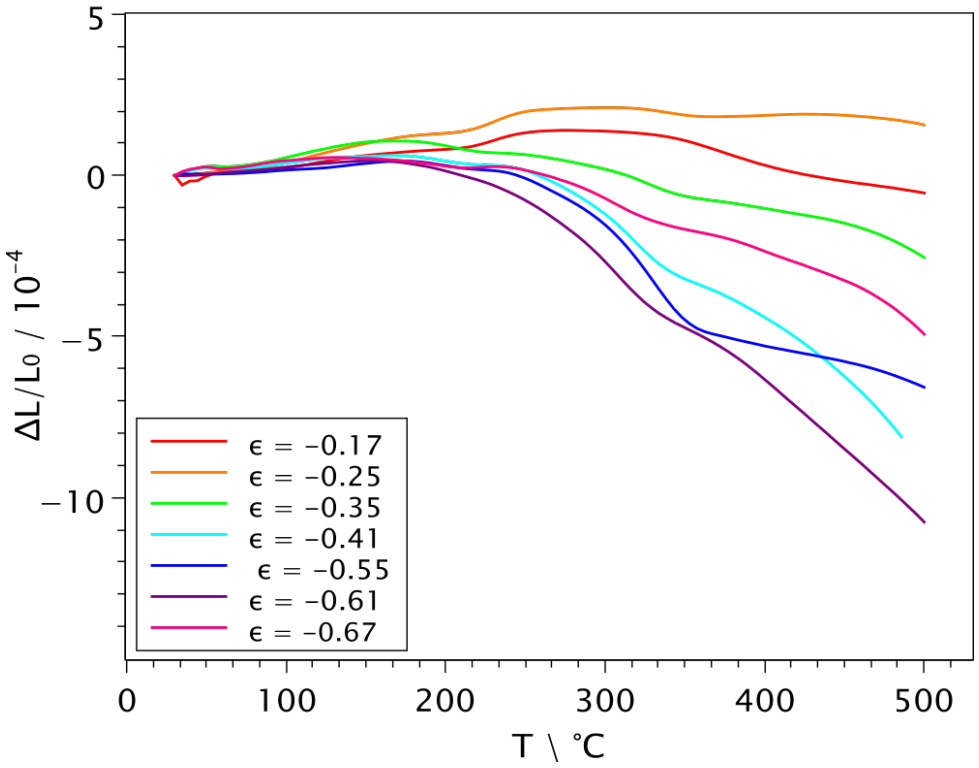

Figure 5.1.7: *Difference dilatometry curves of samples measured parallel to the direction of deformation with a heating rate of* $4\,\mathrm{K\,min^{-1}}$ *for different grades of deformation. The irreversible length change is plotted against the temperature*

Measurements with the same heating rate show a similar behavior for different grades of deformation considering the shape of the curve (Fig. 5.1.7). Having the insights gained from the perpendicular measurements in mind, three stages can also be identified in this series (Fig. 5.1.8), which seem to occur in each of the dilatometer curves in a more or less distinctive manner. Contrary to the dilatometer curves of the perpendicular measurements, the dilatometer curves of this series show an increase in irreversible length change in the low temperature regime of the curve. The onset of decrease in length change following the initial increase in length change seems to be dependent on the grade of deformation, with a higher grade of deformation resulting in an earlier onset. Furthermore, three distinct peaks can be observed, one around 300 °C, one around 200 °C and a broader peak around 100 °C. However, the first two peaks of the derivative curve point to the opposite direction in comparison to the last peak, which is, as mentioned above, due to the positive irreversible length change in stage I and IIa of the dilatometer curves. For higher grades of deformation ($\varepsilon > -0.41$), an increase in irreversible length change is only occurring in stage I.

The broad peak found around 100 °C may be a result of two overlapping peaks as also found in the perpendicular measurements. It may also be a result of an additional process that only has an effect in measurements done parallel to the direction of deformation. This process may cause the expansion in the first regime of the dilatometer curves, resulting in the first peak to be rather broad and blurred, so that only one peak can be identified rather than two.

When considering the total absolute length change difference of each curve, they seem to follow no distinct pattern of behavior, which would show a correlation between the absolute length change of a sample and its grade of deformation. However, contrary to the measurements performed perpendicular to the direction of deformation, a slight trend can be seen, where a higher grade of deformation roughly results in a greater irreversible length change.

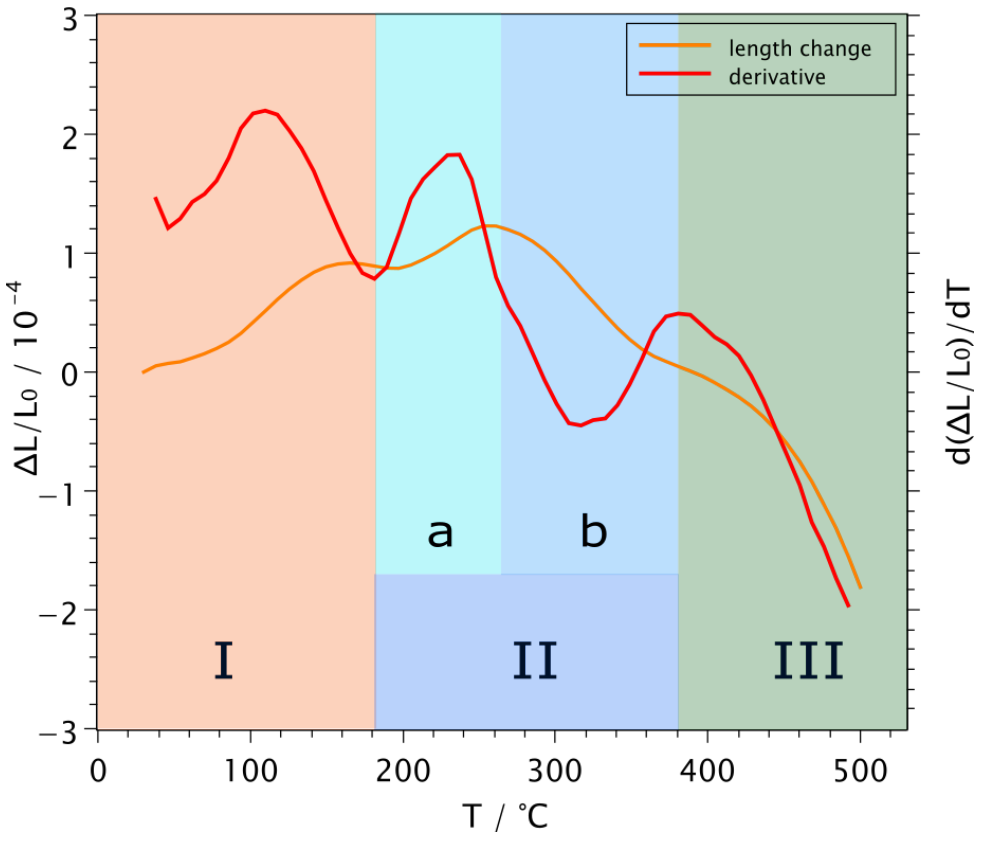

Figure 5.1.8: *Dilatometer curve and its corresponding derivative for a deformation of* $\varepsilon = -0.35$ *and a heating rate of* $HR = 1.5\,\mathrm{K\,min^{-1}}$. *The positions of the peaks are important to identify the different processes occurring in the material during linear heating. In stage I and IIa of the dilatometric curve, the deformed sample seams to expand step wise compared to the reference sample. In stage IIb, there is a sharp, in stage III a more steady decrease in length change.*

When comparing the peak temperatures for peak IIa, found in all dilatometer curves with a heating rate of $4\,\mathrm{K\,min^{-1}}$ (Fig. 5.1.9), no correlation between the grade of deformation and the location of the peak can be found. Process IIa seems to happen at the same temperatures independent on the grade of deformation. This is also true for

different heating rates as shown in Fig. 5.1.10.

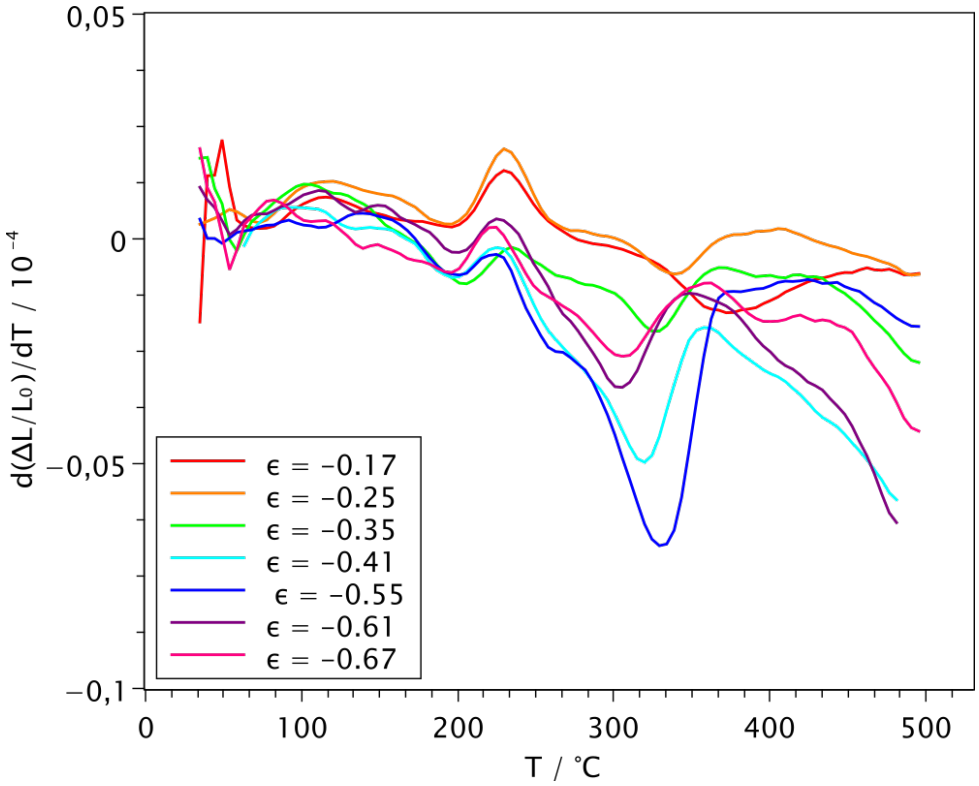

Figure 5.1.9: *Derivatives of the dilatometer curves shown in Fig. 5.1.7. A comparison of the derivative curves of measurements performed under different conditions is important to identify possible dependencies of the previously assigned processes to these parameters. As can be seen, the position of the peak found around* 200 °C *(IIa) does not change upon changing the grade of deformation of the samples, the position of the peaks found around* 100 °C *(I) and* 300 °C *(IIb) however, does.*

For the peak found at 300 °C, a change in peak temperature can be found upon changing either the grade of deformation or the heating rate. When moving to higher grades of deformation, the peak temperature decreases. The same is true when moving to lower heating rates. Therefore, the temperature at which this process occurs seems to be dependent both on the heating rate and the amount of strain previously introduced to the sample. The same is true for the peak found around 100 °C and these tendencies can be found in all measurements of this series (see Fig. 5.1.10 and table 5.1.5).

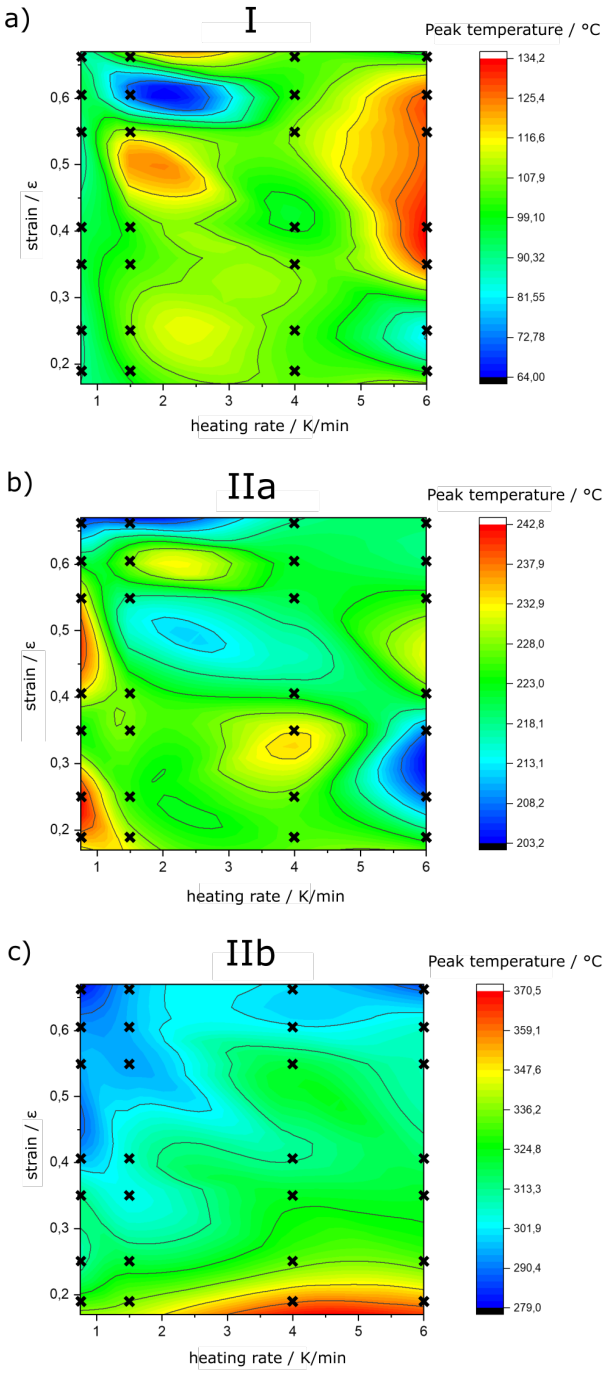

Figure 5.1.10: *Temperatures of the peaks obtained from the derivative curves of the parallel series summarized in a two dimensional interpolated representation with the measured data points marked with an ×. a) peak temperature variation in stage I. b) peak temperature variation in stage IIa. c) Peak temperature variation in stage IIb. When comparing the positions of the peaks found for measurements performed under different conditions, one can conclude the following: The peaks found around* 200 °C *do not change their position when changing either the heating rate or the grade of deformation. The peaks found around 100 and* 300 °C *shift to lower temperatures upon increasing grade of deformation (ε) or decreasing heating rate (HR).*

Table 5.1.5: *Temperatures (°C) of maximum reaction rate of the processes in stage I and II for measurements performed parallel to the direction of deformation, HR = heating rate (*$\mathrm{K\,min^{-1}}$*)*

Peak	ε / HR	**-0.17**	**-0.25**	**-0.35**	**-0.41**	**-0.55**	**-0.61**	**-0.67**
I	**0.75**	90.4	89.6	94.6	93.8	89.2	95.3	88.3
	1.5	98.32	107.3	102.9	102.0	110.3	70.8	111.2
	4	105.8	104.5	107.0	97.7	108.7	102.4	106.0
	6	108.9	81.2	127.9	133.5	127.3	126.36	96.0
IIa	**0.75**	231.7	242.3	223.0	233.5	233.5	219.9	205.0
	1.5	232.1	224.9	-	226.2	217.6	227.7	203.8
	4	226.7	226.8	232.8	220.4	220.8	221.5	217.6
	6	226.35	-	208.6	226.2	224.4	218.5	219.8
IIb	**0.75**	339.0	310.8	313.8	294.9	295.7	293.0	279.4
	1.5	341.9	320.1	304.3	307.4	295.1	296.6	295.6
	4	368.4	333.3	322.6	312.3	320.1	301.3	300.3
	6	364.5	332.9	322.4	316.4	309.3	306.3	286.1

5.2 Analysis of the microstructure with EBSD after quenching from different temperatures

This series was done subsequently to the parallel and perpendicular series to get a better insight into the processes occurring during linear heating of a deformed sample. Figure 5.2.1 shows the temperature program for this series. The dilatometer was heated up to four different temperatures with a linear heating rate . After reaching the distinct temperature, samples were quenched to RT with a cooling rate of $30\,\mathrm{K\,min^{-1}}$.[1]

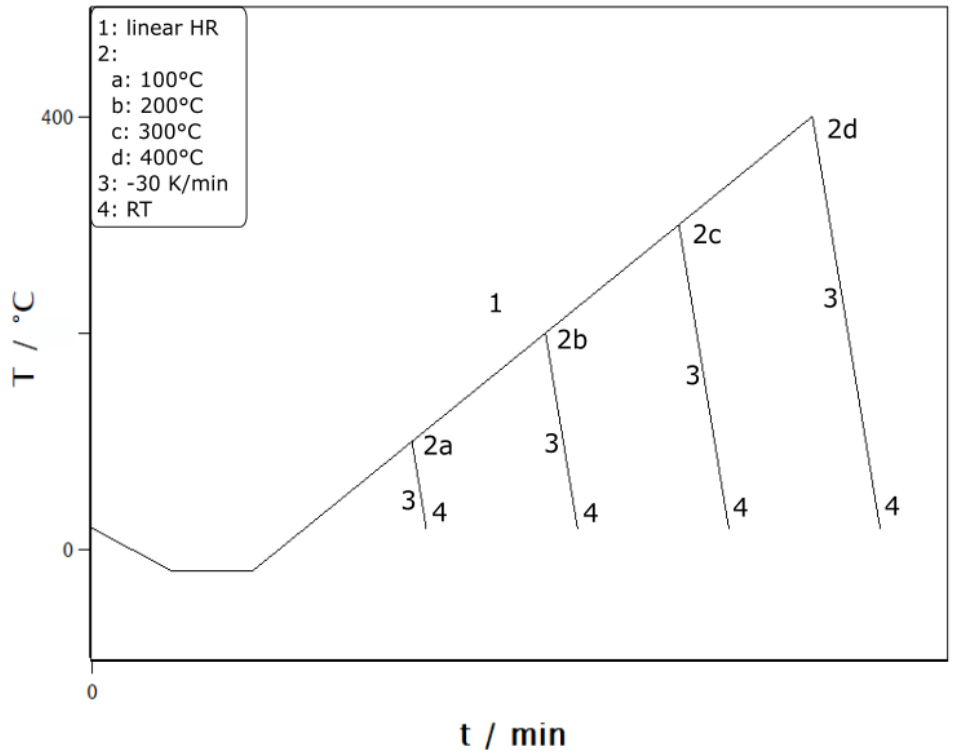

Figure 5.2.1: *Temperature program for partial heating and subsequent quenching for freezing the microstructure at distinct temperatures (2a, 2b, 2c, 2d) for EBSD analysis.*

Samples with two different grades of deformation, either $\varepsilon = -0.25$ or $\varepsilon = -0.61$, all cut perpendicular to the direction of deformation were measured in the dilatometer with either $4\,\mathrm{K\,min^{-1}}$ or $1.5\,\mathrm{K\,min^{-1}}$ and were then quenched at four distinct temperatures as shown in **??** using cold nitrogen gas. Afterwards, EBSD measurements of the quenched samples were performed. Figure 5.2.2 shows the length change curves for $\varepsilon = -0.25$; HR $= 1.5\,\mathrm{K\,min^{-1}}$ as an example. In this measurement series the focus was on the EBSD analysis and the dilatometer results were only used to ensure the same annealing conditions as reported for the measurements in the previous section.

[1] a faster cooling rate was technically not possible

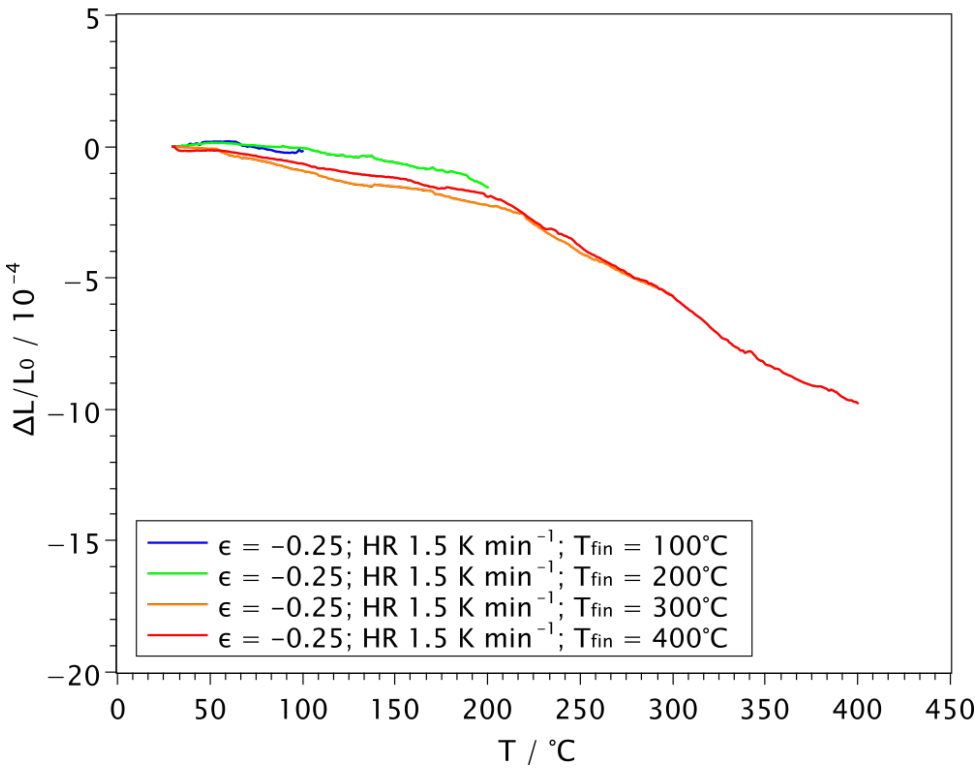

Figure 5.2.2: *Dilatometry curves of measurements with linear heating quenched at distinct temperatures to monitor the evolution of the micro structure at those temperatures T_{fin} with the help of EBSD analysis.*

Results of the EBSD measurements Samples quenched from 100, 200, 300 and 400 °C as well as samples without heat treatment (RT) according to Tab. 5.2.1 were analyzed with EBSD. Samples were chosen that way to ensure, that the results of different heating rates and results of different grades of deformation can be compared. Figure 5.2.3 shows the two planes of the samples, which were examined with EBSD. In each of the following EBSD images, the plane of observation is indicated in the top right corner.

Table 5.2.1: *Sample combinations with different grades of deformation (ε) and heating rates (HR) as measured with EBSD*

HR / ε	1.5 K min^{-1}	4 K min^{-1}
-0.25	•	
-0.61	•	•

The first EBSD images shown are inverse pole figure images of the grain structure without heat treatment (Fig. 5.2.4) and after heating to 400 °C (Fig. 5.2.5). High angle boundaries (HAB) are shown in black, low angle boundaries (LAB) in grey (angle 5° to 12°) and white (angle 2° to 5°). Table 5.2.2 shows the average grain sizes.

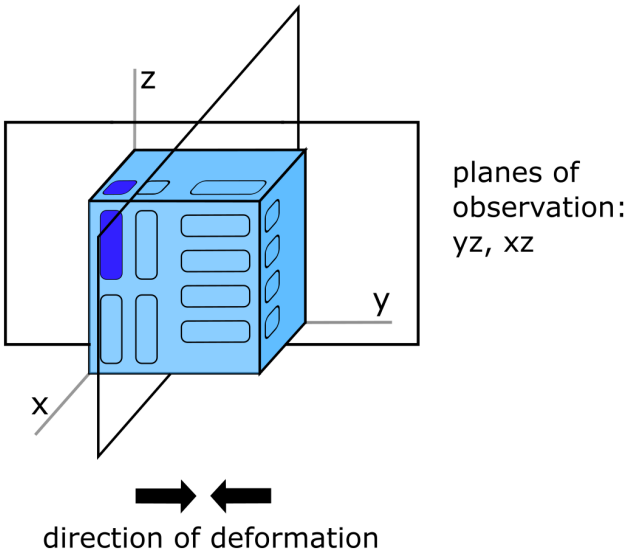

Figure 5.2.3: *Orientation of the samples as measured in the EBSD measurement series. All samples were measured by dilatometry in z- direction (marked dark blue in the image), the planes of observation for EBSD were the yz and the xz- plane. The inclusions present in the sample due to the initial manufacturing process are aligned in x direction*

Table 5.2.2: *Average grain sizes, d, of the microstructures as shown in Figs. 5.2.4 and 5.2.5.*

ε	HR / K min^{-1}	RT	400 °C
		d / µm	d / µm
-0.25	1.5	55,7 ± 16,1	49,4 ± 17,9
-0.61	1.5	56,2 ± 17,6	24,0 ± 10,1
	4		20,4 ± 8,4

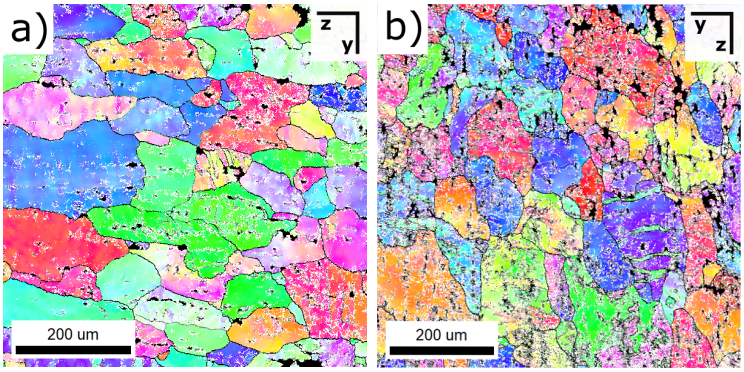

Figure 5.2.4: *Inverse pole figure (IPF) images of two samples with different grades of deformation, $\varepsilon = -0.25$ (a) and $\varepsilon = -0.61$ (b), but without heat treatment.*

The grain sizes in higher deformed samples after heating to 400 °C are about one third

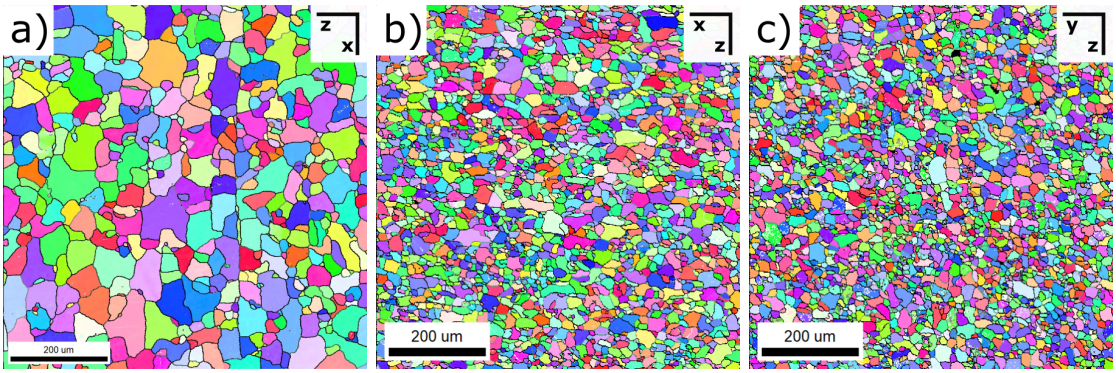

Figure 5.2.5: *Inverse pole figure (IPF) images of three samples with different grades of deformation ε measured with different linear heating rates and quenched at* 400 °C*:* $\varepsilon = -0.25$, $HR = 1.5\,\mathrm{K\,min^{-1}}$ *(a);* $\varepsilon = -0.61$, $1.5\,\mathrm{K\,min^{-1}}$ *(b);* $\varepsilon = -0.61$, $HR = 4\,\mathrm{K\,min^{-1}}$ *(c)*

the size of the grain sizes in the starting material, the grain size of the lower deformed sample remains almost unchanged during recrystallisation. The amount of LAB after heat treatment is considerably low in all three samples as can be seen in Fig. 5.2.5, therefore recrystallisation/ recovery seems to be finished after heating to 400 °C. Since all three images of Fig. 5.2.5 show an equiaxed, homogeneous grain structure, which is in contrast to the grain structure of the starting condition, it can be concluded that recrystallisation played a mayor role during the annealing process of all three sample combinations. What can also be seen is an alignment of the recrystallized grains alongside the aligned particles. As mentioned in chapter 4.2.2, particles are aligned in the rolling direction (x) of the production process as done by the manufacturer. In Figs. 5.2.5 a) and b), the images were taken of the xz- plane of the samples and an alignment of the recrystallized grains in x- direction can be seen. In Fig. 5.2.5 c), the images was taken of the yz- plane of the sample and no alignment of recrystallized grains can be seen.
Additionally, as one would expect, the final grain size of the higher deformed samples is smaller than the grain size of the lower deformed sample after recrystallisation.

To study the evolution of recrystallisation over the period of the four mentioned temperature steps, orientation deviation (GROD) maps are extremely helpful. An orientation deviation map (ODM) shows the deviation in angle of each point amid defined grain boundaries from the standard orientation of this grain. Therefore, these maps can reveal the amount of recovery which has happened between different temperature steps as well as whether and where recrystallisation has already started, since recrystallized grains show no deviation from the standard grain orientation amid its boundaries.

Looking at the ODM of the deformed starting material (see Fig. 5.2.6), one can see, that all three samples show a high amount of misorientation, and as expected, it is higher for the samples with higher deformation.
After reaching a temperature of 100 °C, little of this misorientation has been released, however, after reaching 200 °C some spots, where the misorientation is lower can be seen in all of the three samples. At 300 °C, recrystallisation is in progress. One can see small recrystallized grains amid other non recrystallized grains with higher misorientation. The sample with a low heating rate and a high deformation has the largest fraction of grains re-

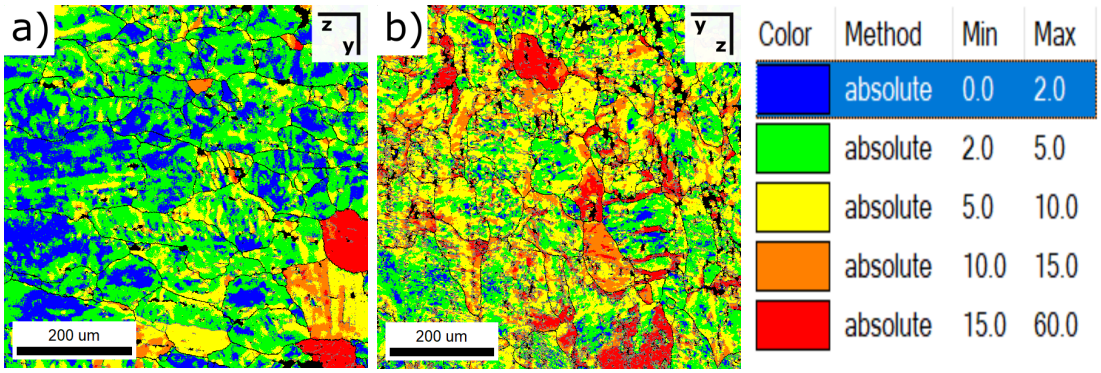

Figure 5.2.6: *ODM for a)* $\varepsilon = -0.25$ *and b)* $\varepsilon = -0.61$ *without heat treatment; key for the coloring of the min, max values of the misorientation in degree*

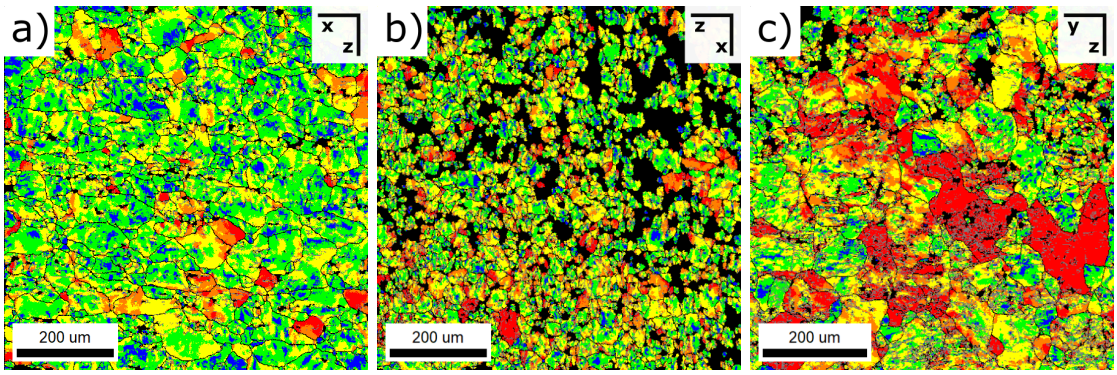

Figure 5.2.7: *ODM for samples quenched from* 100 °C*:*
a) $\varepsilon = -0.25$, $HR = 1.5\,\mathrm{K\,min^{-1}}$*; b)* $\varepsilon = -0.61$, $HR = 1.5\,\mathrm{K\,min^{-1}}$*; c)* $\varepsilon = -0.61$, $HR = 4\,\mathrm{K\,min^{-1}}$

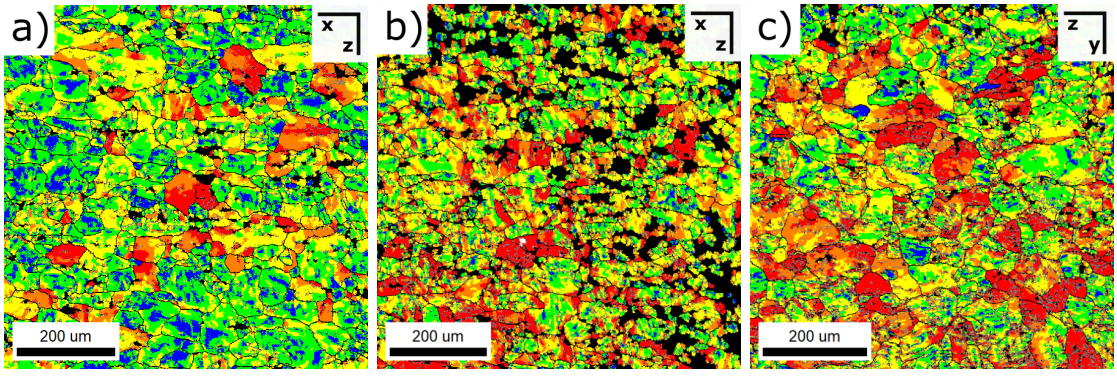

Figure 5.2.8: *ODM for samples quenched from* 200 °C*:*
a) $\varepsilon = -0.25$, $HR = 1.5\,\mathrm{K\,min^{-1}}$*; b)* $\varepsilon = -0.61$, $HR = 1.5\,\mathrm{K\,min^{-1}}$*; c)* $\varepsilon = -0.61$, $HR = 4\,\mathrm{K\,min^{-1}}$

crystallized, the sample with low deformation and a low heating rate has the least fraction of grains recrystallized. Reaching 400 °C, recrystallization has finished for the majority of grains, both samples with a high deformation show an equal number of recrystallized grains of the same size, the sample with low deformation shows larger grains, but also,

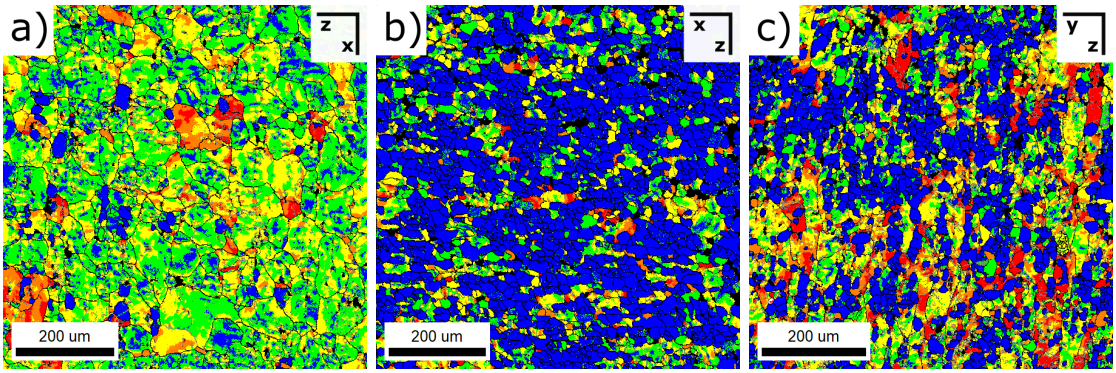

Figure 5.2.9: *ODM for samples quenched from* 300 °C*:*
a) $\varepsilon = -0.25$, $HR = 1.5\,\mathrm{K\,min^{-1}}$*; b)* $\varepsilon = -0.61$, $HR = 1.5\,\mathrm{K\,min^{-1}}$*; c)* $\varepsilon = -0.61$, $HR = 4\,\mathrm{K\,min^{-1}}$

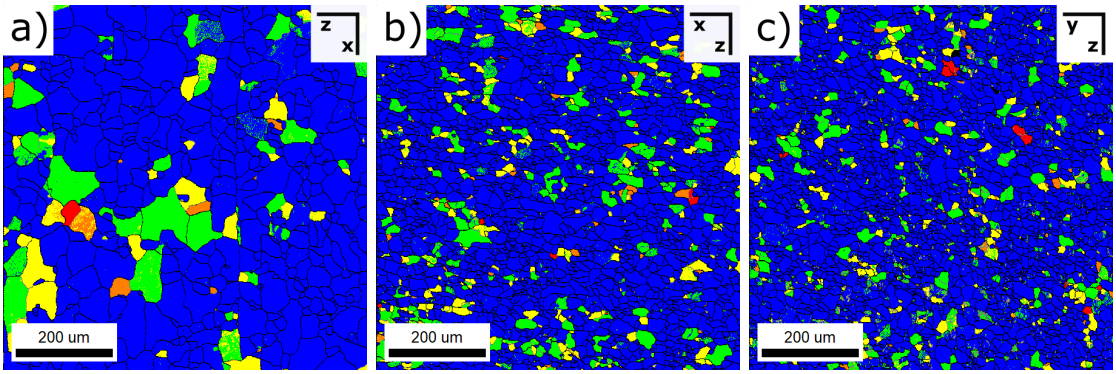

Figure 5.2.10: *ODM for samples quenched from* 400 °C*:*
a) $\varepsilon = -0.25$, $HR = 1.5\,\mathrm{K\,min^{-1}}$*; b)* $\varepsilon = -0.61$, $HR = 1.5\,\mathrm{K\,min^{-1}}$*; c)* $\varepsilon = -0.61$, $HR = 4\,\mathrm{K\,min^{-1}}$

the majority of grains is recrystallized. The above mentioned EBSD micro graphs are shown in Fig. 5.2.6 to 5.2.10.

Another helpful diagram, which can be used to exemplify the fraction of recrystallized grains in a sample is the grain orientation spread (GOS). The GOS works similar to the orientation deviation, where the deviation from the standard orientation of each grain is calculated for the whole area, but contrary to the OD in GOS, this deviation is averaged over the whole grain. Figure 5.2.11 shows a GOS map of a sample with $\varepsilon = -0.61$ heated with a rate of $1.5\,\mathrm{K\,min^{-1}}$ and quenched at 300 °C (compare to Fig. 5.2.9b).

To get an overview over the number of recrystallized grains in a sample, the area fraction each angle of misorientation takes up is calculated and a boundary value of misorientation is set to define the boundary between a recrystallized and a not recrystallized grain. For the following analysis, this boundary value was set to 2° and below for recrystallized grains. The fraction of recrystallized grains ia calculated by an integration of the area fraction from 0° misorientation to 2° misorientation. Figure 5.2.12 shows the fraction of recrystallized grains at each temperature for each measurement combination, Fig. 5.2.13 shows grain images with only recrystallized grains.
The fraction of recrystallized grains from RT to 200 °C is almost zero. When recrystalli-

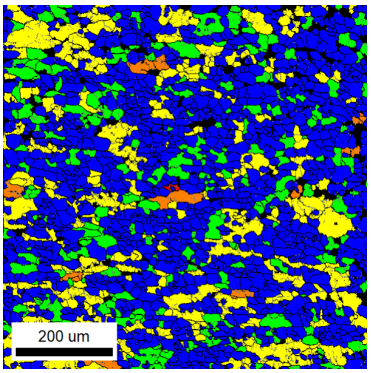

Figure 5.2.11: *GOS image for a sample with* $\varepsilon = -0.61$, *HR* $= 1.5\,\mathrm{K\,min^{-1}}$ *after quenching from* 300 °C *(same sample as shown in Fig. 5.2.9b). A GOS image shows the misorientation to the initial orientation of the grain averaged over the whole grain.*

sation has started at 300 °C, for $\varepsilon = -0.25$, HR $= 1.5\,\mathrm{K\,min^{-1}}$, only a small fraction of all grains is recrystallized, for $\varepsilon = -0.61$, HR $= 4\,\mathrm{K\,min^{-1}}$, a large part is recrystallized and for $\varepsilon = -0.61$, HR $= 1.5\,\mathrm{K\,min^{-1}}$, more than half is recrystallized. At 400 °C, all three sample combinations are almost fully recrystallized, the difference between them is marginal.
So recrystallization seems to start around 300 °C for $\varepsilon = -0.25$, HR $= 1.5\,\mathrm{K\,min^{-1}}$ and before 300 °C for $\varepsilon = -0.61$, HR $= 1.5\,\mathrm{K\,min^{-1}}$ and $\varepsilon = -0.61$, HR $= 4\,\mathrm{K\,min^{-1}}$. This is reasonable, since the starting point of recrystallization is dependent on the grade of deformation. The higher the stored energy in the sample, the earlier recrystallization starts.
For the samples with higher deformation, the one with a lower heating rate has a larger fraction already recrystallized at 300 °C, which is also reasonable, since when heating with a higher heating rate, there is less time for nucleation and recrystallization to take place. Therefore, the fraction of recrystallization at 300 °C is higher for $\varepsilon = -0.61$, HR $= 1.5\,\mathrm{K\,min^{-1}}$.
However, since there is less time for recrystallisation, there is also less time for other processes such as recovery, which take place at lower temperature and therefore less stored is energy is consumed in these processes. This may be the reason why the sample with $\varepsilon = -0.61$ and HR $= 4\,\mathrm{K\,min^{-1}}$ has a slightly larger percentage of recrystallized grains compared to the sample wiht $\varepsilon = -0.61$ and HR $= 1.5\,\mathrm{K\,min^{-1}}$, since more stored energy was available during recrystallisation for the first sample mentioned.

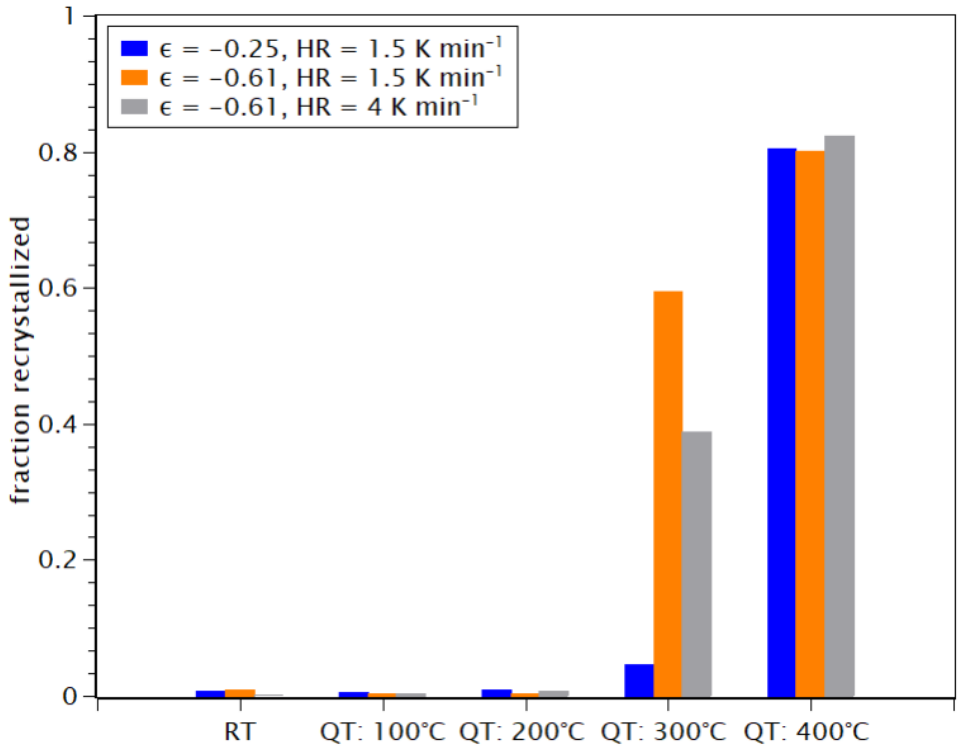

Figure 5.2.12: *Fraction of recrystallized grains for each temperature step calculated as mentioned in the text. At* 400 °C*, the fraction of recrystallized grains is almost the same for all three grades of deformation. However, at* 300 °C*, the fraction of recrystallized grains is highest for the slowly heated, higher deformed sample and lowest for the slowly heated, lower deformed sample.*

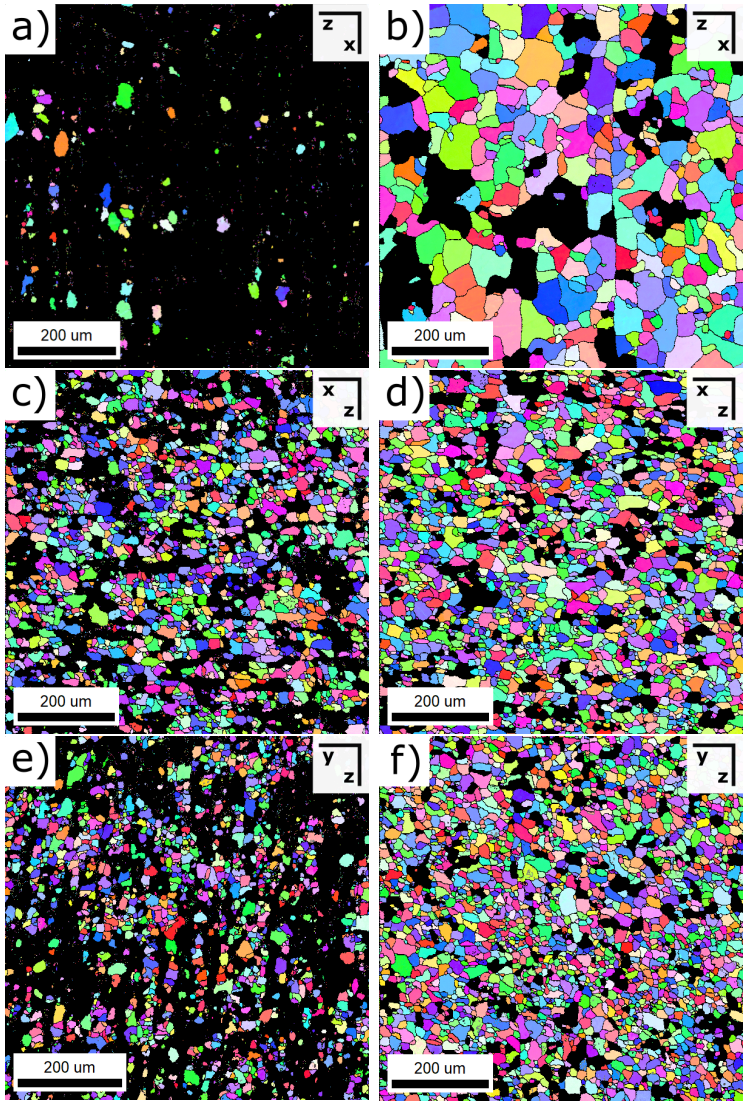

Figure 5.2.13: *Grain images showing only recrystallized grains displayed after quenching from temperatures* 300 °C*(a,c,e) and* 400 °C*(b,d,f):* $\varepsilon = -0.25$, $HR = 1.5\,\mathrm{K\,min^{-1}}$*(a,b);* $\varepsilon = -0.61$, $HR = 1.5\,\mathrm{K\,min^{-1}}$*(c,d) and* $\varepsilon = -0.61$, $HR = 4\,\mathrm{K\,min^{-1}}$*(e,f). These images confirm the conclusions drawn according to the results shown in Fig. 5.2.12*

When analysing the evolution of recrystallisation in the temperature regime between 0 °C and 500 °C, one can also compare the change in the length of the low angle boundaries with increasing temperature (Fig. 5.2.14).

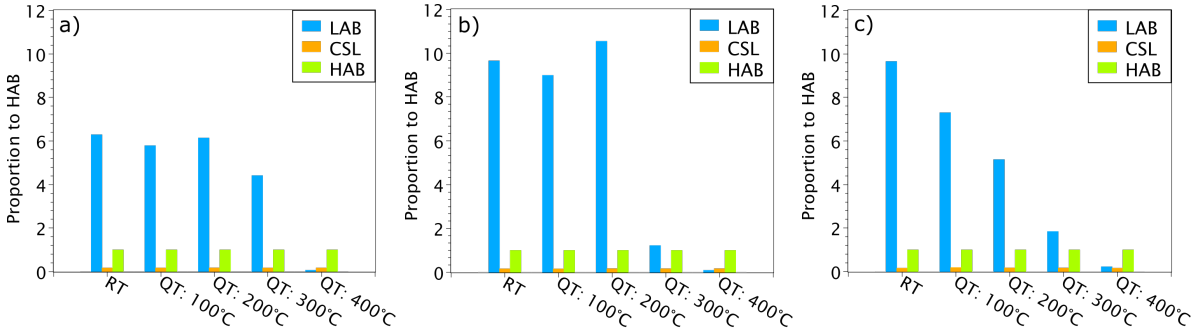

Figure 5.2.14: *Change in low angle boundary length (LAB) at each temperature step normalised to high angle boundary (HAB) length:* $\varepsilon = -0.25$, $HR = 1.5\,\mathrm{K\,min^{-1}}$ *(a);* $\varepsilon = -0.61$, $HR = 1.5\,\mathrm{K\,min^{-1}}$ *(b) and* $\varepsilon = -0.61$, $HR = 4\,\mathrm{K\,min^{-1}}$ *(c).*

In the lower deformed sample, the LAB length changes rapidly between 300 °C and 400 °C, in the higher deformed samples, the change occurs between 200 °C and 400 °C. So in the lower deformed sample, recrystallisation seems to start at temperature higher than 300 °C, in higher deformed samples below 300 °C. Moreover in the sample heated with a higher heating rate, the fraction of LAB is higher at 300 °C than in the sample with a lower heating rate which is also consistent with the conclusions gained before.

5.3 Difference Dilatometry with isothermal annealing

This test series was performed to study the behavior of the deformed material during isothermal annealing. For samples with a deformation of either $\varepsilon = -0.25$ or $\varepsilon = -0.61$ the length change was measured according to the temperature program as sketched in Fig. 5.3.1. The samples were heated up to different temperatures with a heating rate of 10 K/min, held for an hour at this temperature and then cooled back to RT.

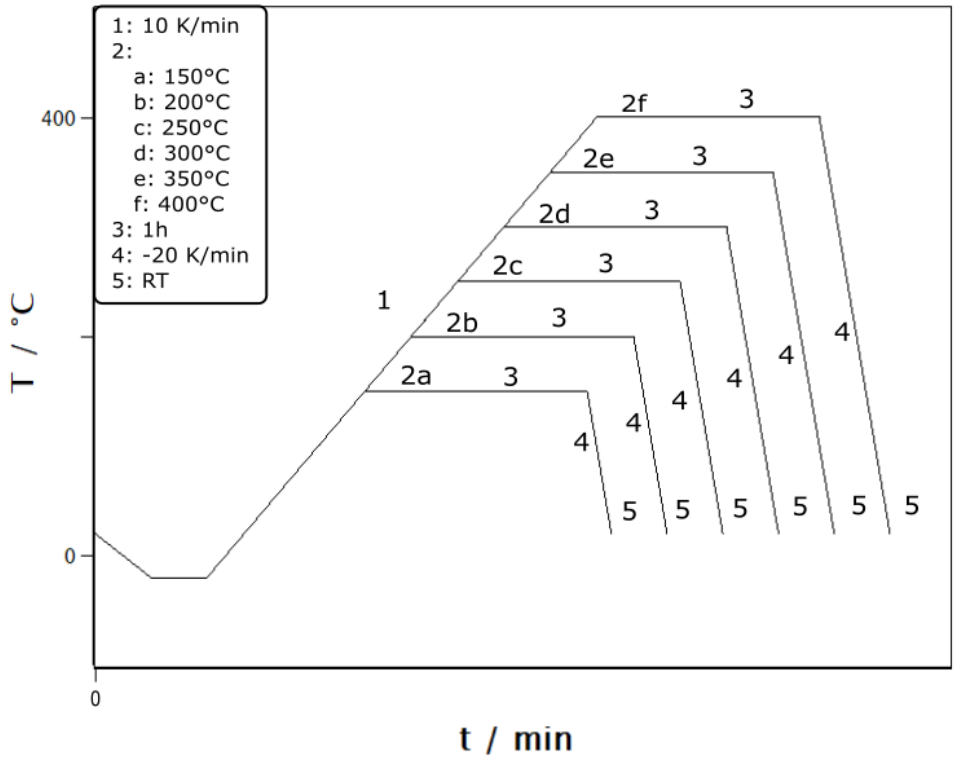

Figure 5.3.1: *Temperature program for the isothermal dilatometric measurement series.*

Figure 5.3.2 and 5.3.3 show the results of the isothermal measurements, displaying the dilatometer curve of the whole measurements (Figs. 5.3.2 and 5.3.3 a) and the length changes during isothermal annealing (Figs. 5.3.2 and 5.3.3 b). The dilatometer curves show a steep decrease in length in the regime of linear heating to the annealing temperature and steady decrease during isothermal annealing. There seems to be a rough trend considering the correlation between the absolute length change and the annealing temperature, namely an increase in length change with increasing annealing temperature. For both deformations, $\varepsilon = -0.25$ and $\varepsilon = -0.61$, the values for the absolute length changes follow the same order when increasing the annealing temperature. A little to no change in length can be seen for a annealing temperature of 150 °C, a greater change in length for annealing temperatures of 200 °C and 250 °C and an even greater change in length when annealing at $T_a = 300$ °C and 350 °C. An exception in this order are the values for the the absolute length change at $T_a = 400$ °C, which are much higher than the values of the other measurements for a the deformation of $\varepsilon = -0.25$ and in the same order of magnitude for a deformation of $\varepsilon = -0.61$. There, the absolute length change at $T_a = 400$ °C is around the values of absolute length change at $T_a = 250$ °C and $T_a = 200$ °C and lower than the

absolute length changes at $T_a = 300\,°C$ and $T_a = 350\,°C$. Considering solely the values for the length changes during isothermal annealing (Figs. 5.3.2 and 5.3.3 b) one can see a steady increase in length change with increasing annealing temperature. However, one exception in this scheme, which occurs for both grades of deformation are the values for the length change at 300 °C, which are even higher than the values of length change at annealing temperatures of 350 °C and 400 °C.
Two different processes occurring at temperatures around 200 °C and 300 °C would be a reasonable explanation for the results described above. A more detailed discussion will be made in the discussion chapter (see chapter 6.1).

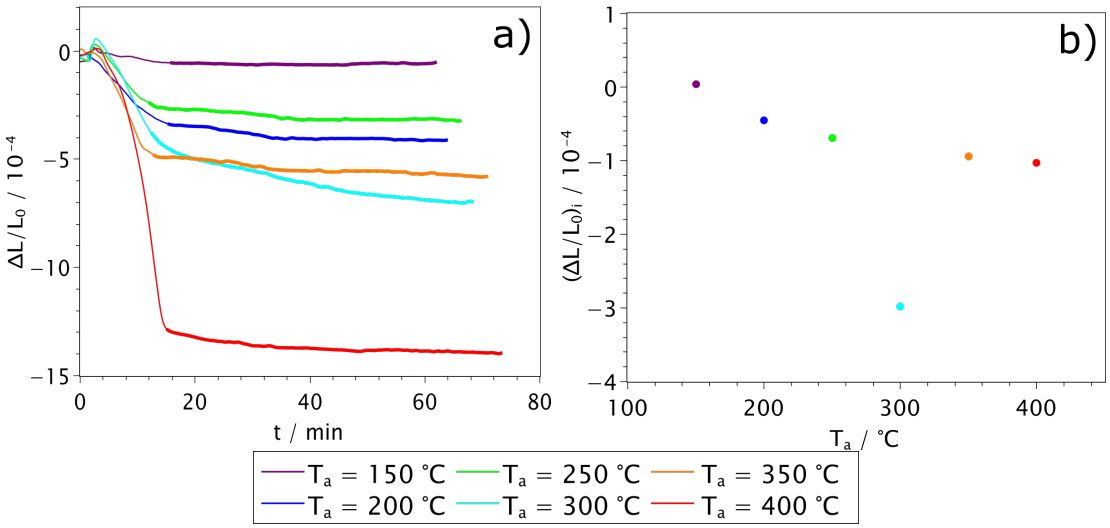

Figure 5.3.2: *Dilatometer curves of the isothermal measurements as function of time for samples with a deformation of $\varepsilon = -0.25$ (a). The region of isothermal annealing after initially heating up with $10\,\mathrm{K\,min^{-1}}$ to the annealing temperature is accentuated with a thick line. The amount of the absolute length change during isothermal annealing $(\frac{\Delta L}{L_0})_i$ is shown in (b) as a function of annealing temperature.*

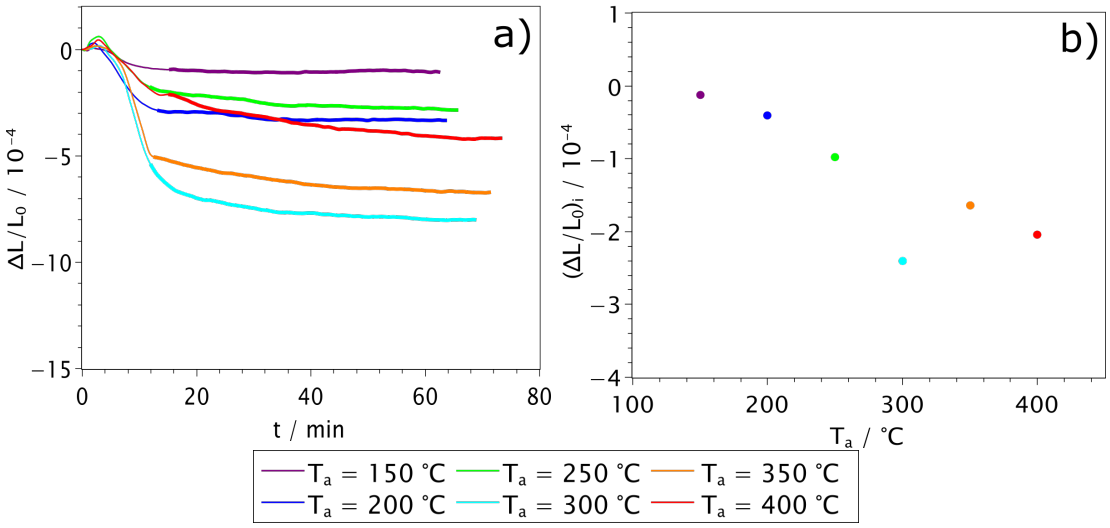

Figure 5.3.3: *Dilatometer curves of the isothermal measurements as function of time for samples with a deformation of* $\varepsilon = -0.61$ *(a). The region of isothermal annealing after initially heating up with* $10\,\mathrm{K\,min^{-1}}$ *to the annealing temperature is accentuated with a thick line. The amount of the absolute length change during isothermal annealing* $(\frac{\Delta L}{L_0})_i$ *is shown in (b) as a function of annealing temperature.*

Hardness measurements To get some more information on the processes believed to occur around 200 °C and 300 °C, an additional type of measurement was made. Samples were deformed with $\varepsilon = -0.61$, annealed at either 200 °C or 300 °C and quenched after a certain amount of time. Then the hardness of the quenched samples was measured and a trend as shown in Fig. 5.3.4 was found.

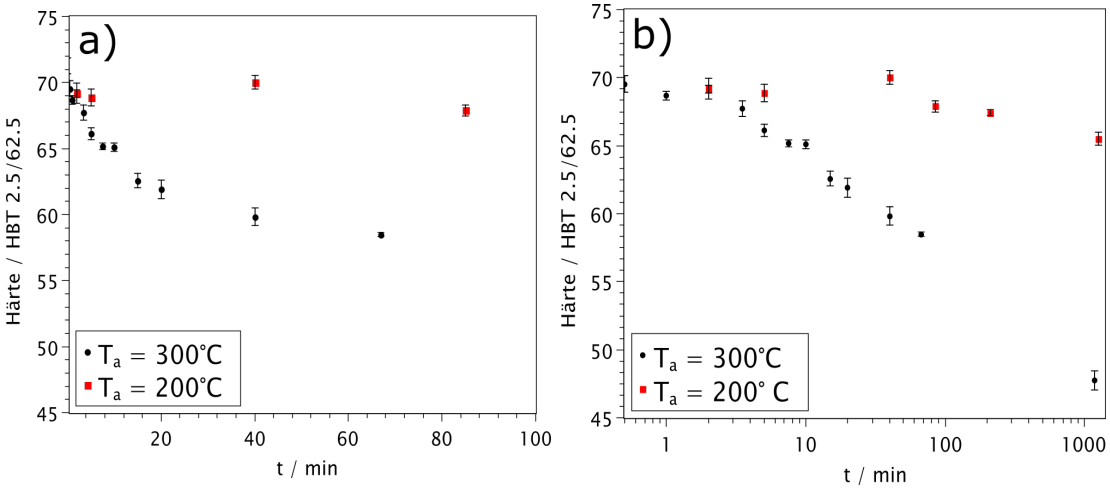

Figure 5.3.4: *Hardness measurements of samples (*$\varepsilon = -0.61$*) annealed at* 200 °C *or* 300 °C*; a) linear scale over a shorter time intervall, b) logarythmic scale over a longer time intervall*

Upon annealing at 300 °C, the hardness value decreases rapidly at the beginning to resolve in a steady decrease over a long time period. Annealing at 200 °C, leads to a less intense decrease in hardness, even after a long period of annealing time.

When using a logarithmic scale, one can see that the decrease in hardness upon annealing at 300 °C follows a logarithmic relation, which is also an indication for recrystallisation occurring at this temperature.

6 Discussion

This chapter deals with the issue of finding reasonable explanations for the results and observations reported in the previous chapters. Hypotheses will be made and it will be tried to verify them with the results of the measurements and other external sources. This will be done for the purpose of combining the results of each measurement type to obtain a reasonable overall picture of the whole annealing process.

As found in chapter 5.1, from the results of the dilatometric measurements three separate stages (I,II,III) can be distinguished, in which different processes occur. Stage II is assumed to be caused by recrystallisation and will be discussed in the first section. It is also reasonable to assume, that stage I is caused by a variety of processes during recovery. Stage III may be caused by grain growth of the freshly recrystallized micro structure. However, no further attention will be paid to this last stage, due to the fact, that data measured at the end point temperature of a dilatometric measurement may not be reliable enough. There is no assurance, that the measurements completely cover all parts of a process occurring in stage III, and that it is finished at the end temperature of the measurement.

6.1 Recrystallisation

Recrystallisation is expected to take place in stage II which can be seen in the dilatometric curves measured parallel and perpendicular to the direction of deformation. Recrystallisation in aluminium alloys usually takes place in the temperatures regime between 300 °C and 500 °C [23, 24, 25] and therefore, the position of the two peaks found in the derivatives of the dilatometer curves seems to fit. The whole process of recrystallisation can be further sub classified into two separate processes, nucleation and then growth of the formed nuclei. It is suggested, that these two processes can be distinguished from a difference dilatometer curve and its derivative so the first peak in the derivative curve in stage II can be assigned to the nucleation process and the second peak to the growth of the nuclei. The results of the isothermal annealing measurements on the other hand also support the occurrence of two different processes in this temperature regime. The small, overall length change upon heating to and annealing at 200 °C and 250 °C may be caused by nucleation occurring in this temperature regime and greater length change may be caused by the process of growth when heating to and annealing at 300 °C and higher temperatures. Now, in the following two subsections it will be tried to proof these assumptions.

6.1.1 Nucleation

During nucleation, small areas of a new crystal structure are formed mostly at the old grain boundaries. The results of the EBSD measurements suggest, that early nucleation in this material starts around 200 °C. The onset of the peaks of stage IIa in samples measured parallel and perpendicular to the direction of deformation is usually found around 200 °C, which can be handled as a first proof, that these peaks are caused by the nucleation process. Moreover, the results of the dilatometric measurements show, that the temperatures of the peaks in stage IIa do vary to some extent when changing the heating rate or the grade of deformation, but this variation does not show a clear pattern of behavior upon the changing of the previously mentioned parameters. Nucleation as a complex process is not fully understood in these alloys until today and the common simplifications used in models suggest, that there is no clear dependence of the onset of nucleation to outer parameters. The lack of a systematic in the shift of the peak temperatures in stage IIa with outer parameters, e.g., the heating rate, can be seen as a second more indirect proof for the assumption previously made, that these peaks are caused by nucleation.

6.1.2 Growth

In stage IIb of the dilatometric curves measured parallel and perpendicular to the direction of deformation, one very distinct peak is found around 300 °C. This process occurring in stage IIb is most likely the growth of the nuclei formed in the previous process occurring in stage IIa. The growth of the nuclei during recrystallisation, which is dependent on the movement of high angle boundaries is a thermally activated process. Therefore, the onset of the growth is dependent on the heating rate, HR, as can also be seen in the shift of the peak temperatures, T_p derived from the dilatometry measurements where a lower heating rate results in a lower T_p. Additionally, the onset temperature for recrystallisation and therefore the growth of nuclei is also dependent on the grade of deformation, ε, introduced to the sample. The movement of high angle boundaries is dependent on the driving

pressure which is proportional to a certain amount of stored energy present in the sample, which increases with increasing deformation. Therefore, a higher grade of deformation results in an earlier onset of recrystallisation, or growth of these nuclei in particular. The peak temperatures in stage IIb of the dilatometry curves shift in the same manner, as would be expected from the shift of the maximum rate of growth during recrystallisation. The results of the dilatometry measurements therefore support the hypothesis, that the peak in IIb can be assigned to the growth of nuclei during recrystallisation. Another support are the results of the EBSD measurements, which show, that the growth of nuclei during recrystallisation starts around 300 °C in a lower deformed sample ($\varepsilon = -0.25$) and at temperatures below 300 °C in a higher deformed sample ($\varepsilon = -0.61$).
The fraction of grains recrystallized at 300 °C is higher for higher deformed samples and additionally, samples with a higher grade of deformation show a decrease in low angle boundary (LAB) share in a temperature range between 200 °C and 400 °C, whereas in samples with a lower grade of deformation, LAB share decreases considerably only, when reaching a temperature of 300 °C. When considering the average misorientation angle that decreases during annealing, the same trend can be seen. Lower deformed samples have a lower amount of misorientation at the beginning but nevertheless, the decrease of misorientaion during annealing is starting at higher temperatures compared to the decrease of misorientation in higher deformed samples, which starts at lower temperatures. Therefore, a clear dependency of the onset of recrystallisation on the previous deformation in the examined alloy is confirmed. It can be concluded, that due to a lower amount of stored energy, the onset of recrystallisation is shifted to higher temperatures in less deformed samples, which is in perfect alignment with the results of the difference dilatometric measurements. Additionally, in annealed samples with a lower amount of deformation previuosly introduced, the final grain structure is more coarse which is also consistent with common literature [2].

6.1.3 Calculation of the apparent activation energy of recrystallisation

Since recrystallisation is a thermally activated process and the temperature of maximum reaction rate of this process shifts with a changing heating rate (HR), the activation energy E_A can be calculated, e.g., according to Kissinger [26, 27, 28], an example is shown in Fig. 6.1.1.

When calculating the apparent activation energies from the peaks received from the analysis of the derivatives of the dilatometric measurements done perpendicular to the direction of deformation one can see a tendency as shown in Fig. 6.1.2. Lower deformed samples seem to need a higher apparent activation energy for recrystallisation to proceed [29]. Since the amount of stored energy is higher in higher deformed samples, it seems only reasonable, that a lower apparent activation energy is needed in higher deformed samples for recrystallisation to start as in lower deformed samples [29].

It is also possible to calculate apparent activation energies for recrystallisation with the shift of the peak positions determined from the dilatometric measurements performed parallel to the direction of deformation. It can be expected, that the values for the apparent activation energy are similar to the values determined by the shift of peaks from the measurements done perpendicular to the direction of deformation. However, a difference to the apparent activation energies determined from the "perpendicular"

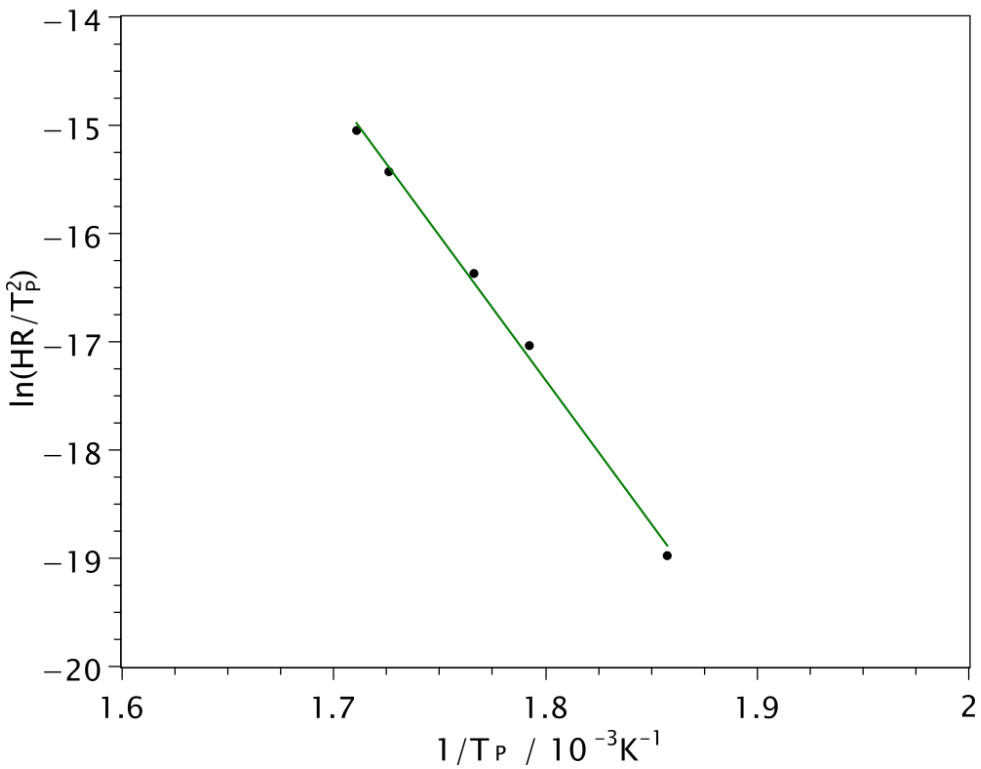

Figure 6.1.1: *Kissinger plot: Heating rates divided by the square of the peak temperature are logarithmically plotted versus the reciprocal peak temperature obtained from measurements with different heating rates for samples with a deformation of* $\varepsilon = -0.61$ *to calculate the apparent activation energy for the recrystallisation process.*

measurements on the other hand would not be surprising due to the anisotropic behavior of the samples during annealing. Unfortunately, it was not possible to do a Kissinger analysis for all the data received from the measurements done parallel to the direction of deformation. The linear fit done for the Kissinger plot was good in some cases, but was not satisfactory in other cases. Therefore, only the data, which resulted in a good correlation were taken to calculate the apparent activation energies for the parallel measurement direction as shown in Fig. 6.1.3. The values for these apparent activation energies are similar to the values determined for the perpendicular direction.

Activation energies E_A in the range of 1.8 eV to 2.2 eV for static recrystallisation in aluminum alloys with similar composition to AW 5754 have also been reported by others [30, 29, 31].

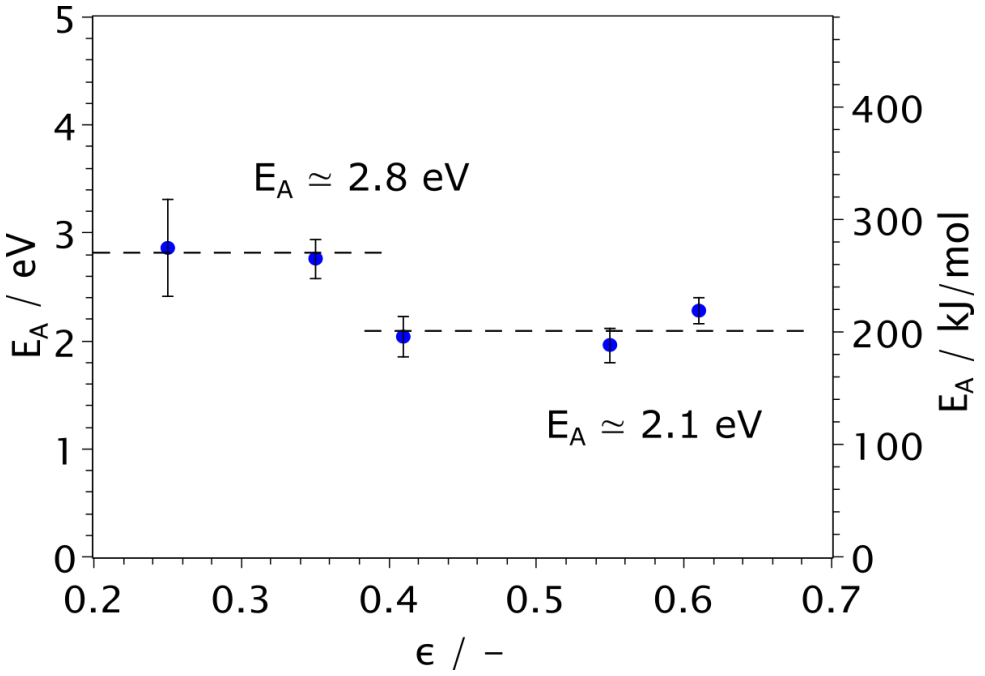

Figure 6.1.2: *Apparent activation energies of recrystallisation for different grades of deformation calculated from the shift of peak positions found in stage IIb of the measurements done perpendicular to the direction of deformation. The apparent activation energy seems to decrease with increasing grade of deformation.*

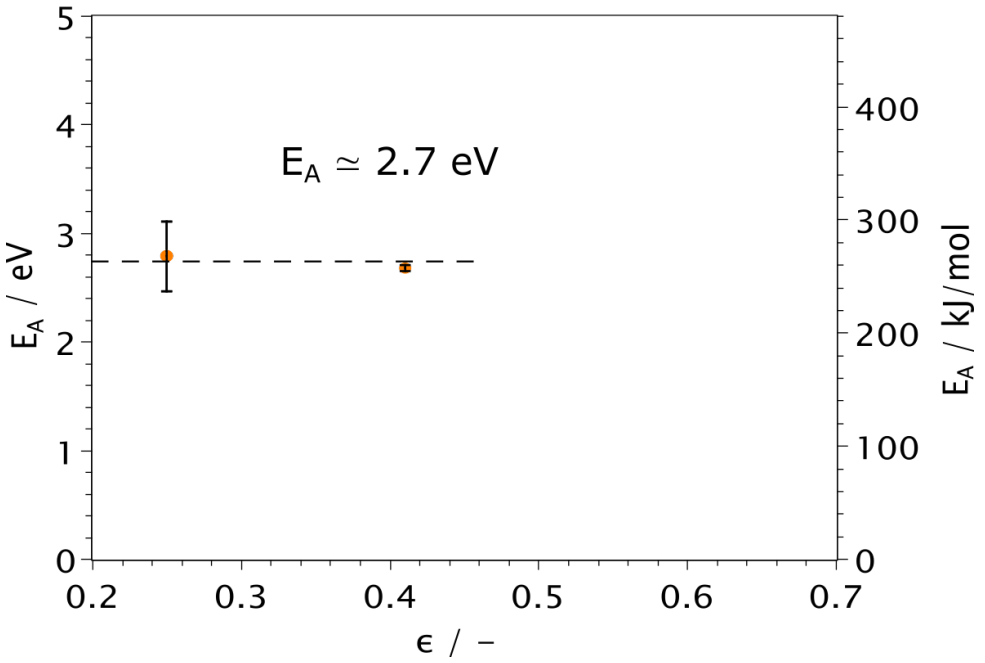

Figure 6.1.3: *Apparent activation energies calculated from the shift of the peaks in stage IIb of the measurements done parallel to the direction of deformation. The apparent activation energies for recrystallisation in this direction are similar in value to the apparent activation energies for recrystallisation perpendicular to the direction of deformation.*

6.2 Recovery

When considering the difference dilatometer curves, samples measured perpendicular to the direction of deformation have been observed to show different behavior compared to samples measured parallel to the direction of deformation considering the length change. Samples measured perpendicular to the direction of deformation show a steady decrease in length change in comparison to a fully recovered reference samples. Samples measured parallel to the direction of deformation on the other hand show an increase in length change in the low- temperature regime, which is followed by a steep decrease in the last stages. The onset of this decrease is dependent on the grade of deformation ε, where a higher grade of deformation leads to an earlier onset. This great decrease in length is caused by the recrystallisation process and therefore, its only reasonable that the onset of this decrease shifts with a changing grade of deformation. Recovery in aluminium on the other hand usually occurs in a temperature range between room temperature and to 100 °C during annealing [32]. The anisotropy in length change can be explained by direction dependent recovery in the low temperature regime of the dilatometer curves. Direction dependent recovery may be a result of the grain shape/ profile, Fig. 6.2.1 shows a schematic view of the micro structure after deformation.

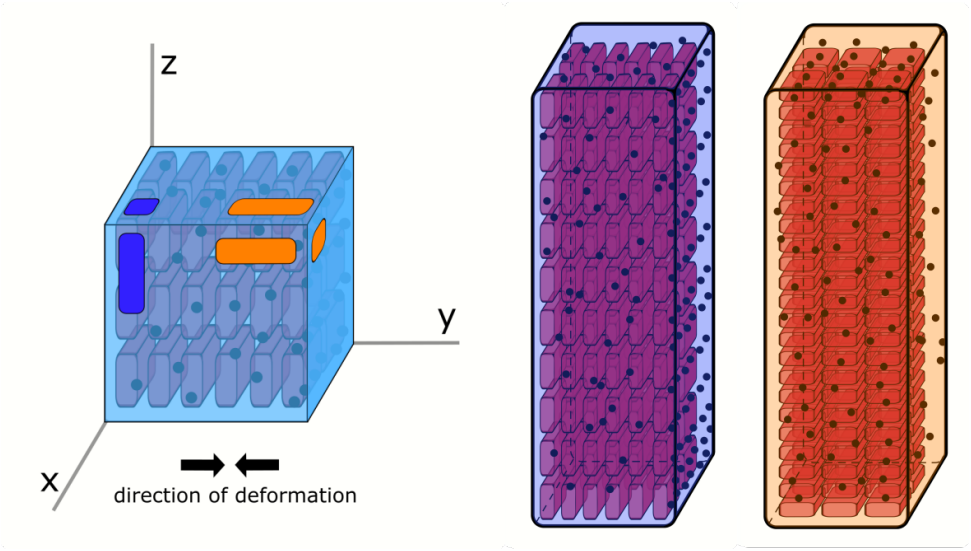

Figure 6.2.1: *Schematic view of the micro structure in the samples cut perpendicular and parallel to the direction of deformation. Grains (outlined red) are disk- shaped and elongated in the xz- plane due to deformation in y direction. Samples were cut perpendicular and parallel to the direction of deformation (outlined blue and orange) and therefore, the disk shaped grains are oriented differently in the measurement direction of both sample types. Inclusions/ particles, indicated by black dots are aligned in x- direction due to the manufacturing process.*

During recovery, dislocations (and vacancies) among other processes like cell formation, move to the high angle boundaries. An increase in dislocation density may cause an expansion of these boundaries, which then counteracts the decrease in length caused by other processes during recovery. Since the density of grain boundaries is much higher parallel than perpendicular to the direction of deformation, these process of grain boundary expansion would have a much greater impact on measurements performed parallel to

the direction of deformation. However, to prove this hypothesis, further analysis of the high angle boundaries at different temperature steps with, e.g., TEM has to be done.

There is another important difference between the dilatometric measurements performed parallel to the direction of deformation and the ones performed perpendicular to the direction of deformation. In the measurements performed perpendicular to the direction of deformation, the process in stage I results in two separate peaks in the derivative curves of the dilatometry curves. In the derivative curves of the measurements done parallel to the direction of deformation, only one broad peak can be distinguished. This may be an indication for some additional process(es) occurring only or to a greater extent in the parallel measurement direction, but not or to a lesser extent in the perpendicular measurement direction.

6.2.1 Calculation of an apparent activation energy of recovery

Similar to the calculation of the apparent activation energy of the recrystallisation process, a calculation of the apparent activation energy for the process occurring in stage I in the "parallel" measurements and in stage Ia in the "perpendicular" measurements can be done by Kissinger analysis. It was possible to do Kissinger analysis with all the data gained from the measurements perpendicular to the direction of deformation as the linear fits of these plots were good, but only a part of the data received from the measurements done parallel to the direction of deformation could be used for Kissinger analysis as not all linear fits met the sufficient requirements.
Fig. 6.2.2 shows the activation energies calculated from the slope of the linear fits of the data received from the measurements done perpendicular (a) and parallel (b) to the direction of deformation.

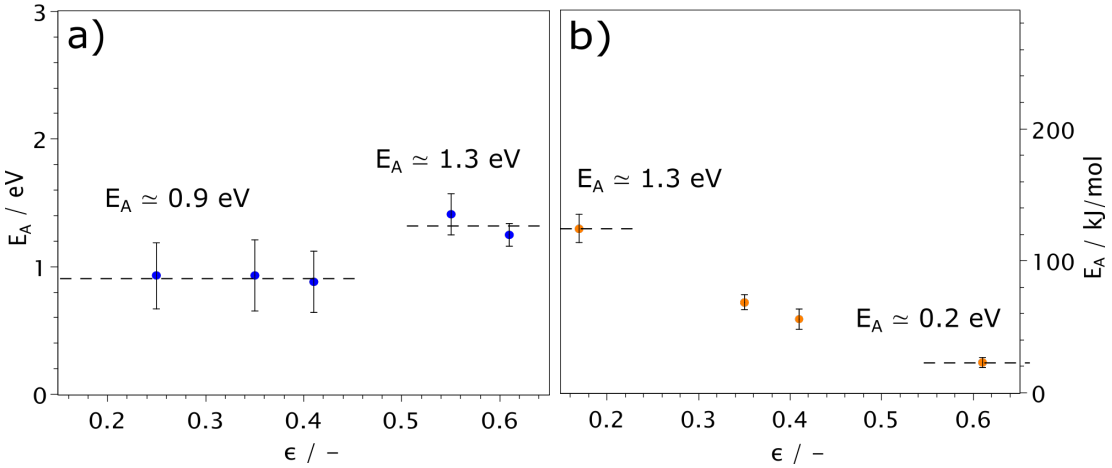

Figure 6.2.2: *Apparent activation energies calculated for the recovery process in stage I for the measurements perpendicular (a) and parallel (b) to the direction of deformation. Activation energies increase with increasing deformation when measured perpendicular (a) to the direction of deformation and decrease with increasing deformation when measured parallel to the direction of deformation (b)*

The apparent activation energies calculated from the data gained from the "perpendicular" measurements are slightly higher for samples with a higher deformation, which

Table 6.2.1: *Apparent activation energies (eV) for the recovery (Rec) and the recrystallisation (REX) process in perpendicular and parallel measurement direction, ε: deformation.*

Process \ ε	**-0.17**	**-0.25**	**-0.35**	**-0.41**	**-0.55**	**-0.61**
$Rec_{\perp}$	-	0.93 ± 0.26	0.93 ± 0.27	0.88 ± 0.24	1.41 ± 0.16	1.25 ± 0.09
$REX_{\perp}$	-	2.86 ± 0.45	2,76 ± 0.18	2.04 ± 0.19	1.96 ± 0.16	2.28 ± 0.12
$Rec_{\parallel}$	1.29 ± 0.11	-	0.71 ± 0.06	0.58 ± 0.08	-	0.24 ± 0.04
$REX_{\parallel}$	-	2.79 ± 0.32	-	2.68 ± 0.03	-	-

is a trend opposite to that seen in the recrystallisation process in stage IIb (Fig. 6.1.2). Contrary to that, the apparent activation energies for this process (stage I) decrease with increasing deformation, when calculated for the "parallel" direction. These findings once again show, that there is an anisotropy in annealing apparent during the recovery process. Activation energies in the range of 0.9 eV to 1.3 eV for different processes occuring during static recovery in aluminum alloys with similar composition have also reported by others [30, 29, 31, 33]

All activation energies that have been calculated in the previous section are summed up in table 6.2.1. The values for the perpendicular direction are average values obtained from two different data sets. First, they have been calculated with the values from table 5.1.2 in chapter 5.1.1 and second, they have been calculated using the values from table 5.1.3 in chapter 5.1.1 which were received from reproducibility measurements. However, reproduciblity measurements have only been done for heating rates of 4 and 1.5 $\mathrm{K\,min^{-1}}$ and for Kissinger analysis, more than three values are needed. Therefore, values for heating rate of 0.1, 0.75 and 6 $\mathrm{K\,min^{-1}}$ have been taken from table 5.1.2 additionally to the values from table 5.1.3 to do the Kissinger analysis.

6.3 Calculation of the total volume change during linear heating annealing

In the previous two sections, the effects of the amount of deformation on the annealing behavior of an AW 5754 alloy during linear heating have been examined. An anisotropy, that means a difference in the annealing behavior parallel and perpendicular to the direction of deformation, has been found and discussed. However, to correlate the total amount of misorientation released from the sample during annealing to various parameters like the grade of deformation, the total volume change of this sample during annealing has to be known. Since measurement of the volume change of a sample is not possible with push- rod dilatometry, it has to be calculated from the relative length changes of different samples with the same grade of deformation measured with the same heating rate. All other parameters like environment temperature, humidity and so forth have been kept alike for all samples measured during the course of this thesis. The age of the sample, which means the time span between the deformation and the measurement of the samples has not been taken into consideration due to the fact, that time of storage at room temperature is believed to have no influence on the annealing behavior of a non age hardenable alloy.

The relative volume change of a cuboid sample as a function of the relative length changes of each side can be derived as following, where V_0, is the original volume, V_1 the volume after (irreversible) length change, x_0, y_0 and z_0 are the original lengths of the cuboid and Δx, Δy and Δz the absolute length changes of each side of the cuboid.

$$V_1 = V_0 + \Delta V = (x_0 + \Delta x)(y_0 + \Delta y)(z_0 + \Delta z) \tag{6.1}$$

Resolving this leads to:

$$\begin{aligned} \Delta V = V_1 - V_0 = x_0 y_0 z_0 + y_0 z_0 \Delta x + x_0 z_0 \Delta y + x_0 y_0 \Delta z + \\ z_0 \Delta x \Delta y + x_0 \Delta y \Delta z + y_0 \Delta x \Delta z + \Delta x \Delta y \Delta z - x_0 y_0 z_0 \end{aligned} \tag{6.2}$$

Deviding by the original volume $V_0 = x_0 y_0 z_0$ leads to the relative volume change $\frac{\Delta V}{V_0}$ as a function of the relative length changes of each side:

$$\frac{\Delta V}{V_0} = \frac{\Delta x}{x_0} + \frac{\Delta y}{y_0} + \frac{\Delta z}{z_0} + \frac{\Delta x}{x_0}\frac{\Delta y}{y_0} + \frac{\Delta y}{y_0}\frac{\Delta z}{z_0} + \frac{\Delta x}{x_0}\frac{\Delta z}{z_0} + \frac{\Delta x}{x_0}\frac{\Delta y}{y_0}\frac{\Delta z}{z_0} \tag{6.3}$$

Assuming, that we have two equivalent directions perpendicular to the direction of deformation x and z and that terms of higher order can be neglected for relative length changes in the range of 10^{-4}, Eq. 6.3 can be simplified as following:

$$\frac{\Delta V}{V_0} = 2\left(\frac{\Delta z}{z_0}\right) + \frac{\Delta y}{y_0} \tag{6.4}$$

Using this equation, an irreversible volume change curve can be calculated from a dilatometer curve measured perpendicular and a dilatometer curve measured parallel to the direction of deformation. Fig. 6.3.1 shows the calculated volume change curves and the corresponding derivatives for a heating rate of $4\,\mathrm{K\,min^{-1}}$.

The volume change curves show the same features as the length change curves. What is more interesting is, that contrary to the single length change curves, now a dependency of the total irreversible volume change on the grade of deformation can clearly be seen. The higher the grade of deformation, the higher is the volume change, a trend, that is hidden, when examining the length change curves only. It seems reasonable, that a greater volume is released during the annealing of a higher deformed sample.

A further analysis that can be made is to look at the total volume change during recrystallisation (stage II) and recovery (stage I), as shown in Fig. 6.3.2. Analysing the volume change during the recovery process occurring in stage I leads to the conclusion, that the overall volume change upon this process seems to be independent on the grade of deformation or the heating rate.

Considering the recrystallisation process occurring in stage II, it can be seen, that the total volume change during this process seems to be dependent on the grade of deformation. A higher grade of deformation seems to cause a higher change in volume which seems also reasonable. The heating rate on the other hand seems to have no influence on the total overall volume change during recrystallisation.

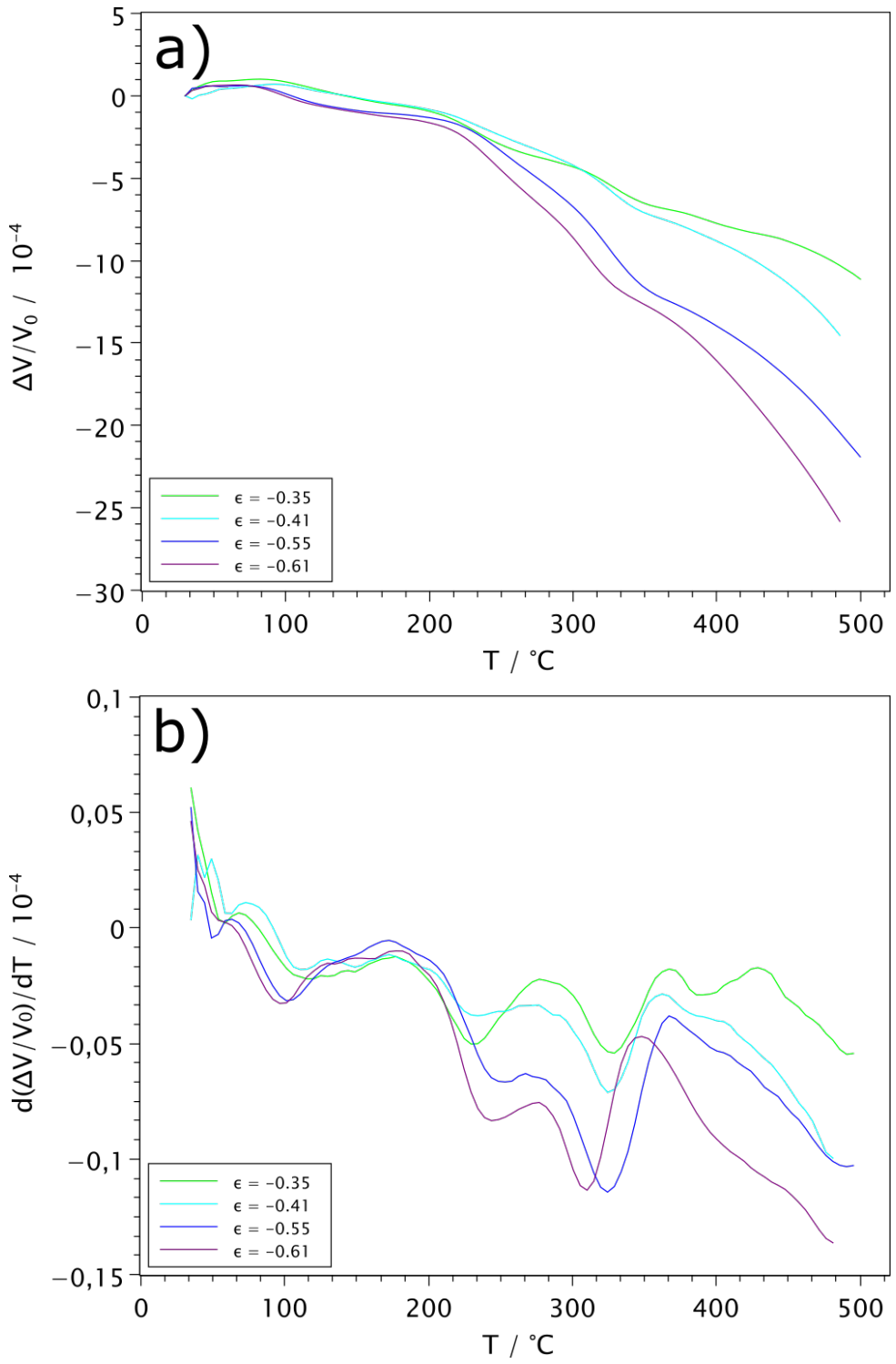

Figure 6.3.1: *Volume change curves for a heating rate of* $4\,\mathrm{K\,min^{-1}}$ *(a) and their corresponding derivatives (b). The curves and the derivatives show the same features as the length change curves: Three stages, two peaks in stage II and one or two peaks in stage I. The peak positions are dependent on the grade of deformation and the heating rate. Moreover, the higher the grade of deformation, the higher is the total irreversible volume change.*

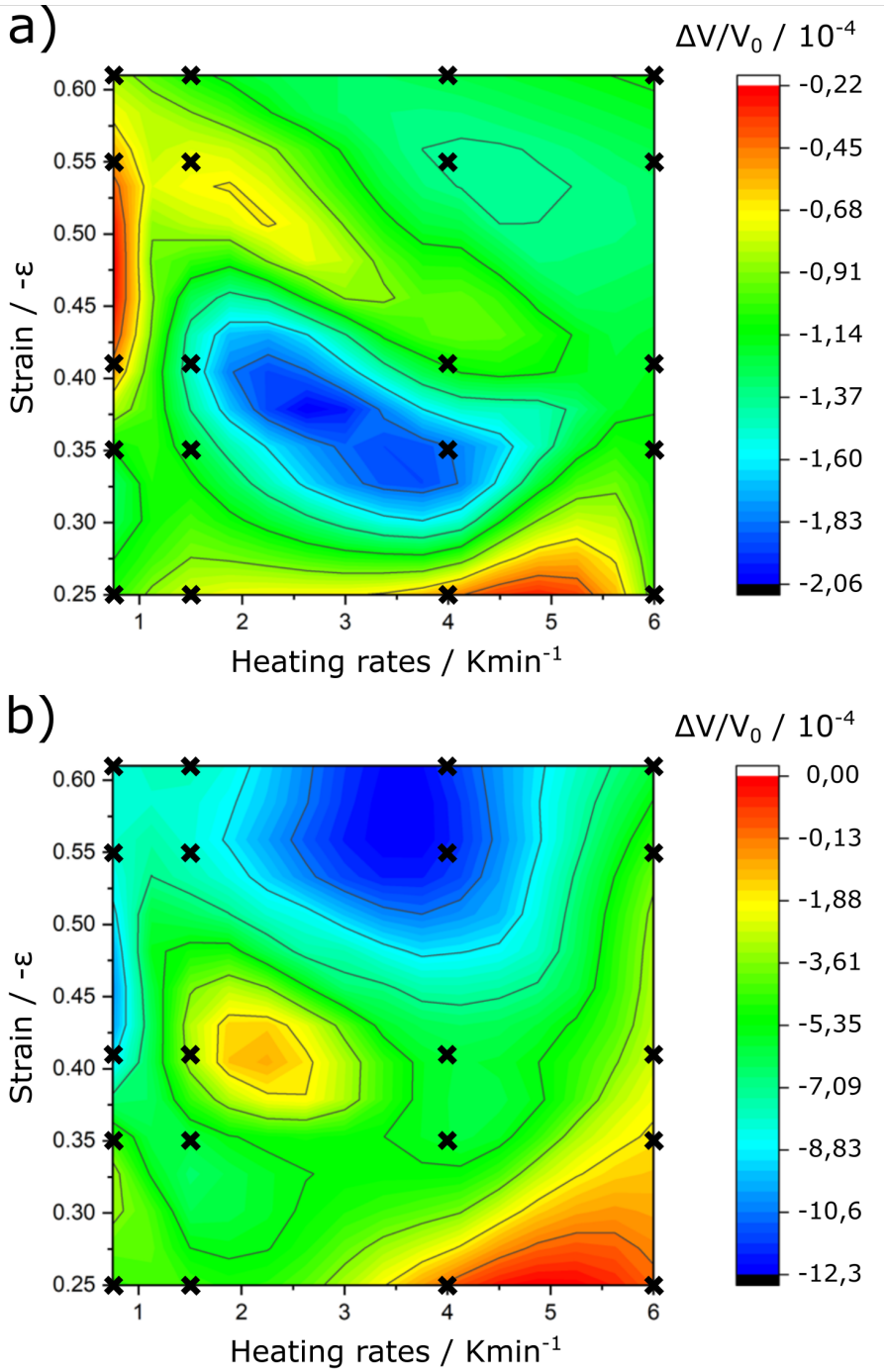

Figure 6.3.2: *Total volume change $\frac{\Delta V}{V_0}$ during recovery in stage I (a) and recrystallisation in stage II (b). For the recovery process, no clear dependency of the total volume change on the grade of deformation or the heating rate is observable.*
For the recrystallisation process on the other hand, no dependency of the total volume change on the heating rate is observed, but a higher grade of deformation seems to cause a higher volume change during recrystallisation.

6.4 Open questions

Finally, some open question remained. First, there has to be done further research for the better understanding of the recovery process. A separate identification of the various processes occuring during recovery with difference dilatometry may be possible. Furthermore, the cause for the anisotropy in length change during the recovery process has yet to be found. Second, the influence of the stable Al_6(Mn,Fe,Si) particles on the annealing procedure and the recrystallized grain structure in combination with the orientation dependency has to be further investigated. Last, the investigation of the influence of changing the composition of the material on the findings of this thesis can give a better view on the overall picture of the annealing process in this kind of alloy.

7 Summary and Outlook

By using dilatometry and electron backscatter diffraction studies of deformed Al-3wt% Mg alloys upon annealing from room temperature up to 500 °C, the main processes of recovery and recrystallisation in this alloy could be assessed. It has been found that the observed irreversible length change upon annealing can be subdivided into three temperature regimes, where the dominant contribution is attributed to recrystallisation.
Recovery has been found to cause a slight decrease in length in comparison to an annealed reference sample in the low temperature regime up to 200 °C. This stage is characterized by various overlapping processes which cause a broad peak in the derivatives of the dilatometry curves. Recrystallisation occurs at temperatures above 200 °C, which results in two seperate peaks, the first one caused by the nucleation process, the second one by growth. Both processes cause a larger change in length in comparison to an annealed reference sample. It has been found, that the onset of growth is shifted to lower temperatures when increasing the grade of deformation or when decreasing the heating rate. The onset of nucleation on the other hand has been shown to be independent on the grade of deformation or the heating rate. With the measurement of extremely high and extremely low deformed samples, it could be shown, that nucleation, and also recovery occur even in very low deformed samples, but for growth during recrystallisation, a minimum grade of deformation of $\varepsilon = -0.04$ is required. There has also been found a dependency of the onset of recovery on these two parameter. Recovery occurs in a temperature range between 60 °C and 180 °C and the onset of at least one process, that occurs in the low temperature regime, is shifted in the same manner as the growth during recrystallisation when changing the heating rate or the grade of deformation. Since the processes occurring during recovery in this material cannot yet be identified with difference dilatometry, further research on the identification of these processes and the capabilities of difference dilatometry to make a separate identification possible is necessary.

It has also been found, that there is an anisotropy in length change during annealing dependent on the direction of measurement. Samples measured parallel to the direction of deformation show an increase in length change in the low temperature regime, which is followed by a decrease when reaching a certain temperature. The temperature of the onset of this decrease has been found to be dependent on the grade of deformation. A higher grade of deformation leads to an earlier onset. Since the onset of this decrease is located in the same temperature range as the onset of recrystallisation, a possible connection between this two apparent processes has been suggested. An earlier onset of recrystallisation, a process which has been found to cause a great change in length in the sample, can lead to an earlier onset of length decrease in samples measured parallel to the direction of deformation.

Measurements done perpendicular to the direction of deformation have shown a different behavior, namely a steady decrease in length during annealing with a great decrease during recrystallisation. However, measurements have been done in one perpendicular direction (z) only and the second perpendicular direction (x) has been assumed to be identical in its annealing behaviour. However, since there is an alignment of stable parti-

cles in one of the perpendicular directions (x), further measurements have yet to be done to prove this assumption. The results of measurements done in x direction could also give further insights into the influence of stable Al_6(Fe,Mn,Si) particles on the annealing process.

The above mentioned anisotropy is mainly caused by processes during static recovery as difference dilatometry shows, presumably as a result of a different orientation of disk shaped grains in samples cut parallel and perpendicular to the direction of deformation. An expansion of grain boundaries upon the migration of dislocations to the gain boundaries, causing an expansion of the sample, that counteracts the decrease in length caused by other processes during recovery has been proposed as a possible explanation. However, this is only a hypothesis to explain the observed anisotropy and further research has to be done for confirmation. Examination of the nature of high and low angle grain boundaries with TEM imaging at different temperature steps during annealing might give a more detailed view on the overall picture.

Kinetic studies have been performed and with Kissinger analysis, the apparent activation energies for recovery and recrystallisation of both measurement directions were calculated. The apparent activation energy of recrystallisation seemed to be dependent on the grade of deformation, where a higher grade of deformation resulted in a lower apparent activation energy, a correlation, that seems reasonable. The apparent activation energy of higher deformed samples is around 2.1 eV, the apparent activation energy of lower deformed samples around 2.8 eV. The calculated energies are consistent with activation energies of recrystallisation found for the same or other aluminum alloys, according to literature. A difference in apparent activation energy for recrystalliation when comparing parallel and perpendicular measurement direction has not been found.

However, a difference was found, when comparing the calculated activation energies for recovery. When calculating the apparent activation energies of recovery for measurements done parallel to the direction of deformation, a steady decrease of energy was found when increasing the grade of deformation, starting with 1.3 eV($\varepsilon = -0.17$) the apparent activation energy of recovery decreases to 0.2 eV($\varepsilon = -0.61$) is reached. The apparent activation energy for recovery when calculated for measurements done perpendicular to the direction of deformation on the other hand increases step-wise when increasing the grade of deformation starting with an energy of 0.9 eV for lower deformed samples and reaching an apparent activation energy of 1.3 eV for higher deformed samples. So the above mentioned anisotropy in length change during recovery is also reflected in the change of apparent activation energy for recovery when changing the grade of deformation. Nevertheless, it still has to be clarified, which processes that occur during recovery can be associated with the calculated apparent activation energies, which is a topic of further research.

Finally, a calculation of volume change curves from length change curves has been done for various heating rates and various grades of deformations. A correlation between the volume change and the grade of deformation has been found, where a higher grade of deformation leads to a greater volume change during recrystallisation as well as during the whole annealing process. Recovery leads to a smaller volume change, which is also not dependent on the grade of deformation. Once again, it could be concluded, that recrystallisation is the dominant annealing process in this material even for slow heating rates.

With the combination of difference dilatometry and EBSD, a method has been developed, that allows the in- situ identification of recovery and recrystallisation with dilatometry. With this new method, following points can be assessed:

- the onset of recrystallisation and recovery
- the dominant annealing process, recovery or recrystallisation
- the threshold grade of deformation ε for recrystallisation
- an orientation dependency of the annealing process

This study can also be seen as an initial first approach for a novel methodical development to determine experimental parameters for recovery and recrystallisation by difference dilatometry in combination with supporting electron backscatter diffraction experiments.

8 Aknowledgements

Last, but not least, I wish to express my sincere gratitude to honor the contribution of the following people to this work, without whom its completion would have not been possible.

Assoc.Prof. Dipl.-Phys. Dr.rer.nat. Wolfgang Sprengel,
for his friendly, competent and extensive supervision of this thesis.

Assoc.Prof. Dr.techn. Cecilia Poletti
for closing the gap between three different fields of expertise in countless helpful and valuable discussions.

Ricardo Buzolin, Eng. Mestr.
for performing the EBSD measurements and his extensive help regarding the interpretation of the results.

Ao.Univ.-Prof. Dipl.-Ing. Dr.techn. Klaus Reichmann
for performing the DSC measurements.

Assoc. Prof. Dipl.-Ing. Dr.mont. Stefan Pogatscher
for performing the chemical analysis of the material.

Ao.Univ.-Prof. Dipl.-Ing. Dr.techn. Karl Gatterer
for quick and straightforward help with issues regarding the etching reagent.

Dipl.-Ing. Robert Enzinger
for his help with the mathematical interpretation of the dilatometer results.

Ing. Wolfgang Rois
for his extensive help regarding the operation of the measurement equipment.

As well as both my colleagues from the Institute of Materials Physics and the Institute of Materials Science, Joining and Forming for their colleagueship.

Bibliography

1. Materials Science International Team, MSIT®. *The Mg-Al binary phase diagram. Datasheet from MSI Eureka in SpringerMaterials,*
2. Humphreys, F. J. & Hatherly, M. *Recrystallization and related annealing phenomena,* 2. ed. (Elsevier, Amsterdam, 2004).
3. Linseis. *Manual DIL L75VX Platinum Series*
4. Wikimedia. *File:LVDT.png,* https://commons.wikimedia.org/wiki/File:LVDT.png.
5. Vasilief, I., Besch, S., Gadiou, R. & Franke, K. *The QtiPlot Handbook,* https://www.qtiplot.com (2004).
6. Unger, K. *Bestimmung der Curie- Temperatur von Nickel zur heizratenunabhängigen Kalibrierung eines Differenz- Dilatometers,* Bachelor thesis: Institut für Materialphysik, TU Graz (2010).
7. *Elektrizitätslehre und Optik* (eds Lüders, K. & Pohl, R. O.) ger. 24., gründlich überarbeitete Auflage (Springer Spektrum, Berlin, 2018).
8. Weck, E. & Leistner, E. *Metallographische Anleitung zum Farbätzen nach dem Tauchverfahren. (English: Metallographic instructions for colour etching by immersion),* ger (Dt. Verl. für Schweisstechnik DVS-Verl., Düsseldorf, 1986).
9. Gao, L., Harada, Y. & Kumai, S. *Microstructural characterization of aluminum alloys using Weck's reagent, part I: Applications,* Materials Characterization **107**, 426–433 (2015).
10. Gao, L., Harada, Y. & Kumai, S. *Microstructural characterization of aluminum alloys using Weck's reagent, part II: Coloring mechanism,* Materials Characterization **107**, 434–452 (2015).
11. Olympus Microscopy Resource Center. / *Light and Color - Optical Birefringence,*
12. Schwartz, A. J. *Electron Backscatter Diffraction in Materials Science,* 2. ed. (Springer Science+Business Media LLC, Boston, MA, 2009).
13. Oxford Instruments. *ebsd.com,*
14. Schick, C., Lexa, D. & Leibowitz, L. *Differential Scanning Calorimetry and Differential Thermal Analysis,* **333**, 27 (2002).
15. Dynamic Systems Inc. https://www.gleeble.com.
16. Mishin, O. V., Godfrey, A., Juul Jensen, D. & Hansen, N. *Recovery and recrystallization in commercial purity aluminum cold rolled to an ultrahigh strain,* Acta Materialia **61**, 5354–5364 (2013).
17. Zwieg, T. *Universelle Methodik für die randscharfe mechanische Präparation und das Farbätzen von Aluminiumlegierungen,* (Bühler, application note, 2001).

18. Macherauch, E. & Zoch, H.-W. *Praktikum in Werkstoffkunde. 91 ausführliche Versuche aus wichtigen Gebieten der Werkstofftechnik,* 11., (Vieweg+Teubner Verlag / Springer Fachmedien, Wiesbaden, 2011).

19. Riontino, G., Antonione, C., Battezzati, L., Marino, F. & Tabasso, M. C. *Kinetics of abnormal grain growth in pure iron,* Journal of Materials Science **14**, 86–90 (1979).

20. Antonione, C., Marino, F., Riontino, G. & Tabasso, M. C. *Effect of slight deformations on grain growth in iron,* Journal of Materials Science **12**, 747–750 (1977).

21. Li, Y. J., Zhang, W. Z. & Marthinsen, K. *Precipitation crystallography of plate-shaped Al6(Mn,Fe) dispersoids in AA5182 alloy,* Acta Materialia **60**, 5963–5974 (2012).

22. Ratchev, P., Verlinden, B. & van Houtte, P. *Effect of preheat temperature on the orientation relationship of (Mn,Fe)Al6 precipitates in an AA 5182 Aluminium—Magnesium alloy,* Acta Metallurgica et Materialia **43**, 621–629 (1995).

23. Sepehrband, P., Wang, X., Jin, H. & Esmaeili, S. *Microstructural evolution during non-isothermal annealing of a precipitation-hardenable aluminum alloy: Experiment and simulation,* Acta Materialia **94**, 111–123 (2015).

24. Huang, K., Li, Y. J. & Marthinsen, K. *Effect of heterogeneously distributed preexisting dispersoids on the recrystallization behavior of a cold-rolled Al–Mn–Fe–Si alloy,* Materials Characterization **102**, 92–97 (2015).

25. Fuller, C. B., Krause, A. R., Dunand, D. C. & Seidman, D. N. *Microstructure and mechanical properties of a 5754 aluminum alloy modified by Sc and Zr additions,* Materials Science and Engineering: A **338**, 8–16 (2002).

26. Matusita, K. & Sakka, S. *Kinetic study of crystallization of glass by differential thermal analysis—criterion on application of Kissinger plot,* Journal of Non-Crystalline Solids **38-39**, 741–746 (1980).

27. Oberdorfer, B. *et al. Recrystallization kinetics of ultrafine-grained Ni studied by dilatometry,* Journal of Alloys and Compounds **509**, S309–S311 (2011).

28. Kissinger, H. E. *Reaction kinetics in differential thermal analysis,* Analytical chemistry **29**, 1702–1706 (1957).

29. Puchi-Cabrera, E. S., Villalobos-Gutiérrez, C. J., Carrillo, A. & Simone, F. *Non-Isothermal Annealing of a Cold Rolled Commercial Twin Roll Cast 3003 Aluminum Alloy,* Journal of Materials Engineering and Performance **12**, 261–271 (2003).

30. Hüller, M., Vlcek, J., Dinkel, M., Höppel, H. W. & Göken, M. *Hardening and thermal stability of nanocrystalline AlMg4.8 powder,* Philosophical Magazine **88**, 1209–1226 (2008).

31. Kang, K., Won, J., Bae, G., Ha, S. & Lee, C. *Interfacial bonding and microstructural evolution of Al in kinetic spraying,* Journal of Materials Science **47**, 4649–4659 (2012).

32. McQueen, H. J. & Blum, W. *Recovery and Recrystallization in Al Alloys Fundamentals and Practical Applications,* Aluminium Alloys, Physical and Mechanical Properties ICAA6 (1998).

33. Vandermeer, R. A. & Hansen, N. *Recovery kinetics of nanostructured aluminum: Model and experiment,* Acta Materialia **56**, 5719–5727 (2008).